Enhanced Oil Recovery Performance of Nanoparticle – Surfactant Stabilized CO_2 Foams in Carbonate Reservoirs

Madiyar Koyanbayev

Lead Supervisor: Prof. Randy Doyle Hazlett

Internal Co-Supervisor: Dr. Lei Wang

External Co-Supervisor: Dr. Muhammad Rehan Hashmet

A thesis submitted in fulfillment of the requirements for the degree of

Doctor of Philosophy

Department of Petroleum Engineering

School of Mining and Geosciences

June 2025

Originality Statement

I hereby state that the work presented in this submission is entirely my own, and I attest that it does not include any materials that have been previously published or written by someone else, except in cases where appropriate acknowledgment is given in the thesis. Furthermore, I affirm that the intellectual content of this thesis is a product of my independent effort, and no substantial parts of this material have been used to fulfill the requirements for any other degree or diploma at Nazarbayev University or any other educational institution.

Signature:_____

Date: June 2025

Dedication

This thesis is dedicated to the three most important pillars of my life: my parents, my wife, and my daughters. To my parents, whose unwavering love, sacrifice, and guidance shaped the person I am today. Your endless support and encouragement were the foundation of my dreams, and I will forever be grateful for everything you've done for me. To my wife, Aida, whose love, patience, and understanding kept me grounded throughout this journey. Your belief in me has been a constant source of strength, and I am beyond thankful for your unwavering partnership. To my daughters, Aizere and Ailana, who fill my life with joy, laughter, and purpose. You are the light that brightens my days, and your innocence and curiosity remind me of the importance of perseverance and hard work.

This achievement is as much yours as it is mine.

With all my love and devotion,

Madiyar Koyanbayev

Abstract

Carbon dioxide (CO_2) flooding is one of the promising techniques for enhancing oil recovery through mechanisms such as dissolving, oil swelling, viscosity modification, and lowering interfacial tension. However, CO_2 flooding faces challenges due to gas channeling and viscous fingering, which are caused by reservoir heterogeneity and the mobility contrast between CO_2 and reservoir oil. These issues can significantly reduce the oil displacement efficiency of CO_2 flooding, limiting its broader application and highlighting the need for CO_2 mobility control techniques. Nanoparticles and surfactant-stabilized foams have gained considerable attention as a solution to mitigate CO_2 conformance and mobility issues. The synergistic blend of interfacial tension reduction by surfactant and the strong adsorption of nanoparticles at the foam lamellae can produce foams that are significantly more stable and stronger in oil reservoirs than those stabilized by surfactant alone. However, the impact of nanoparticles on both the static and dynamic stability of traditional foams is not fully understood due to limited research. Therefore, this study aims to investigate the effect of silicon dioxide (SiO_2) nanoparticles on the bulk and dynamic stability of CO_2 foams stabilized by alpha-olefin sulfonate (AOS) surfactant. The performance of CO_2 foam in both bulk and porous media is influenced by several factors, including pressure and temperature conditions, foaming agent concentrations, the presence of oil, and rock properties. Therefore, designing successful CO_2 foam flooding for enhanced oil recovery requires a deeper understanding of foam performance under varying conditions, necessitating a comprehensive experimental and numerical study.

Bulk static stability tests were conducted to examine the effects of surfactant concentration, temperatures, salinity, and nanoparticle presence on CO_2 foam stability. The influence of oil on the stability of CO_2 foam, both stabilized by surfactants alone and in combination with nanoparticles, was quantitatively assessed during bulk static tests and dynamic foam flooding experiments in porous media. Additionally, the study compared the performance of surfactants, either alone or synergistically with nanoparticles, as CO_2 foaming agents for enhanced oil recovery (EOR) at low and elevated temperatures. A series of core flooding experiments were performed on parallel core systems to assess the flow diversion capacity of CO_2 foam stabilized by surfactants or by the combination of surfactants

and nanoparticles. Dynamic core flooding experiments were conducted using Indiana carbonate cores, including CO_2 foam flooding in the absence and presence of oil with measured oil recovery. The results of experimental works were further employed as input parameters for CO_2 foam simulations. Both 2D and 3D reservoir models were developed to conduct comparative studies between various injection scenarios, including CO_2 foam flooding, CO_2 flooding, and the co-injection of CO_2 and brine. Parameters, such as gas-oil ratio, production oil rate, oil recovery, and oil saturation distribution over time, were used to assess the performance of each EOR method.

Bulk static tests demonstrated that above the critical micelle concentration (CMC), CO_2 foam stability remained unchanged as surfactant concentration increased from 0.1 to 1%. This is attributed to the formation of a saturated interface when surfactant concentration exceeds CMC, which reduces the sensitivity of surface tension to further increases in bulk surfactant concentration. Bulk foam experiments demonstrated a decline in the stability of surfactant-stabilized CO_2 foam with increasing temperature. The addition of SiO_2 nanoparticles had only a marginal effect on foam properties. Increasing the oil concentration from 0 to 5% significantly reduced foam stability, decreasing the foam half-life by approximately 50% when stabilized with a 0.5 wt% AOS. Foam quality experiments indicated that increasing gas fractional flow resulted in higher foam apparent viscosity in porous media. However, when the gas fractional flow exceeded 70%, the foam viscosity decreased, marking the transition point between dry and wet foam regions. This value was selected as the optimal foam quality for further experiments.

Similar to the bulk static tests, foam generated in porous media demonstrated low stability at elevated temperatures. Increasing the temperature from 40℃ to 80℃ reduced the surfactant-stabilized CO_2 foam's apparent viscosity from 30 cp to 20 cp in the absence of oil. The addition of 0.05 wt% SiO_2 nanoparticles substantially improved foam performance in porous media, resulting in 1.5 to 2 times higher apparent viscosities compared to the surfactant alone. Dual-core studies showed that CO_2 foam was effective in diverting flow at various levels of heterogeneity, thereby improving sweep efficiency. Furthermore, CO_2 foam stabilized by the combination of nanoparticles and surfactant recovered 5% more oil than surfactant-stabilized foam under both low- and high-temperature conditions.

It is hoped that the outcomes of the laboratory work and numerical simulations in this research will contribute to the advancement of nanoparticle-surfactant foam applications for controlling CO_2 mobility. These results will also provide valuable input for conducting reservoir simulation and offer practical recommendations for the prospective field application of CO_2 foam EOR.

Acknowledgments

I would like to begin by expressing my deepest gratitude to my Lead Supervisor, Professor Dr. Randy Doyle Hazlett, for his exceptional patience, insightful feedback, and unwavering support throughout my research journey. His guidance has been invaluable in shaping this work. I am also profoundly grateful to my Internal Co-Supervisor, Professor Dr. Lei Wang, and my External Co-Supervisor, Assistant Professor Dr. Muhammad Rehan Hashmet, for their expertise and constant encouragement, which gave me the confidence to pursue this research. Their thoughtful comments and guidance have significantly improved the quality of my work, and I deeply appreciate their expertise and support.

I am truly thankful to the reviewers, Associate Professor Dr. Masoud Riazi and Assistant Professor Dr. Mian Umer Shafiq, for their valuable comments and suggestions on my research. I am immensely grateful to Professor Dr. Peyman Pourafshary, Acting Vice Dean for Academic Affairs and Research of the School of Mining and Geosciences, for his insightful feedback, support, and assistance during the PhD journey. I would also like to acknowledge Associate Professor Dr. Yanwei Wang and Dr. Sagyn Omirbekov, for all their help, support, and insight.

My sincere thanks go to the Department of Petroleum Engineering at Nazarbayev University for providing state-of-the-art laboratory facilities and continuous mentorship. I am deeply thankful to Mr. Gylym Sapinov, Senior Laboratory Coordinator, for his continuous assistance throughout my research.

Lastly, I would like to extend my heartfelt thanks to my defense committee members for their time, valuable feedback, and meticulous review of my work. Their contributions during the review process and oral defense were crucial to my success in completing this thesis.

Contents

List of Figures

List of Tables

List of Abbreviations and Nomenclature

AOS	Alpha-olefin sulfonate
BHP	Bottom Hole Pressure
BPR	Back Pressure Regulator
CMC	Critical Micelle Concentration
CO_2	Carbon Dioxide
DI	Deionized
EOR	Enhanced Oil Recovery
FCM	First Contact Miscibility
f_g	Foam Quality
GOR	Gas Oil Ratio
HPHT	High Pressure High Temperature
IFT	Interfacial Tension
IOR	Improved Oil Recovery
MCM	Multiple Contact Miscibility
md	Millidarcy
MMP	Minimum Miscibility Pressure
MRF	Mobility Reduction Factor
N_2	Nitrogen
NP	Nanoparticle
OOIP	Original Oil in Place
PV	Pore Volume
SDS	Sodium Dodecyl sulfate
SiO_2	Silicon Oxide
S_o	Oil Saturation
S_{oi}	Initial Oil saturation
S_{or}	Residual Oil Saturation
S_{wi}	Irreducible Water Saturation
wt%	Percentage by Weight

CHAPTER 1. Introduction and Overview

1.1 Background

Today, oil and gas are still major energy sources despite significant growth in renewable energy production over the past decade. Renewable energy capacity is expected to steadily increase because of global efforts towards a more sustainable future. In contrast, it was forecasted that the demand for fossil fuels will reduce from 86% to 77% by 2040 [1]. Even so, it was also predicted that, compared to 2013, the world consumption of oil-based energy will rise by nearly one-third, and oil production will reach 115 million barrels per day by 2040 [1]. This rise in energy demand is driven by projected annual economic growth of 3%. However, the exploration of new potential fossil fuel resources, such as oil and natural gas, is becoming technically more complicated, economically less viable, and raises environmental concern. In response to these challenges, maximizing oil recovery from the existing oil reservoirs is a key approach to meet growing energy demand while minimizing the environmental risks.

CO_2 injection into depleted or produced oil reservoirs is a highly effective method for improving oil recovery as well as minimizing the cost of CO_2 storage. The efficiency of CO_2 as an IOR / EOR solvent has been extensively proven through both experimental and numerical studies [2, 3]. It is estimated that CO_2 accounts for about 60% of gas injection EOR projects implemented in carbonate reservoirs, followed by hydrocarbon gases (36%) [4]. The dissolving of CO_2 in crude oil generates the mixture, which improves sweep efficiency and results in higher oil recovery [5]. Moreover, the solubility of CO_2 is higher in oil compared to water, resulting in significant oil expansion, swelling, and viscosity reduction. However, CO_2 flooding has inherent limitations due to the significantly lower viscosity compared to water and most crude oils. This leads to mobility and instability issues such as viscous fingering and gas channeling [6, 7]. Additionally, CO_2 tends to migrate towards the upper part of a reservoir due to the low density, overriding the oil zone and resulting in poor sweep efficiency.

Foam flooding is considered as a promising solution for controlling gas mobility and improving sweep efficiency during gas EOR. Foam is generated in porous media by either simultaneous or consecutive injection of surfactant solution and CO_2 slugs or dissolving

surfactant in supercritical CO_2 [8]. The primary mechanisms for gas mobility control by foam involve increasing the apparent viscosity of the injected gas and reducing gas relative permeability [9]. CO_2 foam is particularly effective in preventing viscous fingering, improving sweep efficiency, and enhancing oil recovery compared to injecting CO_2 or water or even using the WAG process [10]. In heterogeneous reservoirs, the reduction in gas mobility by foam helps redirect the injected fluid from high permeability to low permeability zones, further improving sweep efficiency [11].

Despite its effectiveness, CO_2 foam is thermodynamically unstable, which limits its applicability under reservoir conditions. Particularly, in a crude oil environment and harsh reservoir conditions characterized by high temperature, pressure, and salinity, foam tends to destabilize easily [12]. This leads to weak foam generation, resulting in poor sweep efficiency. To improve CO_2 foam stability, several methods such as adding surfactant, polymer, and nanoparticles have been investigated [13]. Previous research showed that surfactant increases foam lifetime and stability, improving macroscopic and microscopic sweep efficiency, which leads to higher oil recovery. Moreover, surfactant alters wettability, reducing capillary forces and accelerating oil flow [14]. However, under harsh reservoir conditions, surfactant is prone to degradation, which limits its ability to maintain foam stability for a long time [15, 16]. Additionally, surfactants tend to adsorb onto the rock surface, requiring continuous supplementation of surfactants, which makes foam stabilization costly [17].

Recently, using a mixture of surfactants and nanoparticles for foam stabilization, especially under harsh conditions, has attracted great interest. The synergistic blend of IFT reduction by surfactants and the extreme tendency of nanoparticles to adsorb at the foam interface can lead to stronger foamability and greater stability than the surfactant alone [18]. Several previous studies have demonstrated that the mixture of surfactant and nanoparticles results in both high static and dynamic foam stability [19, 20]. Additionally, nanoparticles are solid, which helps improve the resistance of foam to high temperature, pressure, and high salinity [21]. Besides, nanoparticles help reduce the adsorption of surfactant onto rock surfaces [22, 23].

1.2 Problem Statement

One of the primary concerns in the application of CO_2 foam in EOR is the adverse effect of crude oil on foam behavior, as well as the complexity of foam-oil interactions. Key factors affecting foam stability in the presence of oil are surfactant type and oil properties [18]. Numerous studies have examined the impact of oil presence on foam, stabilized either by nanoparticles or surfactants. Generally, these studies show that the presence of oil can destabilize the foam, deteriorating both static and dynamic foam stability [24, 25]. Additionally, the influence of crude oil on foam stability becomes more detrimental with decreasing oil density and viscosity. However, recent studies have shown that combining surfactant and nanoparticles significantly enhances foam stability in the presence of oil because of nanoparticle aggregation at the foam interface [26, 27]. Furthermore, the addition of nanoparticles results in a higher foam apparent viscosity than surfactant alone, further improving oil recovery [12]. Despite numerous studies assessing the influence of oil on the behavior of foam, further studies are needed to investigate the stability of nanoparticle-surfactant-stabilized CO_2 foam in the presence of crude oil.

Foam flooding plays an important role in overcoming mobility issues in heterogeneous reservoirs. Previous foam flooding experiments have been mainly conducted using homogeneous sandpack or core samples, which make it impossible to assess the flow diversion ability of foam [28-30]. More recent studies used double- or triple-core holder systems containing core samples with various permeability to represent different scales of heterogeneity [31, 32]. These studies reveal that foam performance in flow diversion declines as heterogeneity increases. Moreover, foam becomes ineffective above a heterogeneity limit. This limit is significantly lower in the presence of oil compared to its absence, underscoring the detrimental effect of oil on foam efficiency. However, further studies are needed to thoroughly investigate the influence of heterogeneity on foam performance.

Moreover, salinity is one of the crucial parameters. Increasing salinity or ion concentration negatively impacts foam stability, and previous studies have often used low salinity brine to mitigate this effect [29, 30]. However, typical oil reservoirs contain high-salinity brines, making it essential to use reservoir brine in future studies to reduce uncertainty in field applications.

Overall, using the combination of nanoparticles and surfactants to stabilize CO_2 foam is a relatively new approach; thus, it still requires further extensive study to understand the foam behavior under elevated temperature, various salinity, and crude oil conditions.

1.3 Scope and Objectives

This research aims to explore the potential of surfactant-nanoparticle stabilized CO_2 foam in EOR, focusing on an oil field in Kazakhstan. The primary objective of this research is performing static and dynamic foam experiments to assess foam characteristics under various reservoir conditions, such as elevated temperature, heterogeneity, and the presence of crude oil. The study will also compare the performance of CO_2 foam stabilized by a combination of surfactant and nanoparticles against foam stabilized by surfactant alone. Thus, the main objectives of this study are as follows:

1. Evaluate the stability of CO_2 foam stabilized with alpha-olefin sulfonate (AOS) surfactant, with and without the addition of silicon oxide (SiO_2) nanoparticles, using static tests. Additionally, investigate the influence of oil and temperature on CO_2 foam stability.
2. Conduct foam flow experiments in carbonate core samples to understand foam flooding performance and foam behavior.
3. Perform a comparative study to investigate the oil recovery efficiency of CO_2 foam stabilized with the surfactant-nanoparticles and surfactant alone.
4. Determine the impact of heterogeneity on CO_2 foam behavior in porous media in the absence of oil.

1.4 Significance

In recent years, the injection of CO_2 into reservoirs to enhance oil recovery has attracted significant global interest as a viable and efficient carbon capture, utilization, and storage technique aimed at reducing greenhouse gas emissions and mitigating global warming. Therefore, CO_2 injection into the major carbonate oil reservoirs of the Pri-Caspian basin is an attractive option for enhancing oil recovery while simultaneously utilizing and storing CO_2. However, mobility and conformance issues due to the low viscosity of CO_2 and

reservoir heterogeneity may limit its oil recovery efficiency; hence, mobility control techniques such as foam are recommended.

The application of CO_2 foam flooding into Kazakhstani oil fields to enhance oil recovery has not been extensively studied, and available information remains limited. For this reason, this study aims to provide the first detailed insight into the feasibility of CO_2 foam application for oil recovery in the Pri-Caspian basin. Furthermore, this research evaluates the use of Caspian Sea water as an aqueous phase for foam application. Given its regional availability and extensive use for waterflooding to enhance oil recovery from oil reservoirs in the Pri-Caspian basin, assessing its compatibility and performance in CO_2 foam systems—particularly when combined with surfactants and nanoparticles—is crucial. Beyond the technical aspects, CO_2 foam flooding offers both economic and environmental benefits. From one side, this technique enhances oil recovery, increasing profitability, and from the other side, it enables CO_2 sequestration, thereby contributing to climate change mitigation.

1.5 Thesis structure

Chapter 1 introduces the background of the study, outlines the key challenges in the field, and presents the motivation and objectives of the thesis. Chapter 2 introduces enhanced oil recovery methods and defines foam, including its characteristics. Chapter 3 describes the materials, experimental setup, procedures, and methods used for studying the foam characteristics and their application in EOR processes. Chapter 4 summarizes the main experimental results and key findings. Chapter 5 includes the results of numerical simulation of CO_2 foam performance in EOR, using a sector model. Finally, the conclusions of the thesis and recommendations for future work are presented.

CHAPTER 2. Literature Review

2.1 The Concept of Oil Recovery

The traditional oil recovery process includes three distinct phases: primary, secondary, and tertiary recovery. Primary recovery refers to the process of oil extraction and production utilizing natural energies stored within the reservoir. Expansion and liberation of reservoir fluids, such as oil, gas and water, as well as rock compaction, are the main mechanisms of primary recovery [33]. During this phase, reservoir pressure declines due to oil production, reducing reservoir energy available to force hydrocarbons trapped in the reservoirs to the surface.

Once primary recovery becomes less effective, secondary recovery methods are employed to support reservoir pressure and increase oil production by displacing oil toward the production wells. The most common methods are water flooding and immiscible gas injection [34]. However, the estimated average recovery factor after primary and secondary methods is less than 30-40% of original oil in place. This is largely due to high interfacial tension and poor mobility control, which hinder the effective displacement of oil [35].

The huge volume of residual oil remaining after primary and secondary recovery phases is a target for tertiary recovery, which is often used as a synonym for enhanced oil recovery (EOR) processes. The decline in new oil reservoir discoveries and the low recovery efficiency of conventional oil recovery methods have made the application of EOR techniques essential for extracting additional hydrocarbons from mature fields to meet growing global energy demand. EOR methods are designed to improve both macroscopic and microscopic displacement efficiencies, helping to recover the trapped residual oil. The microscopic sweep efficiency, which is described as the flow of oil at the pore level, can be improved by reducing capillary forces, lowering oil viscosity, and decreasing interfacial forces between reservoir oil and the displacing fluid. On the other hand, the macroscopic displacement efficiency refers to the process of sweeping the reservoir by displacing fluid and pushing oil toward a production well. Improving macroscopic sweep efficiency involves creating a more favorable mobility ratio-either by increasing oil mobility or reducing the mobility of the displacing fluid [36].

2.2 Enhanced Oil Recovery Methods

EOR involves a range of techniques to extract residual or bypassed oil from reservoirs. These methods include mobility control, chemical flooding, miscible gas flooding, and thermal recovery techniques [33, 37].

Chemical flooding often uses chemicals, such as surfactants, polymers, and alkali [38-40]. Surfactant flooding is implemented to reduce surface tension at the water-oil interface, which in turn diminishes capillary forces. Moreover, surfactants can alter rock wettability or induce spontaneous emulsification [41]. However, many commercially available surfactants used for EOR are expensive and tend to adsorb on the rock surface, requiring a large volume of surfactant or the use of sacrificial materials to overcome the retention issues, which makes their application economically unattractive. Moreover, surfactants often exhibit instability in high salinity brines and can partially solubilize in the reservoir oil, further limiting their effectiveness in EOR.

Polymer flooding involves the injection of large molecular weight polymers into the reservoir, which increases the viscosity of the displacing fluid and reduces its mobility, leading to better sweep efficiency. Nevertheless, the implementation of polymer flooding is limited in harsh reservoir conditions. Polymers with high molecular weight can easily degrade and lose viscosity when exposed to high salinity and high temperature, making them less effective in such conditions [42].

Alkaline flooding uses cost-effective alkali chemicals and their reaction with acid components of reservoir oil to form soap. This reaction decreases IFT between water and oil and reduces surfactant retention [43]. Alkaline flooding can significantly lower IFT, especially when crude oil has a high soap number [44].

Thermal oil recovery methods are used to heat reservoir oil to reduce its viscosity and improve oil mobility. Common thermal EOR techniques include steam-assisted gravity drainage (SAGD), cyclic steam stimulation (CSS), and steam flooding. These methods involve injecting steam into the reservoir to heat the oil or using in situ combustion to generate heat, making the oil easier to extract.

Miscible gas flooding describes the process of injecting gas into the reservoir that is miscible with the trapped residual oil and forms a single phase under suitable reservoir

conditions. This process effectively diminishes interfacial tension and reduces capillary forces, facilitating oil displacement.

2.3 CO_2-based-EOR

Gas flooding is a widely used EOR technique, particularly effective for extracting light, condensate, and volatile oils. Methane and other hydrocarbon gases, CO_2, N_2, and air are commonly used gases in gas flooding EOR. The selection of gas type and composition for field application is determined by various factors, including gas availability, recovery mechanisms (miscible or immiscible), and economic considerations.

CO_2 flooding EOR has been successfully implemented over the last decades with commercial success [45]. The concept of using CO_2 flooding for oil recovery was first proposed by Whorton et al. (1952) [46]. The first pilot test was conducted at the Mead Strawn Field to assess the effectiveness of CO_2 injection in increasing oil recovery [47]. Following the success of this pilot test, CO_2 flooding was implemented for the commercial project at the Kelly-Snyder Field in the USA [48]. Recent studies show that the injection of low-cost CO_2 currently accounts for approximately 5% of total oil production in the USA [13]. It is estimated that CO_2 EOR could contribute to up to 12% of total crude oil production in the country by 2040. In recent years, the use of CO_2 in EOR has gained more interest because of the growing attention on environmental issues and the need to cut greenhouse gas emissions [49].

2.3.1 CO_2 Properties

Understanding the physical properties of CO_2 under various temperature and pressure conditions is crucial for the successful design and implementation of the CO_2-based EOR process. The phase behavior of CO_2 changes significantly depending on the pressure and temperature, as shown in Figure 2-1. At ambient conditions, CO_2 exists as a gas with a specific gravity of 1.529 and a density of 1.95 kg/m^3. As pressure increases, CO_2 becomes denser and changes from gas to liquid phase. The critical pressure and critical temperature of CO_2 are 73.9 MPa and 31.1ºC, respectively.

Above these critical conditions, CO_2 enters a supercritical state and exhibits liquid-like properties. In this supercritical state, the density of CO_2 is similar to that of liquid, but

the viscosity remains relatively low (0.05-0.08 cp). Compared to gaseous CO_2, the injection of supercritical CO_2 is more favorable for EOR, because it mitigates gravity segregation, resulting in higher incremental oil recovery [45, 50]. Despite poor sweep efficiency due to low viscosity, the dissolution of supercritical CO_2 into reservoir oil reduces the oil viscosity, thereby enhancing oil recovery [51].

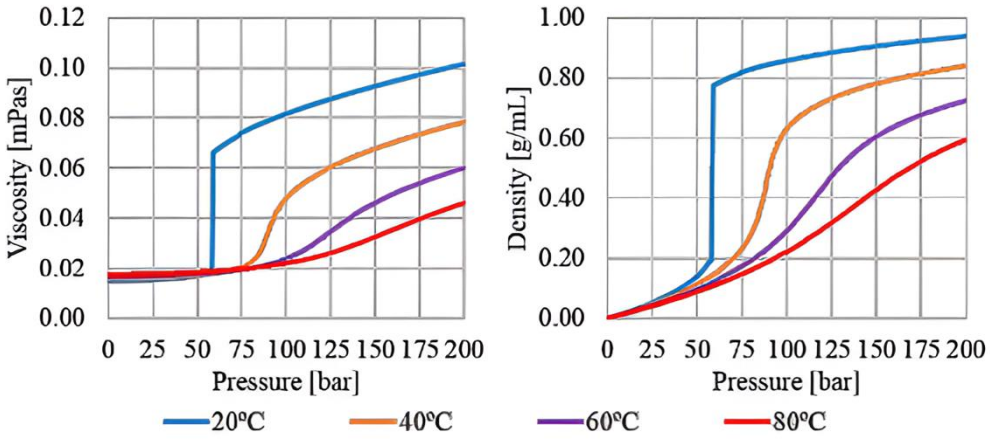

Figure 2-1. Density and viscosity of CO_2 at various pressure and temperature [52].

2.3.2 CO_2 EOR Mechanisms

The primary mechanisms of CO_2 EOR include the following processes that enhance oil recovery:

a) Reduction in IFT at water-oil interface

Upon reaching the reservoir, the injected CO_2 may dissolve in the reservoir brine, reducing the interfacial tension between water and oil. This reduction facilitates high oil production by enhancing the flow mechanism of the reservoir oil.

b) Reduction in oil swelling and viscosity

When CO_2 contacts crude oil under reservoir conditions, it dissolves in the reservoir oil. This dissolution causes the oil volume to expand [45]. The swelling effect that results from this dissolution is beneficial for oil recovery, as it increases the mobility of residual oil. This enhances the relative permeability of oil; thus, oil easily flows towards a production well. In addition to the swelling effect, the dissolution of CO_2 can reduce the viscosity of oil, further improving oil mobility.

c) Solution gas drive

After CO_2 breakthrough during injection, the reservoir pressure may drop to or below the saturation pressure. As a result, the dissolved CO_2 in the crude oil will separate from the oil, generating a gas drive process that provides extra energy to displace the oil.

d) Extraction and vaporization of the light oil fractions

When the reservoir pressure is higher than a threshold value, light components of oil can be extracted and vaporized by CO_2, thereby improving oil recovery. However, the effectiveness of this process largely depends on oil properties.

e) Weak acid formation

The reaction of CO_2 with water forms carbonic acid, which can corrode the carbonate rock, altering its properties, particularly increasing rock permeability. Additionally, the acid helps dissolve inorganic scale, leading to higher oil production.

2.3.3 Miscible and Immiscible CO_2 Injection

CO_2 EOR flooding can be classified as either miscible or immiscible flooding, depending on the oil's characteristics, the composition of the injected gas, reservoir pressure, and temperature. The miscible process is generally preferred due to its potential for higher oil recoveries [53].

For CO_2 flooding to be considered miscible, the reservoir pressure must be higher than the minimal threshold pressure, known as the Minimum miscibility pressure (MMP). If the reservoir pressure is below MMP, the injected CO_2 will not fully dissolve in the reservoir oil. In this case, the CO_2 and oil remain immiscible, and this condition is described as immiscible CO_2 flooding. Even if a portion of injected CO_2 dissolves into the reservoir oil during this process, it can promote oil swelling and viscosity reduction, which can improve oil mobility and enhance recovery. Additionally, immiscible CO_2 flooding can form an artificial gas cap providing extra energy to extract the reservoir oil.

In-situ miscibility between injected gas and reservoir oil can develop if the reservoir pressure exceeds MMP. There are two types of in-situ miscible displacement processes: First-Contact Miscibility (FCM) and Multiple Contact Miscibility (MCM). The FCM occurs when the entire volume of the injected gas completely dissolves into the oil upon the first

contact, while MCM develops gradually over multiple contacts. The MCM involves mechanisms such as vaporizing gas, condensing gas, or a vaporizing/condensing drive [37].

For CO_2 injection, miscibility is typically achieved through the vaporizing drive mechanism, where the lighter components of reservoir oil vaporize into the CO_2, enriching it and leading to miscibility [54]. Moreover, CO_2 requires lower pressure to achieve miscibility with reservoir oil compared to other gases such as N_2 and lean gas [55].

2.3.4 Challenges with CO_2 Injection for EOR

While laboratory studies show that miscible CO_2 flooding can recover over 90% of OOIP, field-scale oil recoveries are often much lower, typically less than 20% [56, 57]. This discrepancy is primarily due to early gas breakthroughs and poor displacement efficiency. As a result, the injected gas can only sweep a small portion of the reservoir, leaving a large fraction of trapped oil, especially in reservoir areas not reached by the injected gas.

Front instabilities and poor volumetric sweep efficiency are common issues affecting the performance of CO_2 EOR. These mobility control problems are mainly due to the low density and viscosity of CO_2, as well as the heterogeneous nature of many reservoirs [37, 58]:

1) CO_2 and most of the gases used for EOR have a low viscosity (in the range of 0.02 and 0.06 cp under reservoir conditions), which makes them significantly more mobile in porous media compared to reservoir oil (which typically has a viscosity of 0.5 cp to 10 cp). This difference in mobility between the injected gas and reservoir oil can cause viscous fingering, where gas flows through more permeable zones, leading to poor oil displacement.

2) The density of CO_2 is significantly lower than that of reservoir fluids, which can result in gravity segregation. Gravity and buoyancy forces cause the less dense gas to rise to the top of the reservoir, while denser fluid remains at the bottom. This phenomenon, known as gravity override, reduces the contact between the injected gas and the trapped oil, particularly in the lower parts of the reservoir.

3) The injected gas tends to flow in the direction of least resistance, just like any other fluid. Therefore, heterogeneous reservoirs with varying permeability can exacerbate mobility issues during CO_2 flooding and can cause gas channeling

through high-permeability zones. In severe heterogeneous environments, this leads to the formation of “thief zones” - areas where the gas flows through the most permeable zones, bypassing much of the oil (Figure 2-2).

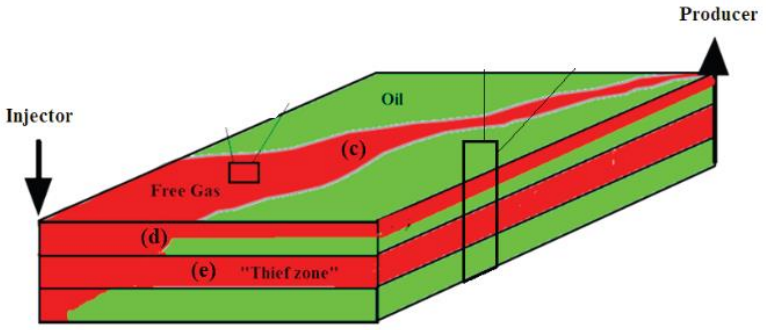

Figure 2-2. CO_2 based enhanced oil recovery process [58].

2.4 Foam CO_2 Flooding

Foam flooding is one of the effective techniques to reduce CO_2 mobility and enhance macroscopic gas displacement efficiency. The application of CO_2 foam for preventing early gas breakthroughs and improving the sweep efficiency of CO_2 flooding was first suggested in the 1950s [59]. The pioneering studies and field tests performed by Mast [60] and Patton et al. [61] revealed that foam could be an effective approach for mitigating CO_2 channeling and viscous fingering phenomena as well as preventing gravity override. Since then, there have been a number of field-scale applications using foam that are successful, as well as some that are not [13, 62].

Foam is a colloidal system in which gas bubbles are dispersed within a continuous liquid phase [63]. As shown in Figure 2-3, the gas phase is trapped in numerous bubbles inside the continuous liquid phase and separated from each other by thin liquid film known as lamellae. This foam structure can be created by injecting gas through a liquid phase or by shaking a container with both phases. In a bulk foam structure, a two-phase system containing water and a gas would rapidly lose its structure due to foam coalescence. However, the addition of surfactants or nanoparticles to the aqueous phase or CO_2 can significantly improve the transitory foam stability [64-66].

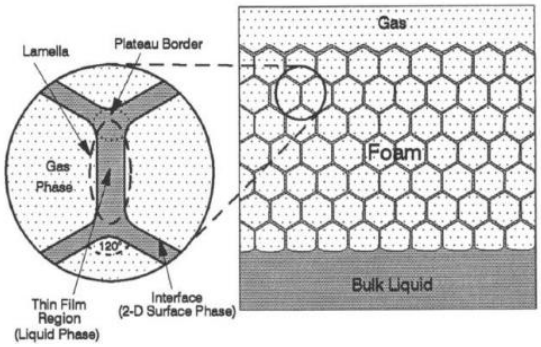

Figure 2-3. Foam structure [63].

In porous media, foam helps prevent conformance and mobility control issues during gas flooding. Foam has a higher viscosity than gas, which allows it to reduce gas relative permeability and increase apparent gas viscosity [67]. Additionally, foam can efficiently block high-permeability zones and divert injected gas or fluid into low-permeability areas, improving sweep efficiency and enhancing oil recovery. Figure 2-4 illustrates the effectiveness of foam in improving displacement efficiency. The foam texture, including bubble size and the quantity of lamellae per unit volume of gas, determines the foam's resistance to gas flow. Smaller bubbles and higher lamellae density increase foam's resistance to flow and improve its stability, positively affecting gas displacement efficiency and contributing to greater oil recovery.

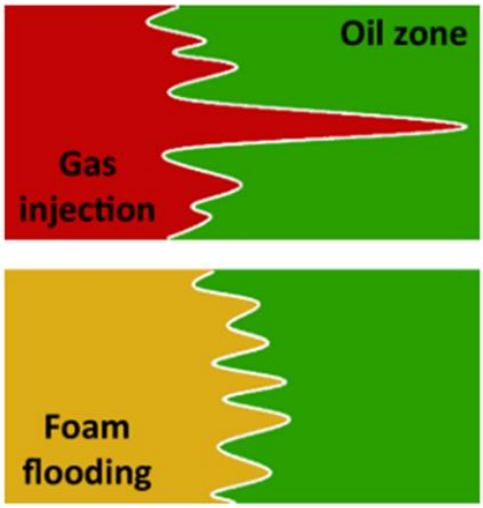

Figure 2-4. Gas flooding versus foam flooding [67].

2.4.1 Foam Generation in Porous Media

Generally, the generation of foam is governed by the formation and coalescence rates of gas bubbles. Foam accumulates in porous media when the formation rate is greater than the coalescence rate. The formation rate of foam is influenced by injection rate, pressure gradient, and pore geometry, such as size, complexity, and aspect ratio [58]. Foam texture, including bubble size, is determined by foam generation mechanisms, which affects the foam flow properties, and its apparent viscosity [68]. Three primary mechanisms responsible for foam generation in pores are leave-behind, snap-off, and lamella division [69].

During the leave-behind mechanism, two gas bubbles approach adjacent pore throats that are initially filled with surfactant solution. As gas bubbles pass around the grain between the pore throats, they converge together in the pore body. The procedure is demonstrated in Figure 2-5. During this convergence, the liquid in the pore body is squeezed with the bubbles, leaving behind a lamellae or liquid lens [70, 71]. This mechanism typically generates weak or coarse foam [72, 73]. Additionally, foam generated by the leave-behind mechanism tends to collapse, as the lamellae are aligned with the gas flow direction [64]. If the liquid phase contains enough surfactant, the lamellae remain quasi-stable; otherwise, they break quickly. Once the lamellae break, the spontaneous generation of new lamellae under the leave-behind mechanism requires delivery of surfactant solution to the pore body.

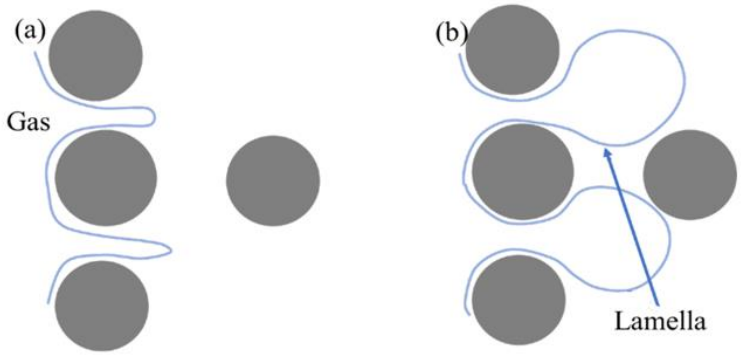

Figure 2-5. Illustration of leave-behind mechanism. (a) gas enters the pore throat; (b) liquid in pore body is squeezed, forming a lamellae [69].

In the snap-off mechanism, the injected surfactant solution initially fills the pore body and pore throat. As the gas phase invades into the pore throat and moves into the

neighboring pore body, the gas bubble begins to grow, as illustrated in Figure 2-6. This causes the capillary pressure at pore entry to decrease, while the pressure within the throat and pore body remains high. This pressure difference drives the surrounding liquid from the pore body into the throat, forming a lens that blocks gas flow. As the gas bubble continues to expand, the capillary pressure at the gas-liquid interface drops below the critical value, causing liquid to eventually snap off and form a discrete bubble, thus making the gas phase discontinuous.

The snap-off mechanism requires a high flow rate, generating enough pressure difference between the pore throat and the pore body. Under this condition, the surfactant solution can spontaneously invade into the pore throat; thus, new bubbles form repeatedly under the snap-off mechanism. For these reasons, it is considered as a dominant mechanism for foam generation in porous media [69]. Two factors affect the occurrence of snap-off: the ratio of pore throat size to pore body size, which must be greater than 2, and the presence of sufficient wetting liquid [74, 75]. Typically, the size of gas bubbles generated under this mechanism is around the size of pore bodies.

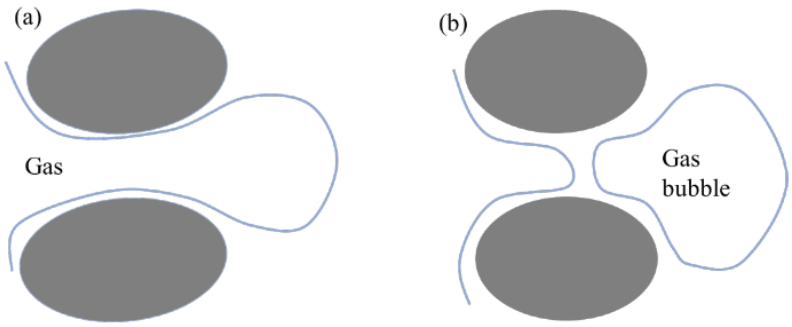

Figure 2-6. The illustration of snap-off mechanism. (a) gas enters into the pore throats; (b) a gas bubble jumps out and form lamellae [69].

The lamella division is a phenomenon that facilitates the expansion of a moving lamella at a branch point, where the pore space is connected to multiple pore channels. At the branch point, a moving gas bubble is split, and the resulting new bubbles proceed into different channels as shown in Figure 2-7. Unlike the snap-off and leave-behind mechanisms, the lamellae division does not generate foam; instead, it leads to gas bubble

fragmentation, which strengthens the dry foams. However, lamellae division only occurs if the foam pressure exceeds the capillary pressure of each channel [76, 77].

Similar to the snap-off mechanism, lamellae division creates gas phase discontinuity either by forming new gas bubbles or by the initial moving bubble. Moreover, this mechanism can happen repeatedly as split bubbles continuously move toward the branch points. The rate of lamellae division is influenced by several factors, including a number of mobile bubbles, the existence of a branch point and the gas injection rate [78-80].

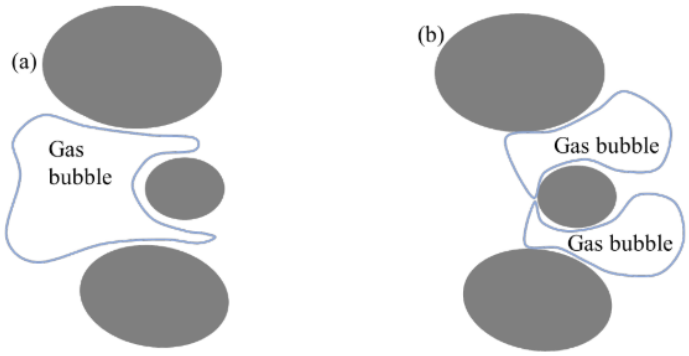

Figure 2-7. The illustration of the lamellae division mechanism. (a) gas enters the pore throat, (b) gas divided into new bubbles [69].

2.4.2 Foam Stability

Foams are inherently unstable and will eventually collapse over time. The ability to sustain the stable foam state is determined by the stability of the lamellae, which means that when the distribution of bubbles is uniform, the lamellae are stronger and thus the foam is more stable [81]. The ongoing changes in foam stability are influenced by foam coarsening, as gas moves through the liquid lamella due to diffusion [82]. The stability of foam is controlled by both the properties of the foam films and petro-physical characteristics [68].

In the absence of oil, foam stability in porous media is primarily governed by two mechanisms: capillary suction and gas diffusion [75].

Capillary suction. The schematic of the foam system is shown in Figure 2-8. Three adjacent lamellae at the junction form a plateau border, with each angle measuring approximately 120º. Typically, the plateau border contains the majority of liquid. The radius of the plateau border is significantly smaller than that of the thin liquid films, resulting in

lower pressure in plateau borders compared to thin liquid films. Because of this pressure difference, liquid in lamellae flows towards the plateau border, which further thins the film. This movement of liquid toward the plateau border is driven by a force known as capillary suction coalescence [83]. Film thinning and lamellae coalescence due to capillary pressure are typically more pronounced inside porous media, especially in pores with small radii, compared to bulk conditions.

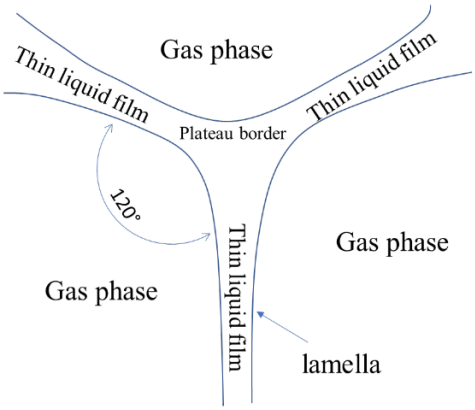

Figure 2-8. The schematic of the foam system [83].

Gas diffusion. A typical foam system may contain bubbles with various sizes. In such a system, small bubbles have a smaller curvature than large bubbles, resulting in greater capillary pressure in the former. The pressure difference between the two bubble sizes causes gas to diffuse from the smaller bubbles into the larger ones. As a result, over time, smaller bubbles disappear, and larger bubbles become more dominant. The resistance of foam to gas flow depends on foam's texture. When large bubbles dominate the system or there are fewer lamellae per unit volume of gas, there is less resistance to gas flow. However, gas diffusion occurs relatively slowly and has a less significant impact when foam flows through a porous medium [63].

The Effect of Temperature and Pressure

Reservoir pressure and temperature are two key factors that influence foam stability. An increase in temperature generally has a negative impact on foam stability. First, as the temperature rises, the foaming agent becomes more soluble in water, reducing its availability to lower interfacial tension between the liquid and gas phases. Second, high reservoir

temperature accelerates the rate of liquid film drainage [81]. A third consequence of elevated temperatures is a decrease in the critical salt concentration (CSC), below which particles begin to aggregate and precipitate. Consequently, when nanoparticles are utilized as foaming stabilizers, the lower CSC weakens their ability to stabilize the foam [84].

In contrast, higher reservoir pressure enhances foam stability by reducing the size of the foam bubbles and decreasing the rate of liquid drainage. However, if the pressure goes above a certain threshold, it can exert additional stress on the foam bubbles, causing them to break [81].

The effect of permeability

Oil reservoirs inherently exhibit some degree of heterogeneity, and this frequently includes variation in permeability. In particular, foam behavior differs significantly between high- and low-permeability areas. Foam tends to be less mobile in high-permeability regions compared to low-permeability zones [68]. When foam is injected into a reservoir with permeability heterogeneity, the stronger foam will be produced in the high-permeability regions, effectively diverting fluid flow into lower-permeability zones [85]. This process helps block the high-permeability layers, as foam formation reduces gas mobility, thus mitigating the effects of reservoir heterogeneity [86].

The Effect of oil

The effectiveness of foam injection in EOR largely depends on the interaction between foam and reservoir oil. Foam films typically degrade upon contact with oil, which limits their stability. Core flood studies have shown that foam will not form in the oil reservoir if the oil saturation exceeds a specific threshold, known as a critical foaming oil saturation [87, 88]. At this saturation point, the oil breaks the gas/liquid interface by spreading across the foam film, displacing the initial liquid phase. [81]. This leads to the formation of an unstable oil film, which causes gas bubble coalescence [89].

Despite these challenges, several studies have reported successful foam generation even at high oil saturations, indicating that foam stability can still be maintained under certain conditions [90-92].

2.4.3 Foam-oil Interaction Theories

In the literature, a number of theories have been developed to predict foam behavior in the presence of oil. The most well-known theories are listed below:

1) Spreading and entering coefficients

2) Bridging coefficient

3) Lamella number

Spreading and entering coefficients

The key parameters to assess the influence of oil on foam stability are the entering coefficient (E), which is calculated using Equation 2.1 [74, 93]:

$$E = \sigma_{w/g} - \sigma_{o/g} + \sigma_{w/o} \tag{2.1}$$

and spreading coefficient (S) is calculated by [74, 94]:

$$S = \sigma_{w/g} - \sigma_{o/g} - \sigma_{w/o} \tag{2.2}$$

where σ_{wg} and σ_{og} are the surface tensions at the water-gas interface, and oil-gas interface, respectively, and σ_{ow} is the interfacial tension at the water-oil interface.

When the entering and spreading coefficients are negative, the foam remains stable in the presence of oil. However, when both E and S are positive, the oil droplet enters the gas-water interface, where it spontaneously spreads along the interface. This process leads to foam instability, such as lamellae collapse or rupture [95, 96].

The impact of oil on the various negative and positive values of the entering and spreading coefficients is displayed in Figure 2-9.

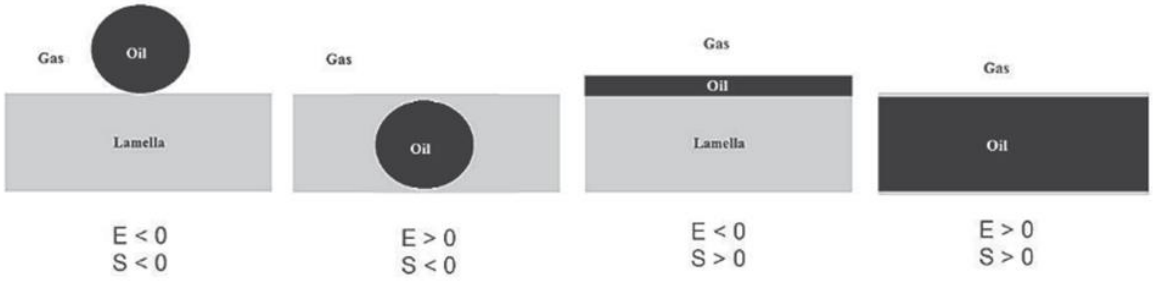

Figure 2-9. The schematic of different entering and spreading cases [74].

Bridging coefficient

Another frequently used parameter to assess the influence of oil on foam stability is the bridging coefficient, which is calculated by Equation 2.3 [97, 98]:

$$B = \sigma_{w/g}^2 - \sigma_{o/g}^2 + \sigma_{w/o}^2 \quad (2.3)$$

If the spreading phenomenon does not occur, the oil droplet may enter the lamellae, forming a lens or bridge. This leads to foam instability even when E is positive and S is negative. Eventually, the lamellae are split by an oil drop into the two film surfaces and rupture.

The following scenarios can be concluded from comparing the entering and bridging coefficients:

• A positive B implies positive E, but the reverse is not necessarily true. Therefore, the bridging coefficient must be positive for the oil droplet to enter the lamellae and destroy it.

• If B is negative, S will also be negative. In this case, the oil droplet does not spread at the lamellae surface, thus the lamellae resist film stretching and rupturing.

It is important to note that the theories governing E, S, and B coefficients were developed by observing foam interactions under controlled conditions. Therefore, they might not accurately describe all foam behavior in oil present.

Lamella number

Schramm and Novosad proposed an alternative parameter to describe foam-oil interactions, based on the degree of oil emulsification [99]. This parameter is defined as the lamella number, and a simplified equation of the lamella number is:

$$L \approx 0.15 \cdot \left(\frac{\sigma_{w/g}}{\sigma_{w/o}}\right) \quad (2.4)$$

where 0.15 represents the ratio of the radius of the curvature of the Plateau border to the radius of an oil droplet absorbed by water. While all of the foams analyzed showed the same

value, Schramm and Novosad noted that the value could vary depending on the experimental setup [99].

The Lamella number indicates the degree of oil emulsification within the foam lamellae. When L<1, the foam exhibits the highest stability, as oil droplets are small and well-dispersed in the foam. However, when L>1, droplets are large, and as they enter the lamellae, they occupy nearly the entire film volume. This leads to various degrees of foam's instability.

Foams have been classified into three categories (A, B, and C) based on the degree of interactions with oil and their stability in the presence of oil [99].

Type A foams (L < 1) exhibit minimal interactions with the oil and show good stability.

Type B foams (1 < L < 7) are moderately stable.

Type C foams (L > 7) have unfavorable interactions with the oil and exhibit low stability.

The three types of foam suggested by Schramm and Novosad are shown in Figure 2-10.

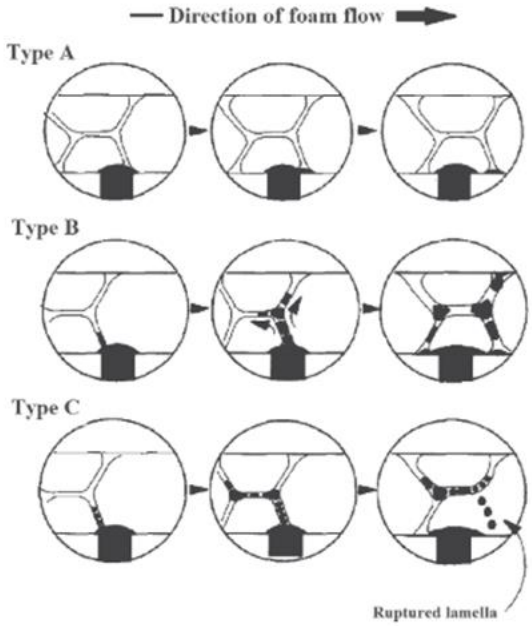

Figure 2-10. The schematic of type A, B and C foams based on different lamella number [99].

The lamella number was first proposed to enhance the understanding of the oil influence on foam in porous media. Studies by Schramm and Novosad demonstrated a good correlation between L values derived from the equation and foam stability in pores containing residual oil under low pressure and temperature [99]. However, subsequent studies revealed that L values poorly describe foam stability in bulk tests and porous media experiments [100 -102].

This discrepancy between calculated L values and foam behavior in oil-saturated porous media arises from the use of constant values of two radii of curvature (i.e., 0.15). Another reason is the assumption of zero capillary pressure for L calculation. However, in reality, the foam lamella encounters large capillary pressure in pores, which leads to disjoining pressure on thin film, affecting foam stability in the presence of oil.

2.4.4 Foam Flow Behavior

Understanding foam flow characteristics is crucial for evaluating the effectiveness of foam flooding to control CO_2 mobility. The ability of foam to reduce gas mobility and improve its stability are critical considerations for designing successful field foam flooding projects. Several parameters have been proposed to assess foam behavior in porous media [5]. Foam efficiency is evaluated based on the following parameters:

Foam quality

Foam quality significantly influences foam flow behavior in porous media. It is defined as the ratio of the gas flow rate to the total of both gas and liquid:

$$f_g = \frac{Q_g}{Q_g + Q_{liq}} \tag{2.5}$$

where F_g is the foam quality, and Q_g is the gas flow rate, Q_{liq} is the liquid flow rate [68].

In general, foam quality represents the gas fraction in foam. Typical values for foam quality range from 0.75 to 0.9 [68, 81]. Foam mobility can be reduced by increasing the gas fraction, but only to a critical point. If the gas fraction exceeds this critical foam stability point, further increases in the gas fraction will no longer effectively reduce foam mobility

[103]. Additionally, gas bubble size plays a significant role in foam quality. Large gas bubbles decrease foam stability, leading to a reduction in foam quality [81].

Apparent viscosity

The primary reason for the negative mobility ratio during CO_2 EOR is the low viscosity of CO_2. Thus, CO_2 foam flooding can be an effective method to increase gas viscosity, improving its displacement efficiency. The apparent viscosity of foam was calculated by combining Darcy's law with gas permeability [104] The equation is given as:

$$\mu_{app} = \frac{kA\Delta P}{q_g L} \tag{2.6}$$

where k is the absolute permeability, A is the cross-sectional area, ΔP is the pressure gradient across a core plug, q_g is the volumetric foam rate, and L is the capillary length.

The apparent viscosity depends on several factors, including the flow rate, differential pressure, size, and distribution of bubbles [105, 106].

Mobility reduction factor

The mobility reduction factor (MRF) is used to evaluate the efficiency of foam in reducing gas mobility compared to the no-foam gas injection scenario. MRF is a dimensionless parameter that quantifies the reduction in mobility during foam flooding. High values of MRF indicate a strong foam generation in porous media.

The MRF can be calculated in the laboratory by dividing the pressure drop across the core during foam flooding by the pressure drop measured in the absence of foam (without surfactant), as shown in the following equation:

$$\text{Mobility Reduction Factor (MRF)} = \frac{\Delta P_{foam}}{\Delta P_{without\ foam}} \tag{2.7}$$

2.4.5 Foaming Agents

Pure brine and gas can be used to create foams, but they are prone to breaking easily. Therefore, a foaming agent is required to both create and stabilize the foam [81]. One of the

widely utilized foaming agents is surfactant or surface-active agents. In recent years, nanoparticles have gained attention as more reliable and alternative foaming agents [107, 108].

Surfactants

Surfactants are frequently used to enhance both the foamability and stability of foam in porous media [13]. They reduce IFT by adhering to the gas-liquid interface because of their amphiphilic structure, which has both hydrophilic and lipophilic characteristics [109]. Based on the polarity of their head groups, surfactants can be divided into four main classes: cationic, anionic, nonionic, and zwitterionic [110] (Figure 2-11).

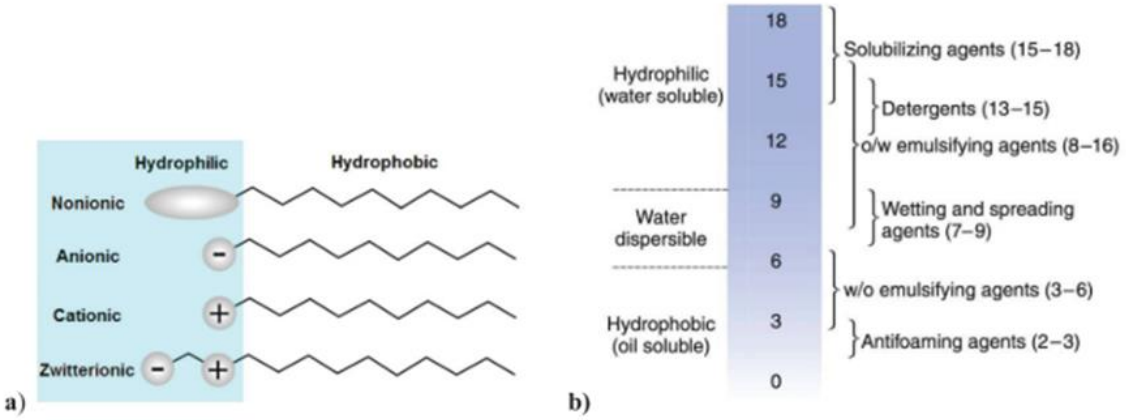

Figure 2-11. (a) the schematic of surfactant molecules (b) classification of surfactant based on the HLB number [110].

Anionic surfactants, which have negatively charged surfaces, are particularly suitable for sandstone reservoirs. Their negative charge creates the repulsive force between the surfactant and the rock surface, reducing surfactant loss due to adsorption. Similarly, cationic surfactants, which have positively charged head groups, are effective for the carbonate reservoirs, where surface area has a positive charge. This helps minimize surfactant loss [37].

Surfactants have been widely used for enhancing the stability of CO_2 foam. Numerous studies demonstrated that the adsorption of surfactant molecules on the gas-water interface increases foam lifetime and stability, while foam mobility is maintained by

continuous regeneration of foam lamellae within the pores, leading to better macroscopic and microscopic sweep efficiency [111- 113]. Additionally, surfactants have the ability to efficiently increase the viscosity of foam, improving volumetric sweep efficiency [103].

Surfactant-stabilized foam for EOR

Numerous studies have been conducted to investigate the efficiency of surfactants in improving the characteristics of foam used for enhanced oil recovery. The presence of surfactants improves foam stability, increasing sweep efficiency and recovering more residual oil through saponification, and reducing IFT [114]. Sun et al. performed laboratory tests using sodium dodecyl sulfate (SDS) to stabilize N_2 foam [115]. Their results show that SDS increased foam stability, with an average foam half-life of approximately 5 minutes. In this study, experiments using silica sandpacks demonstrated the effectiveness of SDS-stabilized foam in improving oil recovery, with incremental oil recovery of around 12% from a homogeneous sandpack and 6% from heterogeneous ones. In the experiments of AlYousef et al. an alpha-olefin sulfonate (AOS) was used to stabilize N_2 foam and improve its oil displacement efficiency [12]. Static foam stability tests showed a reduction in foam half-life from 12.5h to 3.5h upon the addition of oil. In oil displacement experiments, surfactant-stabilized nitrogen foams achieved 6.5% OOIP incremental oil recovery following waterflooding.

The research conducted by Ahmed et al. compared the effects of several commercial surfactants on the rheological properties of supercritical CO_2 foam at 1500 psi and 80ºC [116]. Their study found that AOS outperformed other commercial surfactants used in the study in terms of foam stability under harsh reservoir conditions and in the presence of oil. In another study, Ahmed et al. conducted experiments using sandstone core samples to examine the combined effect of AOS and betaine surfactants on CO_2 foam stability and oil recovery in sandstone cores under the same reservoir conditions [117]. The CO_2 foam stabilized by the mixture of these surfactants at optimum concentrations performed excellently well, recovering up to 20% residual oil after CO_2 flooding, even at high-pressure and high-temperature reservoir conditions.

Despite the abovementioned benefits of using surfactants in CO_2 mobility control, it also has a number of limitations. One significant limitation is the relatively low solubility of surfactants in CO_2 compared to water. As a result, the adsorption layer formed by surfactants

at the CO_2/brine interface is very weak, leading to low foam stability [19, 118]. Furthermore, surfactant-stabilized foam demonstrates inefficient stability in high salinity brines and when in contact with oil, as these conditions accelerate the rupture of lamellae at the gas-water interface [9, 119]. Crude oil reduces the stability of foams through the snap-off process, leading to inefficient thin lamellae formation [77]. Additionally, surfactants have a high tendency to adsorb onto rock surfaces, which requires continuous supplementation of surfactants that makes foam use costly [17, 120]. Surfactants are also prone to chemical degradation under harsh reservoir conditions, including high salinity and high temperature [121]. These limitations and issues make the use of surfactants as a stabilizer for CO_2 foam technically challenging and economically inefficient.

Nanoparticles

In recent years, nanoparticles have gained significant attention for their ability to stabilize a variety of foams. Unlike surfactants, nanoparticles exhibit low retention on rock surfaces, and the energy required to detach nanoparticles from the interface is higher [122]. As a result, nanoparticle adsorption at the water-gas interface is typically an irreversible process, whereas surfactants can easily attach to or detach from this interface. Moreover, foam stabilized by surfactant typically has polygonal bubbles, while nanoparticle-stabilized foam contains tiny and round bubbles. This difference arises because the presence of nanoparticles at the lamella modifies its curvature, creates a robust barrier, and reduces the contact region between bubbles. These changes reduce gas diffusion and liquid drainage, thereby improving foam stability [19, 123]. Additionally, in the aqueous phase, nanoparticles do not form micelles, which eliminates concerns about solubility [124].

Over the past few decades, numerous studies have examined the ability of nanoparticles to stabilize gas foams. Binks and Morozov generated stable air foams using only silica nanoparticles [125]. In the study by Espinoza et al. using 5 nm silica nanoparticles resulted in stable supercritical CO_2 foams [126]. Moreover, flooding experiments through a glass beads column demonstrated that foam stabilized by silica NPs was 2 to 18 times more viscous than without it. They also observed that the foam stability improved with higher NP concentrations in high salinity brine. Zhang et al. analyzed the phase behavior of oil/water emulsion in the absence and presence of silica NPs [127]. They found that the addition of

silica NPs led to a more stable water/oil emulsion. Mo et al. also concluded that NPs enhanced the stability of CO_2 foam in both glass-bead columns and cylindrical cores [128].

The several parameters that influence the effectiveness of nanoparticles in stabilizing foam properties include nanoparticle concentration, type, reservoir brine salinity, and temperature. For example, Zhang et al. reported that foams generated with 5 wt% and 10 wt% silica nanoparticles remained stable for up to two months, while using 0.1 wt% and 1 wt% NPs solutions resulted in foams that were stable for less than five days [129]. In another study, Mo et al. found that a higher concentration of NPs was necessary to improve the stability and the volume of generated CO_2 foam [128]. Similarly, Yu et al. observed that generated foam became less mobile with increasing NP concentration because foam lamellae became more stable and had a greater resistance to coalescence as they passed through the pore spaces [130].

San et al. studied the effect of brine salinity and ion composition on the properties of foam generated by silica nanoparticles [118]. Pressure drop during foam flowing through the core was used to evaluate the foam mobility, while foam stability and texture were assessed through a sapphire cell. Their results indicated that increasing NaCl concentration improved foam quality and stability. Notably, foam mobility decreased by 80% when NaCl concentration was increased from 1 to 10%. However, they observed that further increasing salinity above the threshold values resulted in NPs agglomeration, which led to higher pressure drop and pore plugging. They also observed that higher temperature reduced CO_2 foam stability. A 90% reduction in foam static stability and a 58% increase in foam mobility were observed with increasing temperature from 25ºC to 65ºC. Similar results can be found in other studies [130, 131].

Nanoparticles stabilized CO_2 EOR

Several studies have also investigated the oil recovery efficiency of NP-stabilized foam. Fu et al. conducted coreflooding tests to assess the oil recovery potential of NP-generated CO_2 foam injection after waterflooding [132]. Silica NPs as foam stabilizers and Berea sandstone cores were used in this study. Also, the effect of pressure and temperature on the behavior of NPs-generated foam in porous media was investigated. They found that NPs stabilized CO_2 foam injection recovered 3-6% more residual oil compared to the injection foaming solution without NPs. Furthermore, around 12% more oil was produced

by NPs-generated CO_2 followed by waterflooding while pressure increased by 1300 psi. It can be attributed to generating more stable foam at higher pressure, resulting in better sweep efficiency. However, it was found that higher temperature reduced CO_2 foam stability, consequently, oil recovery. Rognmo et al. performed laboratory-scale flooding tests using Bentheimer sandstone cores to evaluate the oil recovery performance of CO_2 foams generated with silica NPs [133]. Their results showed a 3.5-fold increase in pressure drop across the core in the presence of NPs compared to its absence. Moreover, incremental oil recovery resulting from CO_2 foam injection stabilized by NPs after waterflooding was 2 times higher than the injection case without NPs. In addition, the injection of NPs-CO_2 foam as a secondary method produced 15% more oil compared to the co-injection of CO_2 and brine. Additionally, the presence of NPs delayed CO_2 breakthrough, indicating the generation of stable foam in cores and improved mobility control, leading to better sweep efficiency.

Despite the advantages of using NPs in CO_2 mobility control and enhanced oil recoveries, this method also has its own limitations. Low-cost NPs, including silica NPs, often have a high level of hydrophobicity or hydrophilicity, which can reduce their effectiveness in foam stability due to their low ability to adhere to the CO_2-water interface [134, 135]. Consequently, the generation of strong and stable foams needs specially designed and surface-modified NPs, which can be costly [136]. Additionally, NPs tend to agglomerate under high salinity and temperature reservoir conditions, potentially causing pore plugging and injectivity problems [137, 138]. Furthermore, there are a limited number of studies on the environmental effect of using NPs, which has slowed their adoption in field applications [139].

Surfactant-nanoparticle assisted CO_2 foam flooding

Recently, using the mixture of nanoparticle and surfactant for foam stabilization, particularly in harsh conditions, has attracted great interest. Several studies have shown that using surfactant-nanoparticle solution leads to better static and dynamic foam stability. For example, Worthen et al. reported that blending surfactant with nanoparticles produced significantly viscous CO_2-in-water foam compared to using surfactant alone [19]. Similarly, Singh and Mohanty et al. found that a foam generated with the combination of silica nanoparticles and anionic surfactant outperformed a foam produced by surfactant alone in

terms of stability [140]. Furthermore, the use of nanoparticles reduced the negative effect of temperature on foam stability by reinforcing the foam structure.

In similar work, Babamahmoudi and Riahi showed that combining silica nanoparticles with SDS enhanced foam strength and stability [27]. They observed a 25% increase in the relative foam height after adding nanoparticles compared to using surfactant only. In these studies, stronger foamability and longer stability of foam produced with surfactant-nanoparticles were attributed to irreversible adsorption and aggregation of nanoparticles at the foam interface. Additionally, foam stabilized with surfactant and nanoparticles demonstrated better resistance to high temperature, pressure, and high salinity, as nanoparticles are solid [21]. Nanoparticles also reduce the adsorption of surfactant onto rock surfaces, which can further improve foam performance [23].

Surfactant-nanoparticle stabilized CO_2 foam for EOR

The use of surfactant-nanoparticle mixtures has also demonstrated promising results in improving CO_2 foam stability during oil recovery studies. AlYousef et al. investigated the potential of nanoparticles to enhance the stability of surfactant-generated CO_2 foams [12]. In their study, two experiments were performed in the presence and absence of nanoparticles to evaluate the oil recovery efficiency of the foam. Anionic surfactant, alpha olefin sulfonate, and silica NPs were used. The co-injection of surfactant and CO_2 foam in oil displacement experiments resulted in 6.5% incremental oil recovery with a 7.5 psi pressure drop along the core. In another experiment, combining surfactant and nanoparticles recovered 9.76% of OOIP, and pressure drop reached 17 psi. Overall, the synergistic effect of surfactant and nanoparticles produced 3.26% additional oil compared to surfactant alone, due to lower gas mobility and higher foam viscosity in the presence of nanoparticles. In another study, Guo and Aryana used a 2D microfluidic device to assess the oil recovery efficiency of CO_2 foam stabilized by nanoparticles and surfactants [141]. In this study, silica NPs and the mixture of AOS and LAPB were utilized. Combining nanoparticles and surfactants produced 95% of OOIP, indicating the strong CO_2 foam generation.

Worthen et al. developed a mathematical model and incorporated it into a heterogeneous reservoir model to evaluate the effectiveness of NPs-stabilized CO_2 foam [7]. The reservoir models, which included high- and low-permeable layers, compared the front displacement performance of NP-stabilized foam flooding to the co-injection of CO_2/brine.

The model showed that CO_2 foam stabilized by NPs resulted in more stable front displacement and better sweep efficiency compared to CO_2/brine flooding. These results demonstrated the potential of using NP-generated CO_2 foam in heterogeneous reservoirs. In an experimental study by Risal et al. the stability and pore-blocking abilities of NP-surfactant stabilized foams were tested in a homogeneous glass-bead pack. Surface-modified silica NPs and SDS were utilized to stabilize foams [142]. During the foam flooding, the pressure drop across the glass pack increased, indicating foam stability and its ability to block pore spaces. Overall, the synergistic effect of NPs and surfactants demonstrated excellent performance in oil recovery tests, producing up to 18% of residual oil.

Similar to previous studies, the results of other experimental works demonstrated the positive effect of NPs-surfactants CO_2 foams in enhancing oil production from sandstones and limestones core samples [12, 143]. Combined use of surfactants and NPs generated more stable CO_2 foams compared to either component alone. The application of the hybrid technique in an efficient way may increase the foam viscosity, improve sweep efficiency, and reduce CO_2 mobility, all of which enhance recovery of residual oil. Overall, these studies show that surfactant-NP-stabilized CO_2 foam holds huge potential for enhancing oil recovery. However, more studies are needed to investigate the impact of crude oil on the stability of NP-stabilized foams and to assess the capacity of these hybrid foams to enhance oil recovery under different reservoir conditions.

CHAPTER 3. Materials and Procedures.

3.1 Materials

Surfactants

In all bulk tests and foam flooding experiments, alpha olefin sulfonate (AOS), an anionic surfactant, was used. The selection of foaming agent was guided by promising results from previous research, including bulk screening tests and field trials involving AOS surfactants [144-146]. The molecular formula of AOS surfactant is written as $RCH=CH(CH_2)_nSO_3Na$, and the molecular structure is shown in Figure 3-1. The surfactant had a purity of 38% and was received from Stepan Company.

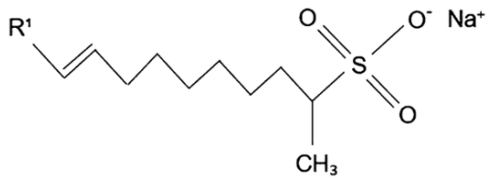

Figure 3-1. Molecular structure of alpha olefin sulfonate (AOS).

AOS are commercially available surfactants, cost-effective to produce at scale, and generally regarded as safe for both human health and the environment. Furthermore, AOS surfactants have demonstrated strong chemical stability and performance in high-temperature foam tests, including under challenging North Sea reservoir conditions of approximately 4000 psi bar and 80-100°C [144, 147]. This proven thermal resilience was a key reason for selecting AOS surfactants for our study under the reservoir conditions of 1500 psi and 80°C.

AOS is a negatively charged anionic surfactant. For this reason, a carbonate reservoir with positively charged mineral surfaces is not a favorable environment for an anionic surfactant because of surfactant adsorption on the carbonate core. Despite that, previous studies have also demonstrated the generation of stable foam with AOS in carbonate core samples [148, 149]. However, adsorption studies conducted using AOS and limestone core materials demonstrated reasonable levels of adsorption [150, 151]). So, using AOS surfactant in a carbonate core, used in this study, may be as effective as in a sandstone core in terms of foam stability and oil recovery.

Carbon dioxide

CO_2 gas with 99.95% purity was used in all experiments. CO_2 was delivered in the bottle pressurized up to 800 psi.

Brine

Distilled water from a Milli-Q Advantage A10 purifier was used to prepare the brine. Specific salts were then added to the distilled water to get the required synthetic seawater, SSW. The types and concentrations of salts/ions utilized in the brine preparation are listed in Table 3-1. The SSW prepared for all experiments was designed to mimic Caspian Sea water, with a salinity of approximately 13,000 ppm [152]. To avoid any chemical reactions between salts, each salt was added to the distilled water separately and stirred for 5 minutes to prevent salt precipitation before the addition of the next salt.

Table 3-1. The composition of brine used in this study.

Ions	**Na^+**	**Ca^{2+}**	**Mg^{2+}**	**Cl^-**	**SO_4^{2-}**	**Total**
Concentration, ppm	3240	350	740	5440	3010	13000

Nanoparticles

Silicon oxide (SiO_2), which are commercially available nanoparticles, was utilized in both bulk tests and foam flooding experiments throughout this research. The nanoparticle stability in brine was the main criterion for selecting these nanoparticles to stabilize CO_2 foam. In the previous study conducted by Muneer [153], the stability of SiO_2 nanoparticles in the brine with the same salt composition used in this work (as shown in Table 3-1) was investigated. The results indicated moderate stability of SiO_2 in the brine, supporting the nanoparticles suitability under the conditions explored in this research. Based on these findings, SiO_2 nanoparticles were selected for use in this study.

The nanoparticles were received in powder form and were purchased from SkySpring Nanomaterials, INC. The nanoparticles have a non-porous structure and nearly spherical shape as shown in Figure 3-2. The size of nanoparticles is less than 50 nm, and their purity is around 99.5%. The bulk density of nanoparticles is 0.08-0.1 g/cm^3.

SiO_2 nanoparticles generally possess a negatively charged surface under low pH conditions [154].

Figure 3-2. The picture of SiO_2 nanoparticles.

Crude oil

The dead crude oil used in the experiments was obtained from an oil field in the West Kazakhstan region. The composition of the oil was analyzed with a gas chromatograph at NIPI Neftegas. The crude oil composition and its density are shown in Figure 3-3. Crude oil was filtered through a 12μm Millipore filter paper to remove any particles that may damage the experimental equipment.

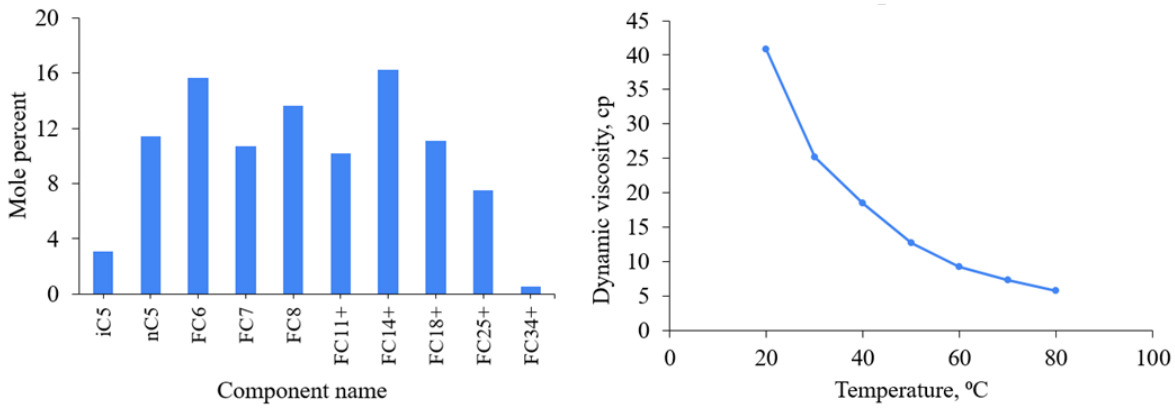

(a) (b)

Figure 3-3. a) Crude oil composition and b) oil viscosity at various temperatures.

Core samples

Outcrop carbonate core samples were used in foam flooding and oil recovery experiments. These core samples were purchased from Kocurek Industries Company. The core diameter was 38 cm, and the length was 30 cm. The cores were cut to the required length for the flooding tests. Table 3-2 lists the core sample properties in this study.

Typically, Indiana limestone consists of more than 95 wt% calcite ($CaCO_3$) with small quantities of silicon oxide (Si_2O_3), magnesium oxide (MgO), aluminum oxide (Al_2O_3), and iron oxide (FeO) [155, 156].

Table 3-2. Core properties.

Core	Length, inches	Diameter, inches	Pore volume, cc	Porosity, %	Permeability, mD
Ind01	5.95	1.5	26.2	15.7	120
Ind02	5.77	1.5	30.6	18.8	66
Ind03	5.94	1.5	27.2	16.3	100
Ind04	5.81	1.5	30.1	18.5	70
Ind05	5.98	1.5	33.4	19.9	103
Ind06	5.67	1.5	28.4	17.8	104
Ind07	5.75	1.5	32.7	20.2	200
Ind08	5.94	1.5	31.6	18.9	28
Ind09	5.91	1.5	29.5	17.7	65
Ind10	5.94	1.5	29.8	17.5	87
Ind11	5.92	1.5	27.5	16.2	11
Ind12	6.1	1.5	32	18.8	45
Ind13	5.75	1.5	30.5	18.9	39
Ind14	5.94	1.5	32.6	19.6	85
Ind15	5.76	1.5	31.8	19.5	45
Ind16	5.87	1.5	33.1	20.1	175
Ind17	5.88	1.5	32.2	19.5	630

The major oil reservoirs in Kazakhstan are primarily carbonate formations. Therefore, Indiana limestone was selected as a representative core sample for this study to evaluate CO_2 foam performance in Kazakhstani oil fields. Furthermore, Indiana limestone is a heterogeneous rock type with a broad range of porosity and permeability distribution, making it comparable to the characteristics of actual reservoir cores [157]. However, it is

well known that carbonate rocks have positively charged surfaces, particularly at low pH conditions [158]. Hence, negatively charged AOS surfactant and SiO_2 nanoparticles can adsorb on the positive carbonate surfaces. This adsorption can lead to the loss of foaming agents and subsequent reduction in foam efficiency. Nonetheless, reasonable adsorption of negatively charged AOS surfactant on carbonate rock surfaces was reported, supporting their applicability for use in carbonate cores, including those used in this study [150, 151]. To reduce possible adsorption of foaming agents and their loss, a core was preflushed with 1 pore volume of foaming solution before CO_2 foam flooding.

3.2 Experimental Equipment and Methods

3.2.1 Rock Sample Preparation and Routine Core Analysis

Firstly, all 12-inch-long outcrop core samples were cut, and then the core ends were trimmed to obtain flat surfaces using the Cutting and Trimming Saw system. A dry-cutting method was employed to prevent damage to the cores from cooling fluids, which could alter their properties. Following this, the physical dimensions and weights of the dry cores were measured. Since the porosity measurement system available in the laboratory was not designed to measure the porosity of core plugs longer than 3 inches, an alternative method was used. The core plug samples were vacuumed and saturated with brine under 1000 psi for 24 hours. After removal from the saturator, the weights of saturated cores were measured. Then the porosity of core plugs was calculated by dividing the weight difference between saturated and dry cores by the density of brine.

For absolute permeability measurements, saturated cores were placed into a core holder, and confined pressure was applied, set 500 psi higher than the pore pressure. Then brine was injected into the core at rates of 1, 3, and 5 cc/min. Differential pressure across the core plug was monitored, and the brine injection continued at each specific flow rate until a steady-state pressure drop was achieved. Brine viscosity, physical length and cross-sectional area of the core, steady-state pressure value, and specific flow rate were used as input values to Darcy's Laws to calculate permeability. Core plug permeability was then determined as the average permeability obtained at various injection rates.

3.2.2 Preparation of Foaming Solution

To prepare a surfactant-only foaming solution, the required concentration of surfactant was added to the brine. The mass percent method was used to calculate both the mass of the surfactant and the mass of the brine needed to achieve the desired foaming solution concentration. Then, the solution was magnetically stirred for 30 minutes at 250 rpm to obtain a homogeneous dispersion. After stirring, the solution was visually inspected to ensure the absence of any precipitation.

For the nanoparticle-surfactant solution, the nanoparticles were first added to the brine. The required amount of nanoparticles was calculated using the same mass percent method. Then, the nanoparticle solution was magnetically stirred for 30 minutes at 800 rpm to prevent nanoparticle aggregation. To ensure complete nanoparticle dispersion, the solution was further bath-sonicated in an ultrasonic homogenizer (BEM-650A) for 45 mins at 600 watts, shown in Figure 3-4. Once the nanoparticles were fully dispersed, the required amount of surfactant was added to the nanoparticle solution. The final solution was magnetically stirred for 30 minutes at 250 rpm to receive a homogenous foaming solution. Finally, the solution was visually inspected to ensure no precipitation. All prepared solutions were stored in closed beakers to prevent any contamination by the environment or evaporation.

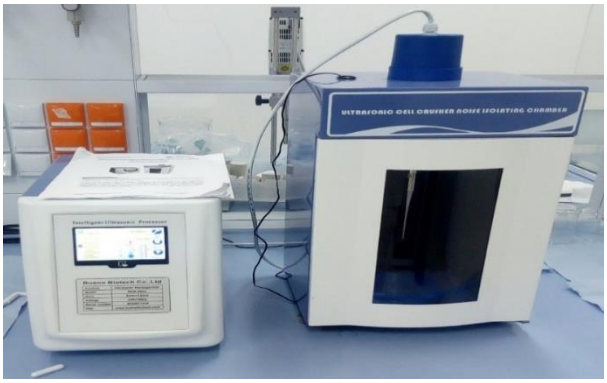

Figure 3-4. Image of the ultrasonic Homogenizer BEM-650 A.

3.2.3 Zeta Potential Measurements

The size distribution of nanoparticles and their zeta potential were measured using the Zetasizer Nano ZS system, shown in Figure 3-5. Zeta potential measurement was performed to assess the stability of silicon oxide nanoparticles in the brine.

Figure 3-5. Zetasizer Nano ZS system used in this study.

In nanoparticle dispersions, oppositely charged ions tend to attach onto the nanoparticle surface, forming a thin layer known as the Stern layer. Surrounding this layer, loosely bound ions create another layer, called as the Diffusive layer. As nanoparticles diffuse through the solution, both layers move with them. As a result, a slipping boundary appears that separates the double layers from the remaining ions in the mobile fluid. The electrical potential at this boundary is referred to as the zeta potential of the nanoparticles.

The value of zeta potential reflects the electrostatic repulsion and attraction between nanoparticles and indicates the colloidal stability of dispersion. A typical range of zeta potential is between +100 mV and -100 mV. Nanoparticle solution exhibits the best stability when the zeta potential value is between +30 mV and -30 mV [159].

3.2.4 Bulk Foam Stability Tests

Bulk tests are often used as a simple, quick, and cheap method for screening and selecting foaming agents, such as surfactants and nanoparticles, for foam generation and stabilization. These tests evaluate foaming agents based on the foamability and foam stability of the obtained foaming solution. Foamability refers to the ability of a foaming solution to generate foam under certain conditions. Foam stability describes the change in foam height or volume over time after foam generation.

The schematic experimental setup for the bulk test is shown in Figure 3-6. The setup consists of a 1000 ml graded glass column (length: 60 cm, diameter: 6 cm), a mass flow meter, CO_2 gas supply lines, and a gas bottle with a pressure regulator. A porous rock is placed at the bottom of the column for gas sparging. A high-resolution camera is used to

record foam decay time for further calculation of foam half-life time and generated foam volume.

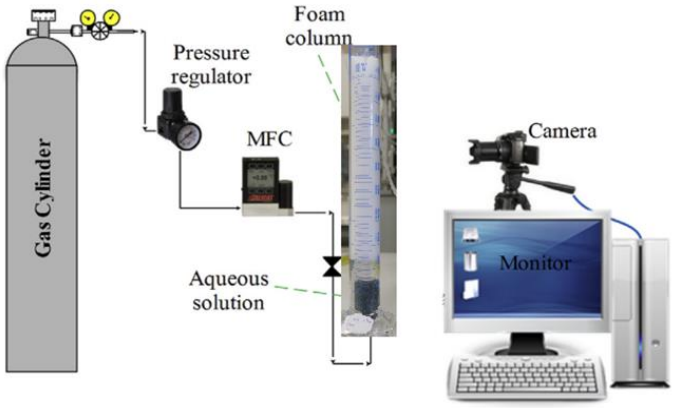

Figure 3-6. Schematic of the bulk test system.

During the bulk test, the foam was generated by injecting CO_2 through the porous rock submerged in the foaming solution. First, 100 ml of the foaming solution was poured into the graded glass column. Then, CO_2 gas was injected at a constant rate (50 cc/min) through the porous rock at the column's bottom to generate foam. The 250 ml of gas was injected in all cases, maintaining the constant liquid and gas ratio of 70%, which had been identified as the best foam quality from screening experiments. After the gas injection was stopped, foam decay was recorded using the high-resolution camera. The recorded data was used to determine foamability and foam stability. To quantify foam stability, foam half-life time was used, which represents the time required for the foam height to decrease to half of its original height.

In the bulk test with crude oil, a predetermined amount of oil was added into the column with foaming solution before CO_2 injection for foam generation. Due to differences in density, the oil phase was located at the top of the foaming solution in the glass column. Thus, foam generation occurred before oil came into contact with foam.

Additionally, bulk tests were conducted to examine the effect of temperature on foamability and foam stability. To achieve this, the glass column and the gas injection line were placed in a high-temperature oven. The temperature inside the oven was controlled and monitored using temperature sensors. CO_2 injection for foam generation was initiated only once the foaming solution in the column reached and stabilized at the required temperature.

The foam behavior was monitored through the sight glass on the side of the oven with the high-resolution camera.

3.2.5 Foam Dynamic Experiments

The schematic of the high-pressure and high-temperature (CFS 700) system used for core flooding experiments in this study is shown in Figure 3-7. In all coreflooding experiments, CO_2 and foaming solutions were co-injected from separate cylindrical accumulators into a core plug. The co-injection method ensures in-situ foam generation as the CO_2 disperses into the aqueous solution.

In the core flooding experiments, a brine-saturated core plug was covered with a sleeve and placed into a Hassler-type core holder. The core holder was then mounted on a horizontal platform. Confining pressure was applied using a Floxlab syringe pump. During the experiments, the confining pressure was maintained at 500 psi higher than the pore pressure to prevent any communication between the confining space and the core plug. Depending on the test type, either brine or surfactant solution and CO_2 were separately loaded into Hastelloy floating piston accumulators, which were placed vertically inside the oven. Two Floxlab dual-syringe pumps were connected to each accumulator, allowing for separate or simultaneous injection of fluids and gas. The dual syringe pumps automatically refilled, ensuring continuous injection throughout the entire experiment.

Pressure values at the inlet and outlet of the core, as well as differential pressure across it, were measured using two pressure transducers and two independent high-accuracy differential pressure transducers. The downstream pressure was regulated by a backpressure regulator (BPR), which was automatically adjusted by the syringe pump to maintain constant pressure. The entire system, except for the injection pumps, was placed into the oven to maintain a constant temperature during the experiment. Effluent fluids were collected in measuring cylinders, and dead volume was applied to the calculations.

An automated data recording system was used throughout all coreflooding experiments, enabling continuous data acquisition and collection. This system improved the accuracy of post-experimental data analysis and interpretation.

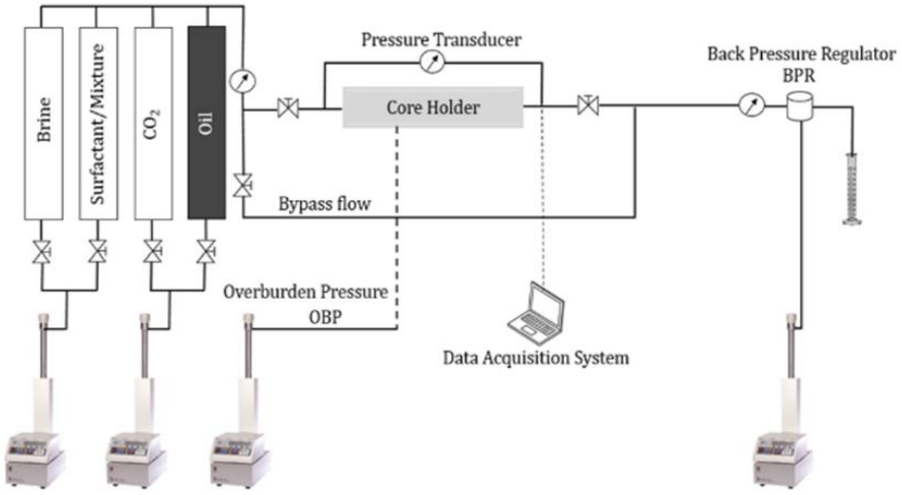

Figure 3-7. The schematic of the coreflood system (CFS 700).

A series of foam flow experiments were conducted to assess the performance of CO_2 foam in porous media. These experiments included foam quality scans, flow rate tests, and foam flooding at various surfactant concentrations. The results from these tests were used as input parameters for foam flooding simulations.

Foam quality scan. The purpose of this experiment was to determine the optimum ratio of injected CO_2 and foaming solution that generates the most effective foam in terms of stability and strength in the porous medium. The total injection rate, defined as the sum of CO_2 and foaming solution injection rates, was kept constant at 1 cc/min throughout the experiment. However, the individual injection rates of CO_2 and foaming solution were adjusted to get various gas fractional flows, which ranged from 40% to 90%. In this work, the fractional flow is defined as the ratio of CO_2 injection rate to the foaming solution injection rate. Pressure drop across the core was monitored, and once steady-state pressure was observed, the injection rates of CO_2 and foaming solution were adjusted to achieve the required gas flow fraction.

Flow rate tests. The foam behavior in porous media depends on the injection rate. Therefore, it is important to understand the effect of varying injection rates on foam generation and stability. In this experiment, the total injection rate was gradually increased from 0.5 to 2 cc/min, maintaining a constant gas fractional flow. As in previous tests, steady-

state pressure drop was used as an indication to adjust the injection rates of CO_2 and foaming solution. The optimum gas fractional flow obtained from the foam quality scan experiment was used in this experiment. The list of foam flooding experiments and reservoir conditions under which they were performed is listed in Table 3-3.

Table 3-3. Cores and corresponding experimental parameters.

Core	Experimental Conditions	Experiment	Injection fluid
Ind01	1500 psi/40ºC	Foam quality scan	0.5% AOS solution
Ind02	1500 psi/80ºC	Flow rate tests	0.5% AOS solution
Ind03	1500 psi/80ºC	Foam flooding	0.5% AOS solution
	1500 psi/40ºC	Foam flooding	0.5% AOS solution
	1500 psi/40ºC	CO_2 and brine co-injection	Brine
Ind04	1500 psi/80ºC	Foam flooding	Brine
	1500 psi/80ºC	Foam flooding	0.25% AOS solution
	1500 psi/80ºC	Foam flooding	0.5% AOS solution
	1500 psi/80ºC	Foam flooding	1% AOS solution
Ind05	1500 psi/80ºC	Foam flooding	0.5% AOS + 0.05% SiO_2 solution
Ind06	1500 psi/40ºC	CO_2 blocking	0.5% AOS solution
Ind07	1500 psi/40ºC	CO_2 blocking	0.5% AOS + 0.05% SiO_2 solution

The effect of foaming agent concentration. This experiment was conducted to investigate the effect of surfactant concentration on foam generation and stability. For this experiment, foaming solutions with AOS concentrations of 0.25%, 0.5%, and 1% were prepared following the procedure described earlier. To minimize surfactant adsorption, 1 PV of surfactant solution was injected as a pre-flush before co-injecting CO_2 and surfactant solution. In this test, steady-state pressure drop monitored over at least 2 PV of injection was used as an indication of foam stability. Subsequently, a surfactant solution with a higher concentration was injected for further testing.

Surfactant and surfactant-stabilized CO_2 foam. Several foam flooding experiments were conducted to compare the performance of surfactant and surfactant-nanoparticles on stabilizing CO_2 foam in porous media under various reservoir conditions.

3.2.6 Dual–core Experiments

In order to determine the diverting and pore-blocking capacity of CO_2 foam stabilized by surfactant, coreflooding tests were performed using parallel cores. The coreflooding system in Figure 3-7 was slightly modified for this experiment., as shown in Figure 3-8. A new core holder was connected in parallel to the existing core holder using tubes. Check valves were placed before each core holder to prevent communication between the cores. Additionally, several valves were installed before each core holder to divert the injection brine from one line to another line during absolute permeability measurement.

Figure 3-8. Dual core holder system.

Once both cores were mounted into their respective core holders, core #2 was isolated using a valve in the upstream line. Then, brine was injected at varying rates (1 to 5 cc/min) through core #1 to measure pressure drop, which was used to calculate its absolute permeability. The same procedure was followed to determine the absolute permeability of core #2. After the permeability measurement, the upstream lines of both cores were opened, and the co-injection of CO_2 and foaming solution was initiated at constant total injection rates of 1 cc/min, maintaining a fixed fractional flow of 70%. The injection rate was kept the same as during single-core experiments to prevent a high-pressure drop across a core when

most of the fluid flows through the one core because of heterogeneity. The pressure transducers were used to measure pressure at the inlet and outlet of both cores. All data were automatically recorded and collected using built-in software. The cores and experimental parameters to study the heterogeneity effect are listed in Table 3–4:

Table 3-4. Overview of core used for dual core experiments with experimental parameters.

Injection fluid	Core	Porosity, %	Permeability, md	Experimental Conditions	Permeability ratio (V_k)
0.5% AOS	Ind08	18.9	28	500 psi/25ºC	2
	Ind09	17.7	65		
0.5% AOS and 0.05% SiO_2	Ind10	17.5	87	500 psi/25ºC	8
	Ind11	16.2	11		

3.2.7 Oil Recovery Experiments

The core flooding system, as shown in Figure 3-7, was also used to investigate oil recovery efficiency of CO_2 foam flooding. In this experiment, a core was saturated with crude oil through a drainage process. Precise measurements of production fluid volumes were crucial to accurately estimate the initial water and oil saturation in the core. The oil recovery experiments included several main stages:

Absolute permeability measurements

After mounting a coreholder with a brine-saturated core plug, 2 PVs of brine were injected to ensure complete saturation of the core. The required backpressure was then set, and the absolute permeability of the core plug was determined by injecting brine at three different injection rates following the procedure described in the previous section. Pressure data was recorded and used to calculate permeability.

Primary Oil Drainage

In this stage, crude oil was injected into the core to displace the brine to reach irreducible water saturation (S_{wi}). Oil was injected at three different rates: 0.5, 3, and 5

cc/min. Higher injection rates were required to overcome the capillary pressure in pores. During the drainage process, brine production was monitored and measured using 5 ml measuring cylinders to accurately calculate S_{wi} and S_{oi} (initial oil saturation).

At S_{wi}, the oil originally in place (OOIP) was determined using the following equation:

$$OOIP = S_{oi} \cdot PV \tag{3.1}$$

where S_{oi} is the initial oil saturation, and PV is the pore volume [cc]. In this calculation, it is assumed that all produced water from the core was displaced by oil during the drainage process, meaning that the sum of S_{wi} and S_{oi} equals 1.

It is important to note that not all of the produced water came from the core plug itself. Usually, small amounts of brine or oil remain in upstream and downstream tubes. This volume of fluid is defined as the dead volume, and knowing it is crucial for precise fluid saturation calculations and estimating oil recovery. Therefore, dead volumes were considered in calculations during both the drainage process and later oil recovery by waterflooding, CO_2 flooding, and CO_2 foam flooding.

Waterflooding

Waterflooding is a widely used, inexpensive method for secondary oil recovery. Therefore, in some of the experiments, waterflooding was employed prior to CO_2 flooding to compare the performance of both methods in terms of oil recovery. During waterflooding, brine was injected into the core plug to displace oil from the core. The brine injection rate was gradually increased from 0.5 to 5 cc/min to overcome the capillary pressure in pores. The produced oil was collected downstream of the BPR in measuring cylinders, and the volume of production was measured as a function of time. Pressure gradients from pressure transducers and the differential pressure transmitters were monitored and recorded throughout the waterflood process.

Oil recovery factor was calculated to assess the displacement efficiency of the waterflood. The oil recovery factor is defined as the ratio of the volume of produced oil during waterflooding to the original oil volume in a core.

$$\text{Oil recovery } (R_f) = \frac{N_{o,prod}}{OOIP} \quad (3.2)$$

where $N_{o,\,prod}$ is the volume of produced oil [cc], and OOIP-original oil in place-is the oil originally in place defined during the drainage process [cc].

CO_2 flooding

After the waterflood, CO_2 flooding was performed to evaluate EOR potential. CO_2 was injected at constant rate of 1 cc/min for about 3 pore volumes (PV) until no more oil was produced. The minimum miscibility pressure for the CO_2/oil system, calculated using CMG WinProp, was 2500 psi at 80°C, and so CO_2 flooding in this study was immiscible displacement.

Co-injection of CO_2 and foaming agent

Following the CO_2 flooding, the co-injection of CO_2 and foaming agent was initiated to evaluate the oil recovery efficiency of CO_2 foam. Foam flooding was performed at a constant gas fractional flow, which had been identified as the optimal value for achieving the highest foam apparent viscosity in previous foam quality scan tests. Throughout the foam flooding process, the total injection rate was maintained at 1 cc/min. Pressure drop and oil production volume were continuously monitored and recorded to assess the efficiency of CO_2 foam in recovering oil from the core.

Final oil saturation and oil recovery were calculated based on the difference between initial oil volume in the core and the produced oil volume, with adjustments made to account for dead volume. The internal volume of the tubing, valves, and fittings located upstream and downstream of the core holder is not part of the porous medium but still contains fluid. In coreflood experiments, dead volume can impact the accuracy of fluid saturation, breakthrough timing, and pressure measurements by introducing a delay between fluid injection and its entry into the core.

To properly account for dead volume and improve the accuracy of oil recovery measurements, oil, foaming solution, and brine were injected through separate lines, which were connected to the tee positioned close to the core holder inlet. Additionally, the dead volume before and after the core holder was measured multiple times, and it was calculated that the total dead volume in the coreflood system was approximately 10 ml.

3.2.8 Interfacial Tension Measurement

The HPHT Interfacial Tension meter (IFT 700), shown in Figure 3-9, was used to measure the IFT in oil−brine, oil−CO_2, and brine−air systems. The measurement range of the equipment is 0.05-70 mN/m. The IFT between oil and brine was determined using the rising bubble method. In this technique, a visual cell with sapphire windows was filled with brine, and oil was injected downward into the cell using a needle. For the IFT measurements in CO_2-oil and CO_2-brine systems, the pendant drop method was employed, where the cell was filled with CO_2, and fluid was injected from the top. A syringe pump and microvalve were used to regulate injection rate and pressure. The pressure of the injected fluid was kept 100 psi higher than bulk pressure in accordance with the manufacturer's recommendations.

Figure 3-9. HPHT Interfacial Tension Meter (IFT 700).

Before running the IFT measurements, the scale of the digital image was calibrated based on the needle size to accurately determine the dimensions of the droplets. During experiments, images of the droplets were captured by the camera, and built-in software automatically fitted the drop shape and calculated IFT using the Young-Laplace equation [160]:

$$\Delta P = s \cdot \left(\frac{1}{r_1} + \frac{1}{r_2}\right) \tag{3.3}$$

To ensure accurate measurements, the droplet (oil or brine) was allowed to stabilize for at least 20 minutes for reaching dynamic equilibrium with the bulk phase (CO_2 or liquid). All IFT measurements were performed at 25 ℃.

3.3 Experimental Precautions

Conducting experiments under high-pressure and high-temperature (HPHT) conditions requires the following special procedures and the use of specific materials. This section discusses the key experimental precautions taken in this study, with a particular focus on CO_2 handling.

Corrosion

Generally, steel and low-alloy materials do not corrode when exposed to dry CO_2. However, when CO_2 reacts with water or brine, it forms carbonic acid, which can cause significant corrosion of the laboratory equipment. To mitigate these corrosion issues, we used a coreflood system consisting of components made from Hastelloy material, including a coreholder, accumulators, and BPR. This measure helped reduce equipment degradation, minimize downtime during experiments, and ensure safe operations, particularly under HPHT conditions.

CO_2 diffusion

CO_2, due to its molecular structure and physical properties, is more mobile compared to fluids, leading to higher permeability through solid materials. Gas diffusivity and solubility are the important factors affecting its permeability through rubber materials. The solubility of CO_2 in Teflon or rubber is significantly higher than that of N_2 and most other gases, as shown in Figure 3-10. Therefore, CO_2 diffuses through Teflon materials up to 15 times faster than N_2. As a result, Teflon sleeves and O-rings used in the coreflooding system can swell upon contact with CO_2, damaging equipment and leading to leakage. Furthermore, CO_2 diffusion from the core through the Teflon sleeve can affect the accuracy of gas flow rate and its fraction in flow.

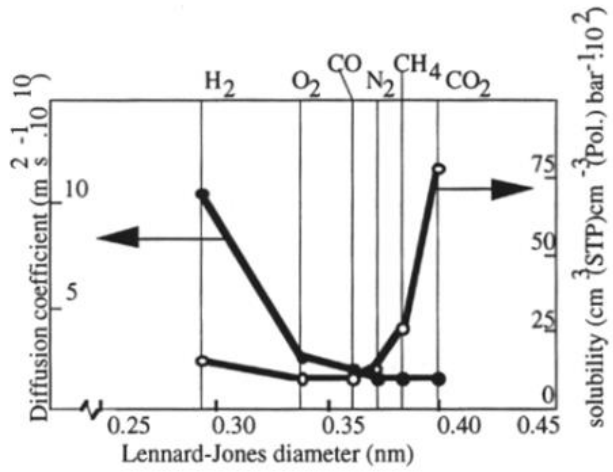

Figure 3-10. The solubility and diffusivity of CO_2 in [161].

To minimize gas leakage and experimental equipment failure due to the high solubility of CO_2 and its diffusivity, several precautions were implemented:

1. Aflass sleeves were used in the coreholder, as they exhibit higher resistance to CO_2 compared to typical rubber or Teflon materials.
2. The Teflon O-rings on the end caps of the coreholder were replaced with Aflass O-rings.
3. The Teflon O-rings on parts of the accumulator exposed to CO_2, particularly on the end cap and one side of the piston, were replaced with Aflass O-rings.
4. Empty accumulators were filled with high-pressure CO_2 at a low rate by adjusting the valve. Similarly, CO_2 was released from the accumulator at a very low rate to prevent the swelling of O-rings due to rapid CO_2 influx.
5. Aflass O-rings were also used in the piston of the BPR to prevent CO_2 diffusion.

Joule-Thomson effect

The temperature of high-pressure CO_2 can drop significantly when it is released from the BPR to ambient pressure. This cooling rate due to gas expansion, expressed in °C/bar, is referred to as the Joule-Thomson effect. Compared to most gases, CO_2 has a significantly high Joule-Thomson coefficient [162]. As a result, when the temperature of CO_2 suddenly drops, the hydrate of carbon dioxide can form in the presence of water, freezing the outlet

of the BPR and the production lines. To mitigate this issue, the BPR and outlet flow/lines were placed into the oven during HPHT coreflood experiments.

CHAPTER 4. Experimental results

4.1 Nanofluid Stability

The zeta potential values of solutions with varying nanoparticle concentrations were measured to assess the stability of nanoparticles in CSW with a salinity of 13000 ppm. The NP solutions were observed over five consecutive days through zeta potential measurements and visual inspection. Figure 4-1 compares the zeta potential values for three NP solutions at the concentrations of 0.05 wt%, 0.1 wt%, and 0.2 wt% SiO_2. The zeta potential for the 0.05 wt% SiO_2 solution fluctuated between -10 and -12mV, while it decreased from approximately -14mV to -9mV for the other two solutions. On the second day, the measured zeta potential for the 0.05 wt% SiO_2 solution was slightly lower than on the third day, likely due to a measurement error. However, the variation was within an acceptable range. Overall, zeta potential values for all three solutions showed similar values over time, indicating that nanoparticle concentration had a minimal effect under the examined conditions.

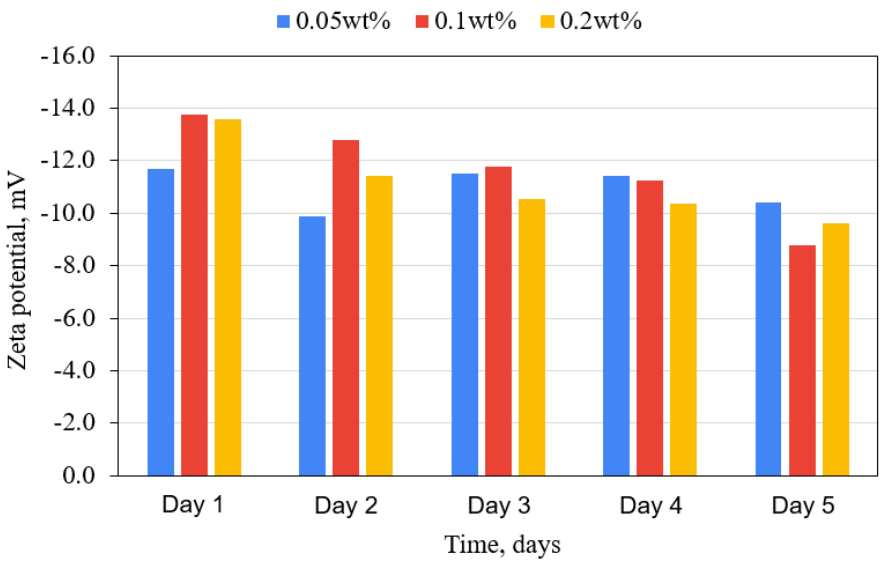

Figure 4-1. Zeta potential values for various concentration of SiO_2 in brine.

Table 4-1 presents the stability indicator values for SiO_2 based on the zeta potential measurements. This table was developed by Salaudeen based on the experimental results. According to this table, all three solutions used in this experiment are characterized as unstable [163].

Table 4-1. Nanoparticle stability indicator [163].

Zeta Potential Values (mV)	Stability
-25 and Below	Highly Stable
-20 to -25	Stable
-15 to -20	Less Stable
-13 to -14	Fairly Stable
-10 to -12	Unstable
-9 and above	Highly unstable

Table 4-2 presents the stability assessment of SiO_2-based nanofluids over a five-day observation period. The formulations containing 0.1 wt% and 0.2 wt% SiO_2 exhibited signs of instability as early as the second day, characterized by visible cloudiness and significant nanoparticle precipitation that accumulated at the bottom of the beakers. This sedimentation indicates a loss of colloidal stability, likely due to agglomeration of nanoparticles. In contrast, the nanofluid containing 0.05 wt% SiO_2 remained visibly clear and free from sedimentation throughout the entire five-day period, indicating dispersion stability.

Additionally, nanoparticle precipitation was observed during a preliminary foam flooding experiment conducted at 80°C and 1500 psi. In this experiment, CO_2 and the solution containing 0.3 wt% SiO_2 were co-injected at a constant injection rate of 1 cc/min, maintaining a fixed fractional flow of 70%. Throughout the experiment, the pressure drop across the core and the pump injection pressure were continuously monitored. After approximately 6 PV of co-injection, a sudden drop in inlet pressure accompanied by a rise in pump injection pressure was observed, indicating potential injectivity problems. Upon disassembling the core holder after the experiment, visual inspection revealed nanoparticle precipitation on the inlet plug surface, which blocked flow paths, as illustrated in Figure 4-2. These observations are consistent with the data presented in Table 4-2, which show that SiO_2 nanoparticles exhibit only moderate stability in the brine at concentrations above 0.1 wt%, leading to precipitation in porous media and subsequent flow blockage.

Table 4-2. The illustration of SiO_2 stability at various concentrations in saline brine at room conditions over the five-day period. Precipitations are circled in red.

SiO_2, wt%	1st day	2nd day	5th day
0.05	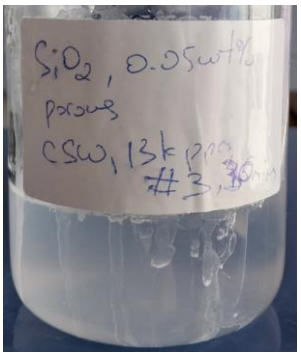	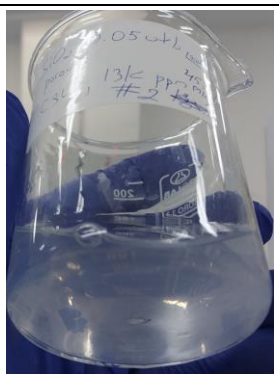	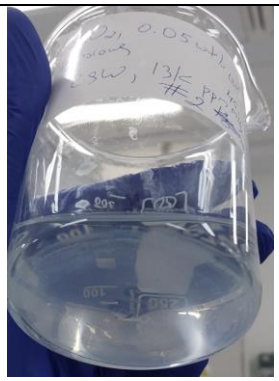
0.1	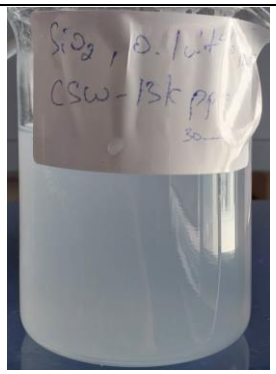	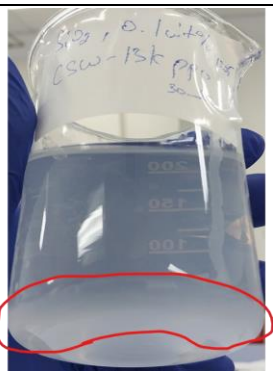	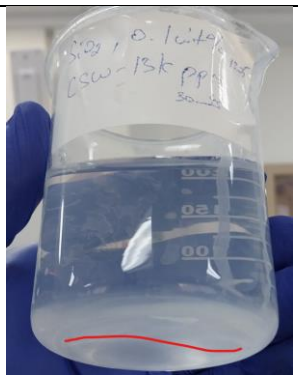
0.2	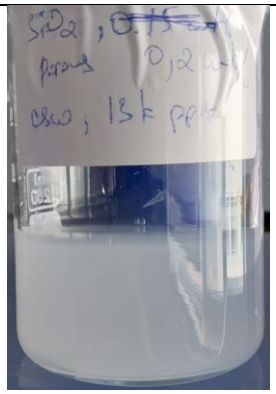	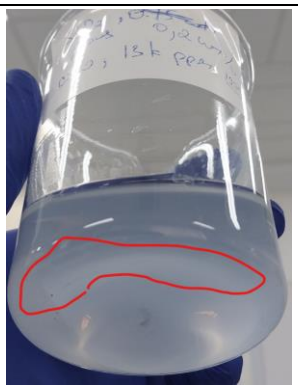	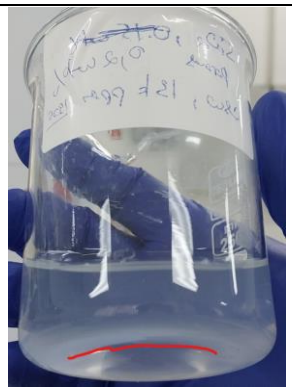

Figure 4-2. The surface of inlet plug of the core-holder.

Based on these observations, the 0.05 wt% SiO_2 concentration was identified as the most stable formulation. These results align with previous findings reported by Salaudeen [163], who also noted that lower concentrations of SiO_2 in brine solutions tend to enhance dispersion stability.

The reduced stability at higher SiO_2 concentrations can be attributed to the ionic strength of the saline brine, which diminishes the electrostatic repulsion between nanoparticles. In such environments, the high concentration of dissolved ions screens the surface charge on the SiO_2 particles, leading to destabilization through van der Waals attractions and subsequent aggregation [164]. This highlights the critical importance of optimizing nanoparticle concentration to maintain stable suspensions in saline conditions.

4.2 IFT Measurement

The interfacial tension of the oil-surfactant-CO_2 system was measured to qualitatively analyze the oil-foam interactions. All measurements were performed at 25ºC and 250 psi pressure conditions. The droplet of oil or surfactant solution was held for at least 10 minutes to allow equilibrium between the two phases. Figure 4-3 illustrates the IFT of the oil-gas system, determined using the pendant-drop method. As shown in the figure, the IFT value gradually decreased and stabilized at 5.8 mN/m after 500 seconds.

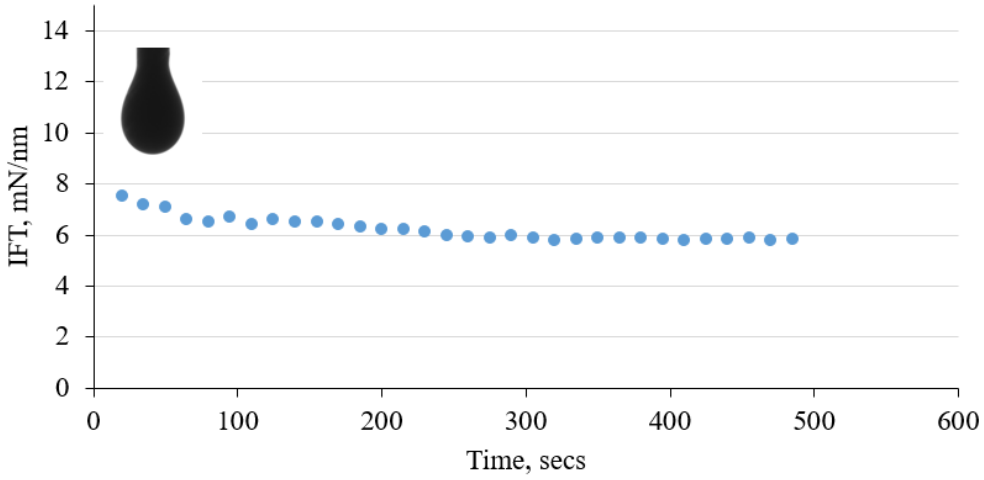

Figure 4-3. IFT measurements for oil-CO_2 system at 25ºC and 250 psi.

Table 4-3 presents the measured IFT for the oil-CO_2-surfactant system and summarizes the results of three coefficients: entering, spreading, and bridging, along with the lamella number, which were calculated based on the measured IFT using equations 2.1-2.4. Positive entering and bridging coefficients indicate that oil will enter the lamellae and generate a bridge between two liquid interfaces. However, a positive spreading coefficient implies that once oil enters the gas-surfactant solution interface, it tends to spread on the surfaces of foam bubbles, quickly breaking the lamellae and destabilizing the foam system. These observations imply that the crude oil has a detrimental effect on the foam stability, which supports the findings from the bulk tests.

Table 4-3. Interfacial tension data and calculated parameters at 25ºC and 250 psi.

System	Interfacial tension, (mN/m)	Parameters	(mN/m)
oil – gas	5.8	Entering coefficients	2.12
oil-surfactant	8.2	Spreading coefficients	2.68
gas-water	0.28	Bridging coefficients	33.7
		Lamella number	4.4

The lamellae number indicates that in the presence of crude oil, the foaming system exhibits moderate stability, corresponding to a type B foaming system [99]. However, both entering and spreading coefficients yield positive values, which contradict the concept of type B foams. The entering coefficient for type B foam is typically positive, while the spreading coefficient is negative. Therefore, the obtained lamella number does not provide a reasonable description of the foam stability in the presence of oil in this study. A similar observation has been reported previously [96].

The values of these three coefficients would be the same for the oil-gas-surfactant-nanoparticle system, as the presence of nanoparticles has an insignificant effect on surface tension values [12, 20].

4.3 Bulk Foam Stability

4.3.1 The Effect of Surfactant Concentration

The effect of AOS surfactant concentration on foamability and foam stability was investigated through several bulk tests conducted without oil. All foaming solutions were prepared following the procedure described in the Section 3.2.2. These tests were performed at room temperature and ambient pressure. After CO_2 foam generation, the foam volume and foam half-life were measured. In this study, foam half-life is defined as the foam decay time from its initial height to half. Figures 4-4 and 4-5 demonstrate the changes of foam half-life time and volume with increasing AOS concentration from 0.1 wt% to 1 wt%. As depicted in the Figure 4-2, both foam stability and foamability remained constant despite the increase in surfactant concentration.

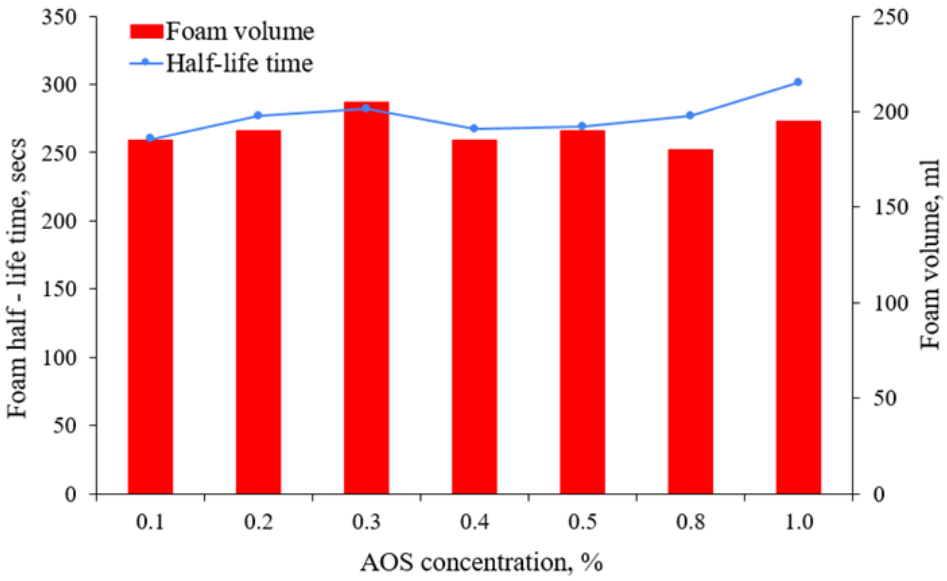

Figure 4-4. The effect of surfactant concentration on foam half-life time at ambient conditions.

The observed behavior of foam at various surfactant concentrations can be attributed to its critical micelle concentration (CMC) value, which is typically lower than 0.01 wt% [24]. CMC is defined as the minimum concentration of surfactant required to form micelles. It is determined by measuring the surface tension at various surfactant concentrations and finding the intersection between the regression straight line and the line of the plateau region. Above CMC value, additional surfactants added to a bulk phase form a double layer, thus surface activity is not enhanced [34, 165]. For this reason, surface tension becomes independent of surfactant concentration and remains unchanged. In the bulk test, the concentration of surfactant in all foaming solutions was significantly higher than the CMC value; thus, both foam volume and foam stability showed stable trends as they depend on surface activity. Based on the results of this test and previous studies, the optimum surfactant concentration was selected as 0.5% for further studies [166].

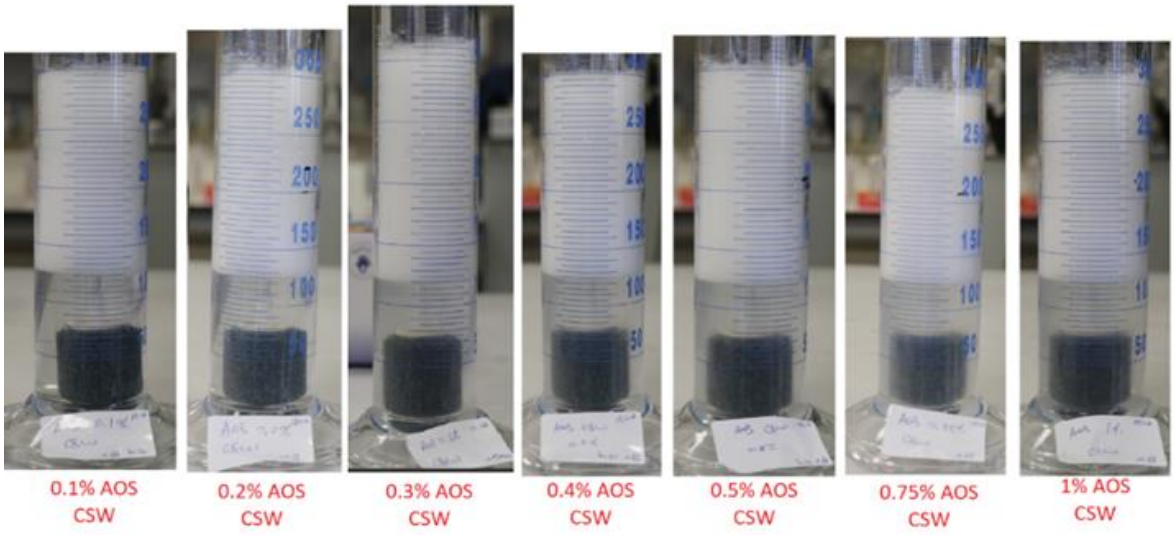

Figure 4-5. Visual observations during bulk tests at various surfactant concentrations after 500 seconds of gas injection at ambient condition.

4.3.2 The Effect of Temperature

Foam stability and foamability strongly depend on temperature. Typically, increasing temperature accelerates foam degradation, reducing its effectiveness in controlling CO_2 mobility. In this study, three bulk tests were performed at various temperatures (20ºC, 50ºC, and 80ºC) to investigate the effect of temperature on AOS-stabilized CO_2 foam. The highest temperature (80ºC) was selected to mimic harsh reservoir conditions. The tests were performed using foaming solutions at 0.25 wt% and 0.5 wt% concentrations, where the latter was determined as the optimum concentration in the previous test. These two concentrations were chosen to explore the relationship between surfactant concentration and temperature.

Figure 4-6 illustrates the changes in foam half-life and volume at various temperatures for both surfactant solutions. As shown, the stability and volume of CO_2 foam at both surfactant concentrations remained relatively unchanged when temperature was increased from 20ºC to 50ºC. Both 0.25 wt% and 0.5 wt% foaming solutions exhibited similar foam behavior at both temperatures. However, the foam volume of the 0.25 wt% AOS foaming solution reduced almost half when the temperature increased from 50ºC to 80ºC, while the 0.5 wt% foaming solution showed only a 20% reduction in foam volume. Similarly, foam half-life showed a significant decrease for both foaming solutions. However,

high-concentration solutions exhibited slightly longer stability compared to low concentration.

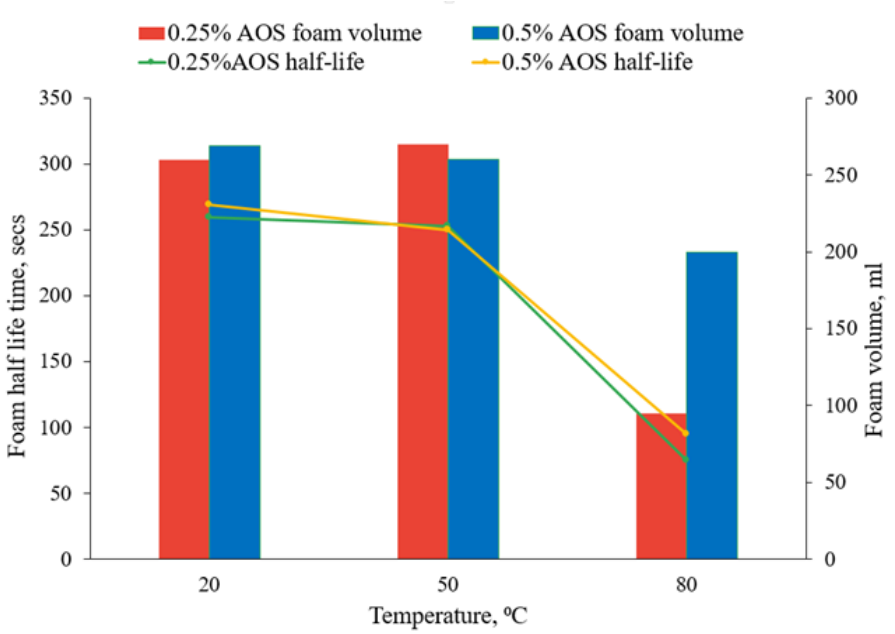

Figure 4-6. The effect of temperature on foam half-life time at various temperature and ambient pressure.

4.3.3 The Effect of Brine Salinity

In order to investigate the effect of salinity on CO_2 foam performance using AOS surfactant, CSW was diluted to create brines with salinities of 3,250 ppm, 6,500 ppm, and 9,750 ppm. Additionally, one test was conducted using DI water as a base case. For each test, 0.25 wt% and 0.5 wt% AOS surfactant solutions were prepared, and the same bulk test procedure with CO_2 was applied.

CO_2 foam stability and foamability at various salinities are shown in Figure 4-7. Typically, increasing salinity has an adverse effect on foam behavior, reducing its stability and capacity. However, in this test, increasing brine salinity had an insignificant effect on foam stability and volume. The maximum stability of 300 seconds was observed at a 0.25 wt% foaming solution when DI water was used as a bulk phase. Other foam half-life values were between 260 and 290 secs. The small variation in foam stability and volume across the tested salinities can be attributed to the relatively low salinity of the brine solutions.

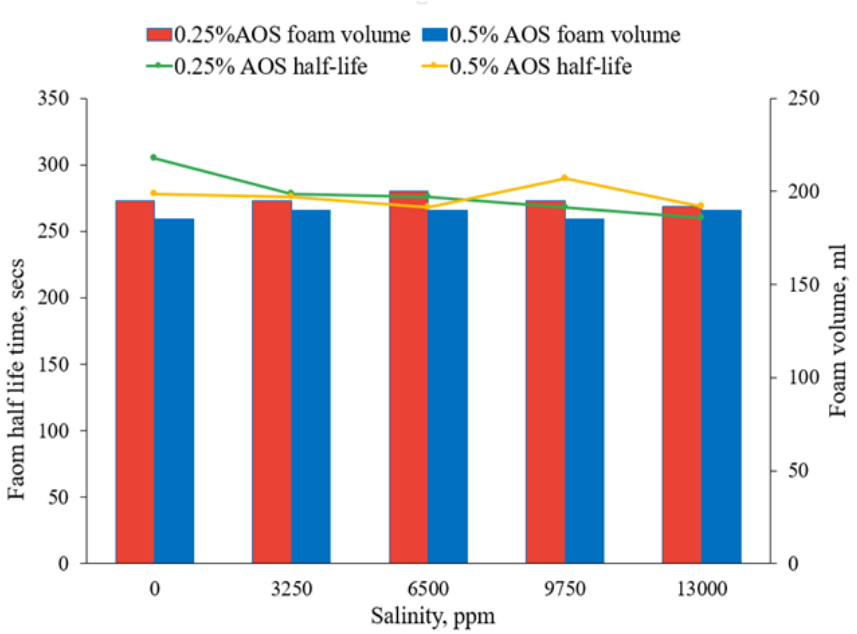

Figure 4-7. The effect of brine salinity on foam half-life time at 20ºC and ambient pressure.

4.3.4 The Effect of the Presence of Oil

A series of the bulk tests were carried out to understand the influence of oil on foam behavior. In these foam stability tests, the oil volume was varied to assess its effect on foam performance. Crude oil was added to surfactant solution at ratios of 1%, 3%, and 5% of foaming agent volume, introduced from the top of the cylinder before CO_2 injection. In these tests, both 0.25 wt% and 0.5 wt% AOS surfactant solutions were used.

Figure 4-8 illustrates the foam stability and volume in the presence of varying oil proportions. Both foaming solutions showed a decreasing trend in foam stability and volume with increasing the amount of oil present. When 1 wt% oil was added to the foaming solution, the half-life time decreased to 240 seconds, and foam volume decreased by half for low surfactant concentration compared to the case without oil. However, the addition of 1 wt% oil had minimal effect on foam stability and volume for higher surfactant concentration. Increasing the oil content from 3% to 5% resulted in a reduction of foaming volume and stability for both solutions. As discussed in section 4.2, both the spreading and bridging coefficients for oil-foam interactions are positive, indicating that oil droplets enter the gas-brine interface and form bridges, thereby destabilizing foam bubbles. Moreover, a positive spreading coefficient suggests that once oil enters the interface, it spreads along the lamellae

interface and ruptures it [167]. Based on these entering-spreading theories, it can be concluded that oil has a destabilizing effect on CO_2 foam, significantly reducing both its stability and foamability. This conclusion is consistent with bulk test results presented in Figure 4-8.

The weakest foam and lowest foam volume were observed in the solution with 5% oil. Compared to the no-oil case, adding 5% oil reduced foam stability by 2- and 1.5-fold for 0.25 wt% and 0.5 wt% foaming solutions, respectively. Additionally, foam volume decreased by nearly 42% for the 0.5 wt% concentration solution, while the 0.25 wt% solution experienced a 60% reduction in volume with 5% oil. Overall, the foam generated with 0.5 wt% AOS foaming solution demonstrated better stability and foamability in the presence of oil compared to the solution with 0.25 wt%. This confirms that 0.5 wt% AOS solution is an optimal concentration for further experiments.

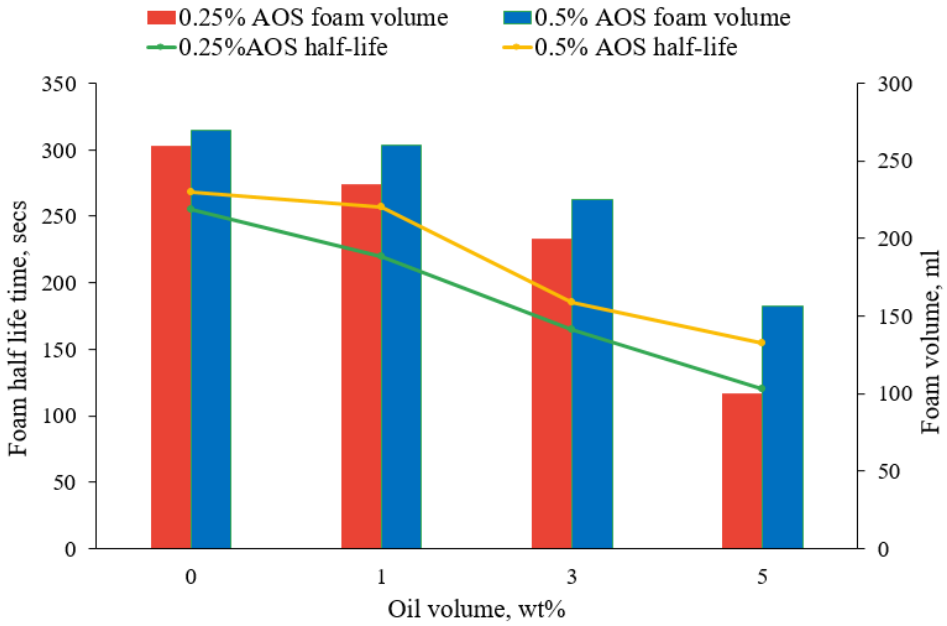

Figure 4-8. The effect of oil on CO_2 foam at 20ºC and ambient pressure.

One bulk test was conducted at 80ºC with 5% oil using 0.25% wt and 0.5% wt AOS solutions. The purpose of this test was to examine the effect of oil on foam performance at elevated temperatures, which represents reservoir conditions for this study. After adding the foaming solution and oil into the cylindrical column, the column was placed in an oven. Once the temperature of the foaming solution stabilized at 80ºC, CO_2 injection was initiated.

The results of this test are shown in Figure 4-9. Similar to the previous test conducted without oil, elevated temperature accelerated the degradation of CO_2 foam, reducing foam stability and foamability for both foaming solutions. Overall, foam stability decreased 80% and 65% for the 0.25 wt% and 0.5 wt% AOS solutions, respectively, when the temperature increased from 20ºC to 80ºC. These findings show the advantage of using higher surfactant concentration to stabilize CO_2 foam in the presence of oil at elevated temperature.

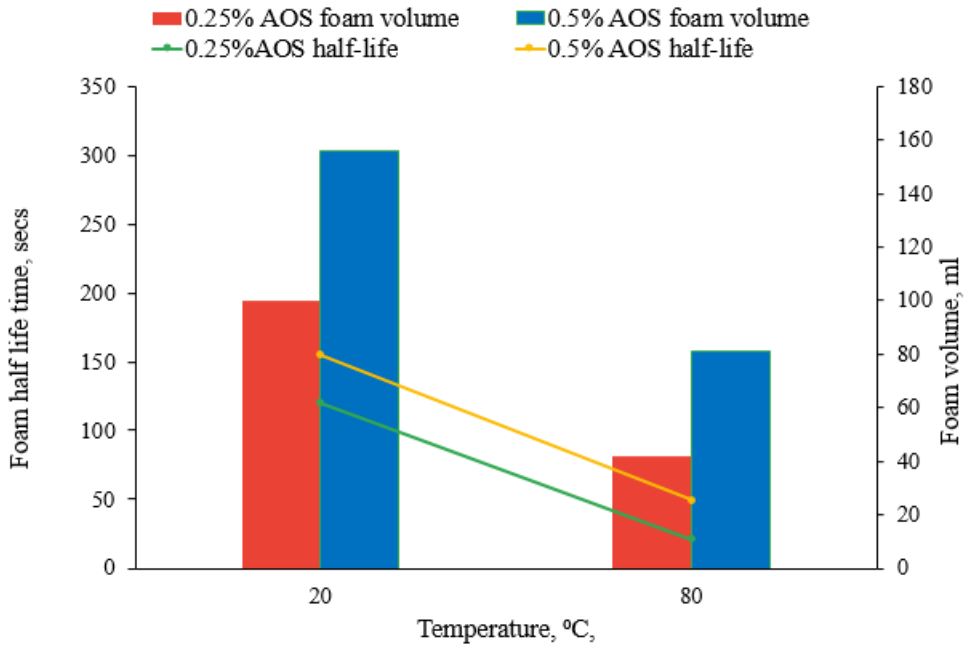

Figure 4-9. Foam stability at 20ºC and 80ºC in the presence of 5% oil.

4.3.5 The Effect of Nanoparticles

A series of bulk tests were performed to investigate the influence of nanoparticles on the behavior of surfactant-stabilized CO_2 foam. Following the procedure outlined in Chapter 1, nanoparticle solutions with concentrations ranging from 0.1 to 1% were first prepared. Then, 0.5 wt% surfactant was added to each nanoparticle solution. The same bulk test procedure was employed for this experiment, with all tests being carried out under ambient conditions.

Figures 4-10 and 4-11 illustrate the stability and volume of CO_2 foam stabilized with the combination of surfactant and nanoparticles. As shown in the Figure 4-10, the highest foam stability was achieved with 0.3% SiO_2 nanoparticle concentration, resulting in a foam

half-life time around 400 seconds. Above this concentration, further increases in nanoparticle concentration led to a slight reduction in foam stability. In general, 0.3 wt% nanoparticle solution performed much better than others. A similar trend was observed in the measurement of foam volume. The improved foam stability and foamability observed in the presence of nanoparticles can be attributed to several mechanisms. First, nanoparticles on the surface of foam bubbles create electrostatic repulsion forces, which prevent bubble coalescence. Additionally, the steric layer formed by the surfactant on the surface of bubbles is reinforced by nanoparticles, reducing the drainage of lamellae due to gravity. These mechanisms in the presence of NPs generate more stable foam [168, 169].

However, as seen in the Figure 4-10, the change of foam volume was insignificant in the presence of NPs. One of the possible reasons for that is the low stability of NPs in brine, resulting in immediate nanoparticle precipitation, as it was found in previous nanoparticle stability tests in the Section 4.1. Despite better performance, using a 0.3% SiO_2 solution may lead to pore plugging problems due to the high rate of nanoparticle precipitation. For this reason, 0.05% SiO_2 was selected as the optimum concentration since no precipitation was observed in previous tests. However, using a 0.05% SiO_2 solution resulted only in a small increase in foam stability compared to the surfactant alone case; nanoparticle solution stability is the main criterion for conducting further core flooding experiments.

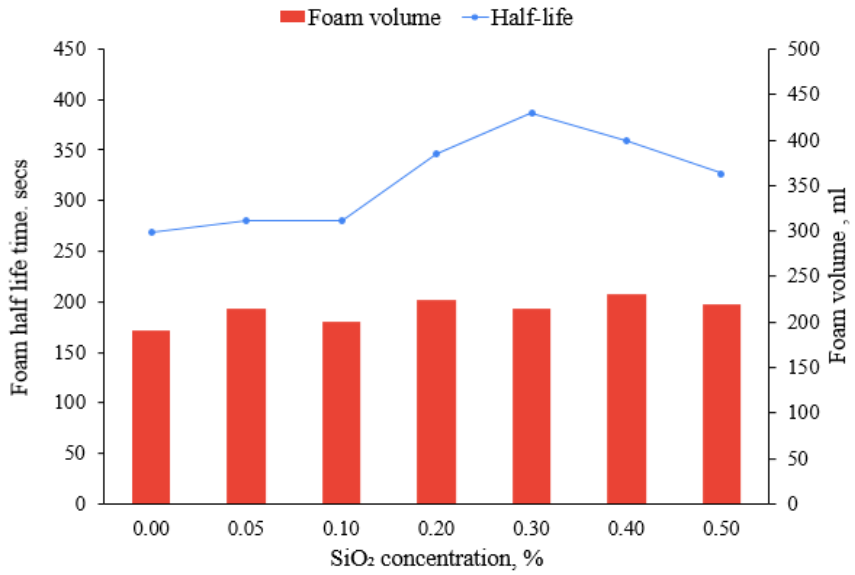

Figure 4-10. The effect of adding SiO_2 to 0.5wt% AOS at 20°C and ambient pressure.

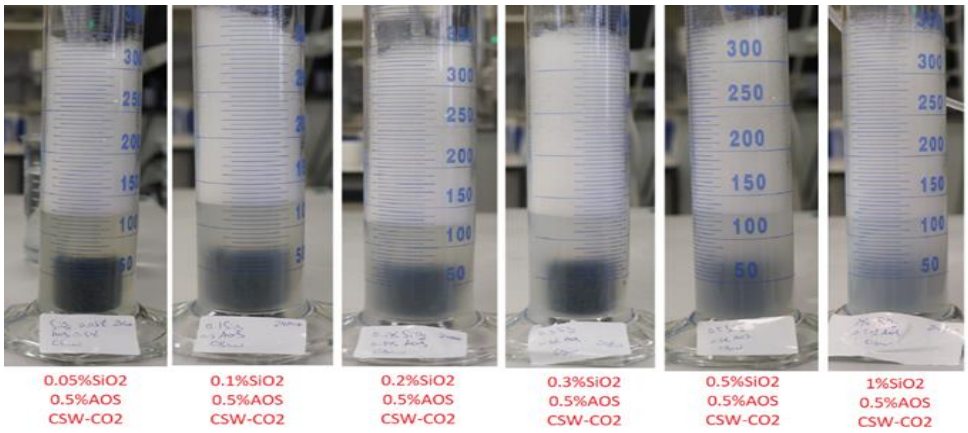

Figure 4-11. The CO_2 foam generation by the mixture of SiO_2 and AOS at 20ºC and ambient pressure.

The selection of surfactant and nanoparticle concentration

Figure 4-4 demonstrates that CO_2 foam stability was not significantly affected by surfactant concentration, as the concentrations tested were significantly greater than CMC value (0.01 wt%). Thus, from the economic standpoint, using the lowest effective surfactant concentration is desirable. However, additional experiments conducted at elevated temperatures (Figure 4-7) and in the presence of oil (Figure 4-8) showed improved foam performance at higher surfactant concentrations compared to the lower. This enhancement can be attributed to the higher liquid viscosity of the 0.5 wt% AOS solution compared to the 0.25 wt% AOS solution, which reduced the foam drainage rate and improved stability as a result.

Furthermore, the injection of negatively charged AOS surfactant into a carbonate core, which has positively charged surfaces, may result in surfactant adsorption due to electrostatic attractive forces. To compensate for this surfactant loss and maintain effective surfactant availability within the porous media, a higher concentration is recommended. Additionally, previous studies have also reported the positive experiences of using 0.5 wt% AOS for CO_2 foam stabilization under elevated temperature and pressure reservoir conditions, similar to those considered in this study [166, 170]. For these reasons, 0.5 wt% was selected as the optimal concentration for the AOS surfactant and used in subsequent experiments.

The stability of SiO_2 nanoparticles in brine was the primary criterion for their use in subsequent foam flooding experiments in porous media. An unstable nanoparticle

suspension can result in nanoparticle precipitation, which may block fluid flow paths and cause injectivity issues. As shown in Table 4-2, nanoparticle precipitation was observed at concentrations above 0.05 wt%. Therefore, a foaming solution containing 0.05 wt% SiO_2 was selected for the subsequent foam flooding experiments using a core to ensure nanoparticle stability and minimize the risk of flow impairment.

It is important to note that the bulk foam tests are typically performed for screening foaming agents. However, the formation, stability, and behavior of foam in porous media cannot be assessed through bulk foam tests, as the physics behind foam performance at bulk and pore scale is different [18]. For this reason, the findings from the bulk foam tests are not directly applicable to foam generated by surfactants and/or nanoparticles in porous media, whether in foam scans or CO_2-foam flooding for enhancing oil recovery, as discussed in the upcoming chapters. Nevertheless, the bulk foam tests demonstrated the effectiveness of the nanoparticle-surfactant combination in improving foam stability.

4.4 Foam Dynamic Experiments

The foam behavior was evaluated in brine-saturated core plugs to determine foam strength at various gas fractional flows (foam quality scans) and injection rates. This was done prior to conducting experiments with oil-saturated core plugs to study the oil recovery efficiency of CO_2 foam. The results from the foam flow tests in this chapter serve as input parameters for the simulation model.

Pressure drop across the core and the apparent viscosity of foam generated by co-injection of the foaming solution and CO_2 were used to evaluate foam strength in porous media. The apparent viscosity of the foam was calculated using Darcy's law:

$$\mu_{app}(\text{cP}) = \frac{\text{k(mD)} * \text{A(cm}^2) * \Delta\text{P(psig)}}{14700 * \text{Q}_t\left(\frac{\text{cc}}{\text{s}}\right) * \text{L(cm)}} \tag{4.1}$$

where μ_{app} is the apparent viscosity of foam, k is the effective permeability to gas, A is the sectional area of the core, Δp is the pressure drop across the core, Q_T is the total flow rate of gas and surfactant solution, and L is the core length.

4.4.1 Foam Quality Scan

The purpose of this experiment is to study the foam strength at various gas fractions to determine the optimum ratio. Co-injection of CO_2 and surfactant was performed in the Ind01 core with a permeability of 120 mD, gradually increasing the gas fraction from 0.4 to 0.9. The pressure drop across the core was continuously measured during the foam injection. The steady-state pressure drop at each specific gas fraction was used as an indicator to adjust the gas fraction. The experiment was conducted at 40°C and 1500 psi.

Figure 4-12 shows the foam's apparent viscosity and steady-state pressure drop at different gas fractions. As seen in the figure, the apparent viscosity of the foam initially increased with the gas fractional flow until it reached a maximum point, after which it declined as the foam was enriched with CO_2. The highest apparent viscosity, 50 cp, was obtained at f_g = 0.7, which was selected as the optimum gas fraction for further experiments.

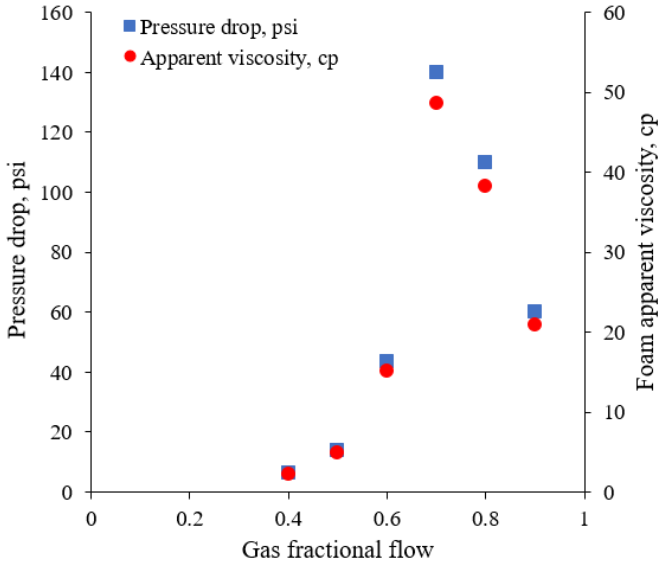

Figure 4-12. Pressure drop and apparent viscosity at 40°C and 1500 psi.

From the Figure 4-12, it can be observed that the apparent viscosity at f_g =0.7 represents a transition point, which divides the foam quality regime into two distinct areas. The region on the left corresponds to the low-foam quality regime, while the high-foam quality regime is on the right. Similar observations have been reported by previous studies [171, 172].

In the low-foam quality regime, the dominant mechanism resisting gas flow is foam bubbles trapped in intermediate-sized pores, while the remaining gas flows through the largest pores [78]. Typically, the ability of foam to resist flow is determined by the amount of lamellae per unit of capillary length, referred to as lamellae density. Foam resistance to flow becomes stronger as lamellae density increases. As the gas fractional flow rises, the quantity of lamellae per capillary length increases, resulting in higher flow resistance. However, under this condition, capillary pressure increases too, and when it reaches a limiting pressure value, the lamellae become unstable and begin to collapse, leading to a reduction in lamellae density [85]. Moreover, in the high-quality regime, the reduction in liquid fraction leads to lower lamellae density and bubble enlargement [173]. As a result, increasing the gas fraction beyond the transition point generates weaker foam and reduces its flow resistance ability.

4.4.2 Flow Rate Tests

Foam propagation in porous media occurs only when injection pressure exceeds the minimum pressure gradient required to mobilize foam. This experiment examined the effect of foam injection rate on foam behavior in porous media. Ind02 core with a permeability of 66 md was used for this experiment. The co-injection of CO_2 and 0.5 wt% AOS solution was performed at a constant gas fractional flow of 70%, which resulted in the best foam characteristics during the foam quality scan test. The experiment was conducted at 80°C and 1500 psi.

Figures 4-13a and 4-13b depict the variation of differential pressure across the core and the apparent viscosity of foam as the injection rate increases. The results demonstrate that co-injecting CO_2 and the foaming solution at a total injection rate of 0.25 cc/min resulted in a pressure drop of 8 psi and an apparent viscosity of 3 cp, indicating the generation of weak foam. When the flow rate increased from 0.25 cc/min to 0.5 cc/min, the apparent viscosity increased to 5 cp, while the pressure drop reached 14 psi. As the injection rate was further increased from 0.5 cc/min to 2 cc/min, the pressure gradient gradually rose from 14 psi to 95 psi, while the foam's apparent viscosity almost doubled, from 5 cp to 15 cp.

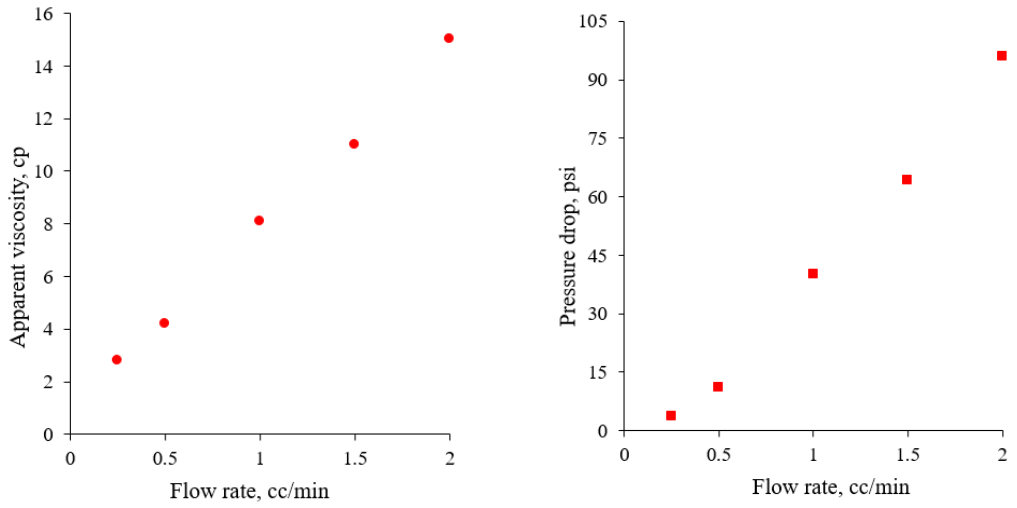

a) b)

Figure 4-13. Pressure drop and apparent viscosity for Ind02 at 80℃ and 1500 psi.

Overall, these figures indicate that foam exhibited shear-thickening behavior. This suggests that the apparent viscosity of foam is higher near the wellbore due to the high flow velocity than deeper within the reservoir. Similar observations have been reported by other researchers [116-117].

4.4.3 Foam Flooding in the Absence of Oil

The brine-saturated Ind03 core with a permeability of 100 mD was used for a foam flooding experiment conducted at 80ºC and 1500 psi, representing reservoir conditions. To minimize surfactant loss due to adsorption onto the rock surfaces, one pore volume of surfactant solution was injected into the core as a pre-flush. During surfactant injection, the pressure drop across the core was approximately 3 psi. In subsequent steps, CO_2 and a 0.5 wt% AOS solution were co-injected into the core at a constant total injection rate of 1 cc/min, with gas fractional flow maintained at 70%.

Figure 4-14 illustrates the change of pressure drop during foam flooding. It is seen that the pressure profile during foam flooding can be divided into three distinct periods. During the first period (0-1 PV), the injected gas and the foaming solution mixed, causing a slight increase in pressure. During the second period (1-2PV), foam generation occurred; therefore, pressure rose gradually until it stabilized at 60 psi with an apparent viscosity of 20 cp. In the third period, further foam flooding helped maintain pressure at a steady state, indicating stable foam generation. Overall, the experiment demonstrated a strong foam generation in porous media under reservoir conditions, which effectively reduced CO_2 mobility.

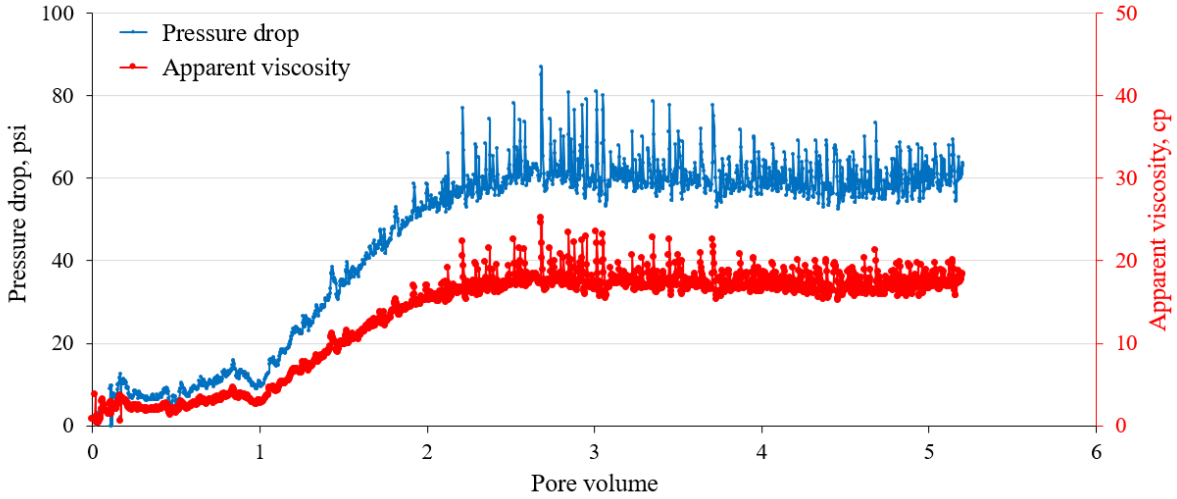

Figure 4-14. Average pressure drop across Ind03 core during the co-injection CO_2 and 0.5 wt% AOS solution at 80ºC and 1500 psi.

Before the next experiment, the core was cleaned by injecting 20 PVs of brine and 5 PVs of isopropanol. During this process, the pore pressure was released several times to remove any trapped gas within the pores. Following this, several PVs of brine were injected into the core to measure the pressure drop and calculate the absolute permeability. If the core permeability deviated significantly from its original value, an additional 10 PVs of brine were flushed through the core.

The second foam flooding experiment was conducted at 40°C and 1500 psi to evaluate foam generation and stability in porous media at a lower temperature. Under these

conditions, CO_2 remained in the supercritical state, similar to the previous high-temperature experiment.

Figure 4-15 illustrates the pressure drop and apparent viscosity buildup profile during foam flooding. Compared to the high-temperature experiment at 80°C, the lower temperature resulted in stronger foam generation, as shown in the figure. Similar to the previous experiment, the pressure drop gradually increased due to foam generation in porous media and reached approximately 100 psi with the apparent viscosity of 30 cp after 6 PVs of foam injection. Following this, the pressure remained relatively stable until the end of the foam flooding. Overall, stronger foam was generated at a lower temperature compared to the high-temperature conditions, similar to the results observed during the bulk foaming tests.

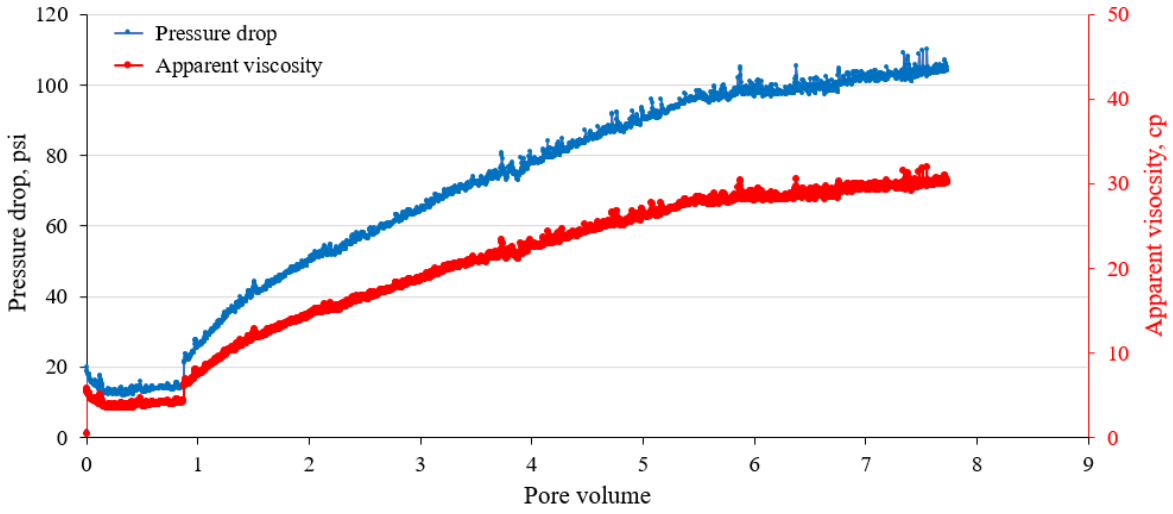

Figure 4-15. Average pressure drop across Ind03 core during the co-injection CO_2 and 0.5 wt% AOS solution at 40ºC and 1500 psi.

After cleaning following the same procedure as in the previous experiment, the core sample was used again in the subsequent experiment, where CO_2 and brine were co-injected under the same reservoir conditions of 1500 psi and 40°C. The objective of this experiment was to evaluate the effectiveness of the co-injection of CO_2 and brine without surfactant for mobility control and compare it with foam injection. As in previous experiments, the total injection rate was maintained at 1 cc/min, with a constant gas fractional flow of 70%. Figure

4-16 presents the differential pressure profile during this experiment. The pressure drop across the core during the co-injection of CO_2 and brine without surfactant fluctuated between 5 and 15 psi, which was significantly lower than that observed during foam injection. These results demonstrate that the co-injection of CO_2 and brine was less effective in reducing CO_2 mobility compared to foam injection under the same injection and reservoir conditions.

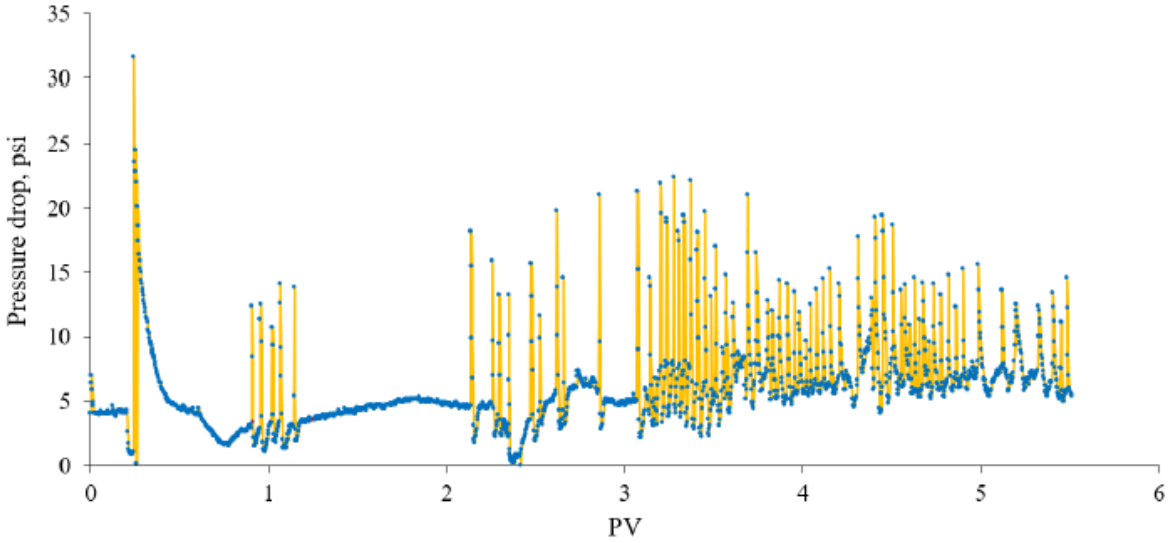

Figure 4-16. Average pressure drop across Ind03 core during the co-injection CO_2 and brine (without foaming agent) at 40ºC and 1500 psi.

4.4.4 Effect of Surfactant Concentration on foam in Porous Media

Understanding the influence of surfactant concentration on foam stability is a crucial step in a foam flooding project. Therefore, a series of foam flooding experiments were conducted to assess the effect of AOS concentration on CO_2 foam stability under reservoir conditions of 1500 psi and 80ºC. The Ind04 core with a permeability of 70 mD was used for this study, which was cleaned after each experiment following the same procedure described in the previous section to restore permeability. Four foaming solutions were prepared with AOS concentrations of 0%, 0.25%, 0.5%, and 1%. The co-injection of CO_2 and the foaming solution was performed at a constant total rate of 1 cc/min and a gas fractional flow of 70%.

Figure 4-17 illustrates the variation in pressure drop across the core for different surfactant concentrations. As shown in the figure, the pressure drop during CO_2 foam

injection without surfactant was approximately 8-9 psi, demonstrating its low efficiency in controlling CO_2 mobility.

During the injection of foaming solution with 0.25 wt% of AOS, the differential pressure gradually increased and reached its maximum of 28 psi after 2 PV of injection. However, as CO_2 foam injection continued, the pressure slowly declined and stabilized around 22 psi by the end of this process. The co-injection of CO_2 and 0.5 wt% AOS solution, initially, resulted in a lower pressure drop compared to the 0.25 wt% solution. However, the pressure rose steadily and finally stabilized at 30 psi, outperforming the 0.25 wt% solution in terms of pressure drop. Similar foam behavior was observed during the co-injection of CO_2 and a 1 wt% AOS solution. However, the final pressure drop during this experiment was 40 psi, which was higher than in previous tests. Overall, the results demonstrate that foam strength increases with surfactant concentration. This can be attributed to the higher blocking capability of foam at higher concentrations.

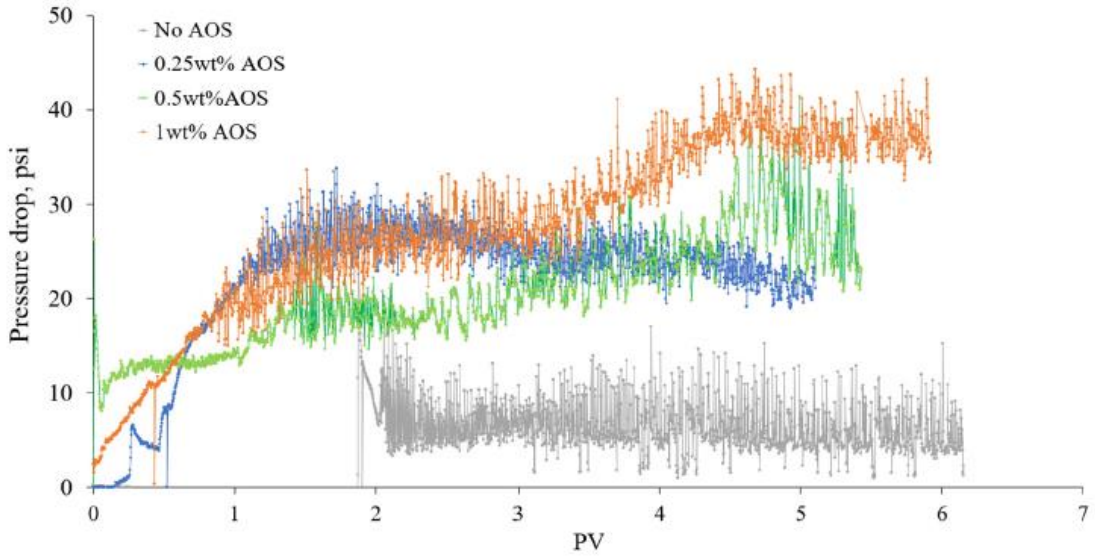

Figure 4-17. Average pressure drop across Ind04 during the co-injection of CO_2 and foaming solution at various concentration of AOS, 80ºC and 1500psi.

4.4.5 The Effect of Nanoparticles on foam in Porous Media

The series of foam flooding experiments was conducted to investigate the influence of nanoparticles on the behavior of surfactant-stabilized CO_2 foam. In this experiment, the Ind05 core with a permeability of 103 md was used, which possessed the same rock

properties as the core used in the previous foam flooding experiment with surfactant alone. Similar to the previous experiment, the reservoir pressure was maintained at 1500 psi, and temperature was kept at a constant 80°C throughout the experiment. CO_2 and the foaming solution, containing 0.5 wt% AOS and 0.05 wt% SiO_2, were co-injected at a constant total injection rate of 1 cc/min with a gas fractional flow of 70%.

As shown in Figure 4-18, the pressure drop during foam flooding with a surfactant-nanoparticle mixture exhibited a similar trend in the first period (from 0 to 1 PV) as the case with surfactant alone. However, a slightly longer time was required for the pressure to stabilize in the presence of nanoparticles. The steady-state pressure drop for the hybrid method was significantly higher compared to the surfactant-only case. Specifically, the steady-state pressure drop with nanoparticles was around 100 psi, while it was approximately 60 psi without nanoparticles.

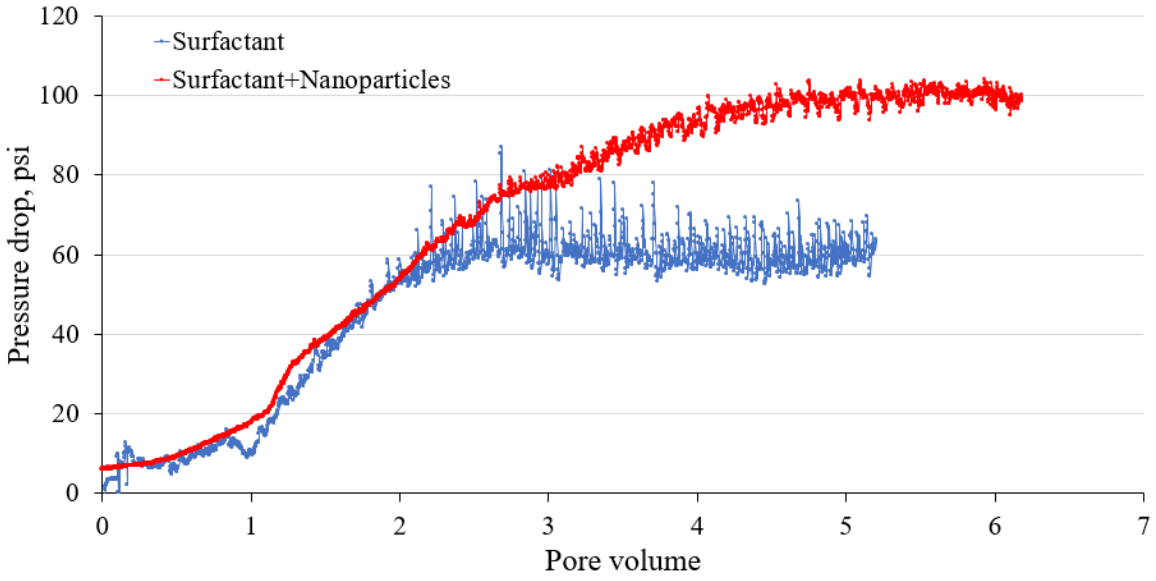

Figure 4-18. Pressure drop during the co-injection of CO_2 and surfactant solution with and without nanoparticles, 80℃ and 1500 psi.

Figure 4-19 illustrates the change in apparent viscosity during both foam flooding experiments. The apparent viscosity of the foam with the nanoparticles-surfactant mixture was 30 cp, nearly twice that of surfactant-stabilized foam, which had a viscosity of 20 cp. These results highlight the ability of nanoparticles to improve the strength and stability of surfactant-stabilized CO_2 foam in porous media.

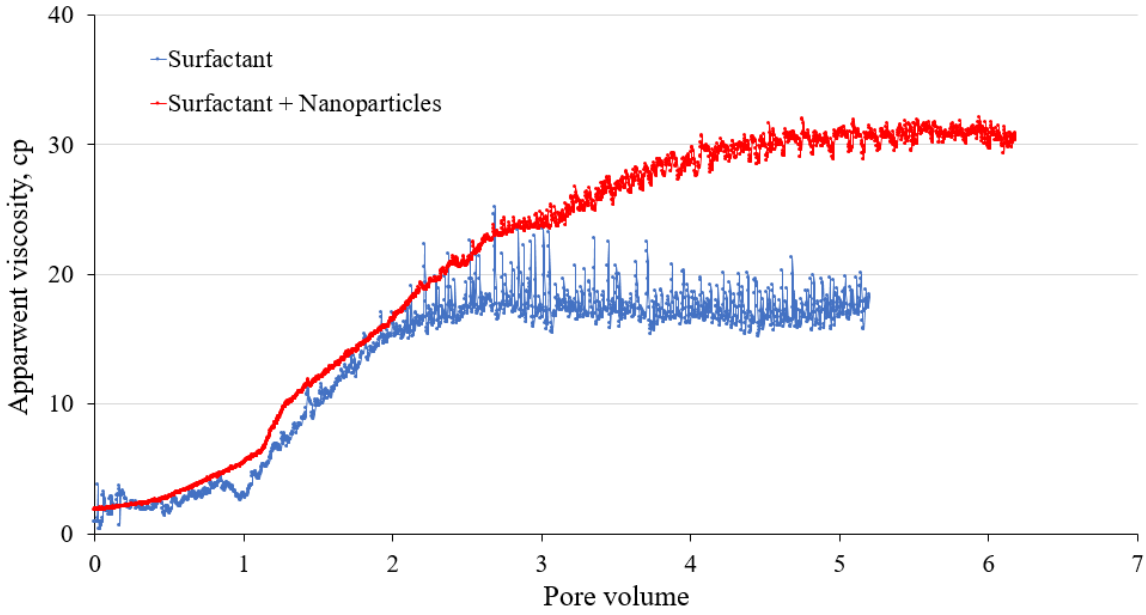

Figure 4-19 . Apparent viscosity during the co-injection of CO_2 and surfactant solution with and without nanoparticles, 80°C and 1500 psi.

4.4.6 CO_2 Mobility Control Using Foam at Low Temperature

Two foam flooding experiments were conducted at 40°C and 1500 psi to compare the ability of surfactant or surfactant-nanoparticle stabilized foam in the reduction of CO_2 mobility in porous media. In the first experiment, 0.5 wt% AOS was used, while the second experiment employed the mixture of 0.5 wt% AOS and 0.05 wt% SiO_2.

Figure 4-20 illustrates the pressure drop and viscosity profiles for the surfactant-only case during foam flooding experiments in the absence of oil through Ind06 core with a permeability of 104 md. As shown in the figure, 1 PV of 0.5 wt% AOS solution was pre-flushed to reduce the surfactant loss due to adsorption on the mineral surfaces. During the pre-flush, the pressure drop was around 4 psi. Then, the co-injection of CO_2 and AOS solution was conducted at a constant total rate of 1 cc/min with 70% foam quality. During the foam flooding, the pressure drop increased gradually as foam formed inside the pores and stabilized at 80 psi after 5 PV of injection. The maximum apparent viscosity in this process reached 26 cp. Foam production was observed at the outlet of the production line, as shown in the inset picture. This confirms the successful formation and movement of foam within the core. In the subsequent step, CO_2 flooding was carried out, resulting in a marked

reduction of pressure drop to 4 psi during 2 PV of injection due to the lower viscosity and density of CO_2 compared to foam. These results demonstrate the short lifetime of foam in porous media after ceasing surfactant injection.

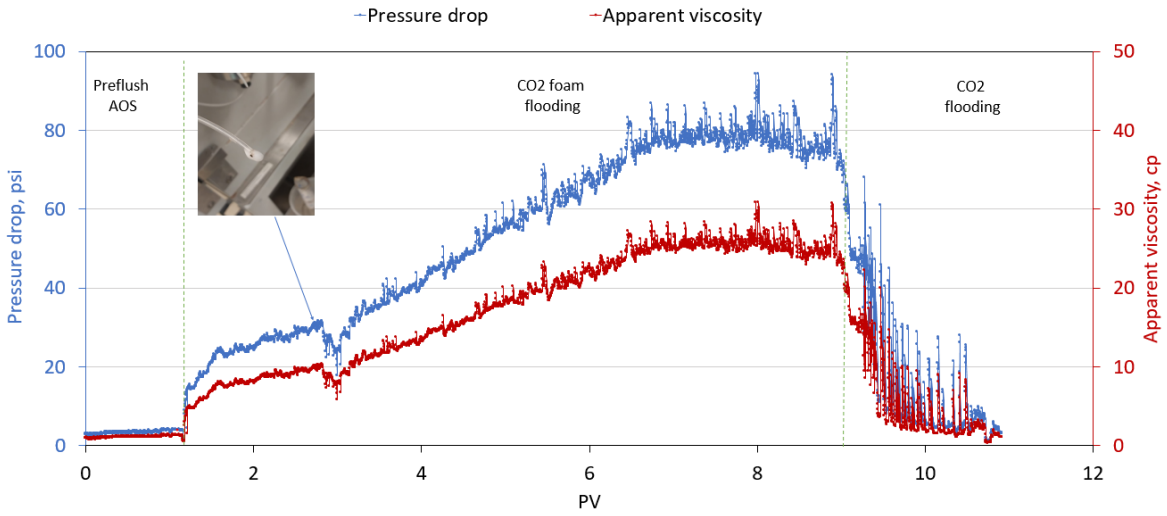

Figure 4-20. Pressure drop and apparent viscosity during the co-injection of CO_2 and 0.5wt% AOS surfactant solution, 40°C and 1500 psi.

In the subsequent experiment with nanoparticles, Ind07 core with a permeability of 200 md was used. First, 1 PV of the foaming solution was pre-flushed to reduce surfactant loss due to adsorption, as shown in Figure 4-21. The pressure drop during the pre-flush was approximately 5 psi. Afterward, CO_2 and the foaming solution were co-injected following the same injection procedure as in the previous experiment. Compared to the surfactant-only foam experiment, the rate of pressure increase was higher in the presence of nanoparticles, indicating the generation of stronger foam within the pores, After 7 PV of foam injection, the pressure drop reached approximately 140 psi, nearly twice the steady-state pressure observed in the surfactant-only case. Similarly, the maximum apparent viscosity for the mixture reached 80 cp at this point, doubling the viscosity of foam stabilized with surfactant alone.

However, the pressure gradient began to decrease as CO_2 injection started, dropping to 10 psi after 3 PV of injection. During the CO_2 flooding, the pressure decreased at a slower rate compared to the surfactant-only case, demonstrating that the foam formed

in the presence of nanoparticles was more stable. As a result, the remaining foam was more effective at controlling CO_2 mobility.

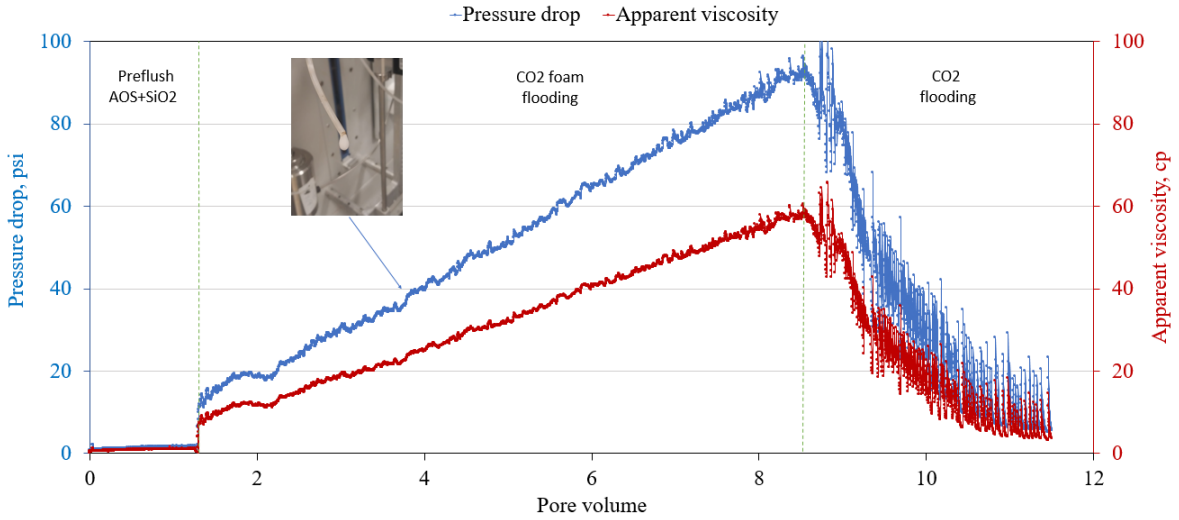

Figure 4-21. Pressure drop and apparent viscosity during the co-injection of CO_2 and the mixture of surfactant and nanoparticles solution (0.5wt% AOS+0.05wt% SiO_2), 40°C and 1500 psi.

A comparison of the two experiments revealed that the presence of nanoparticles resulted in a stronger and more stable foam generation in porous media compared to its absence. The foam viscosity doubled when the mixture was injected, compared to the surfactant-only case. The nanoparticles strengthened the thin liquid film, reducing the liquid drainage rate and thereby enhancing the stability of the produced foam. Thus, foam exhibited longer stability in the presence of nanoparticles compared to its absence when the foam injection was ceased, more efficiently reducing CO_2 mobility.

A comparison of Figures 4-19 and 4-21 reveals that at 40 °C, the foam produced using the hybrid method exhibited a significantly higher apparent viscosity than at 80 °C. At the lower temperature, the maximum apparent viscosity reached 60 cp, whereas at the higher temperature, it was only 30 cp.

4.4.7 Dual-core Experiments

Two foam flooding experiments using a dual-core holder system with parallel cores of varying permeabilities were conducted to assess the flow diversion performance of CO_2

foam. In the first experiment, a 0.5 wt% AOS surfactant was used as a foaming agent, while the second experiment utilized a mixture of 0.5 wt% AOS and 0.05 wt% of SiO_2. Both experiments were carried out at 25°C and 500 psi, conditions under which CO_2 exists in the gas phase. The measured pressure drop across both core samples and the diversion ratio were used to characterize the flow diversion performance of the foam. The diversion ratio was calculated by dividing the effluent fluid volume produced from high- and low-permeability cores by the total production volume. The diversion ratio is expressed as the percentage in this study. Additionally, the permeability ratio (V_k) was used to quantify the level of heterogeneity. This ratio was defined as the ratio of high permeability to low permeability.

In this experiment, primary water injection at a constant rate of 1 cc/min was first performed, followed by CO_2 foam injection stabilized either by surfactant or the surfactant-nanoparticle mixture. The co-injection of CO_2 and foaming solution was conducted at a constant total injection rate of 1 cc/min, with a gas fractional flow of 70%. Subsequently, post-water injection was performed to assess the foam-blocking capacity in a heterogeneous environment.

Figure 4-22 shows the change in diversion ratio and pressure gradient throughout the parallel-core experiment for the surfactant-only case. The permeability ratio for this experiment was approximately 2, indicating relatively weak heterogeneity. As a result, the primary water injection showed good brine displacement in both high- and low-permeability cores. Approximately 65% of brine production came from the high-permeability core, which was significantly higher than the production volume from the low-permeability core. The average steady-state pressure drop during the primary water injection was approximately 3 psi.

When co-injection of CO_2 and a 0.5 wt% AOS solution began, the diversion ratio for the low permeability core significantly increased, while fluid production from the high-permeability core decreased. This result demonstrates the good diverting capability of surfactant-stabilized CO_2 foam under this degree of heterogeneity. The pressure gradient increased slightly when CO_2 foam injection was initiated, but it remained relatively stable during the next 2 PV of injection, indicating the effective mixing of CO_2 and the foaming agent in cores. Afterward, the pressure gradient gradually rose from 2 psi to 30 psi until the end of co-injection, demonstrating the foam generation within porous media.

However, the diversion ratio for the low permeability core dropped from 80% to 35% after 4 PV of co-injection, while the opposite occurred in the high permeability core. Following this, the diversion ratio for both cores fluctuated between 40-60% as CO_2 foam continued to inject. This behavior can be attributed to the inability of foam to enter small pores in the low permeability cores due to high capillary pressure. Additionally, foam generated in both core samples blocked some flow paths, resulting in similar resistance pressures, thus allowing fluid to flow through both cores.

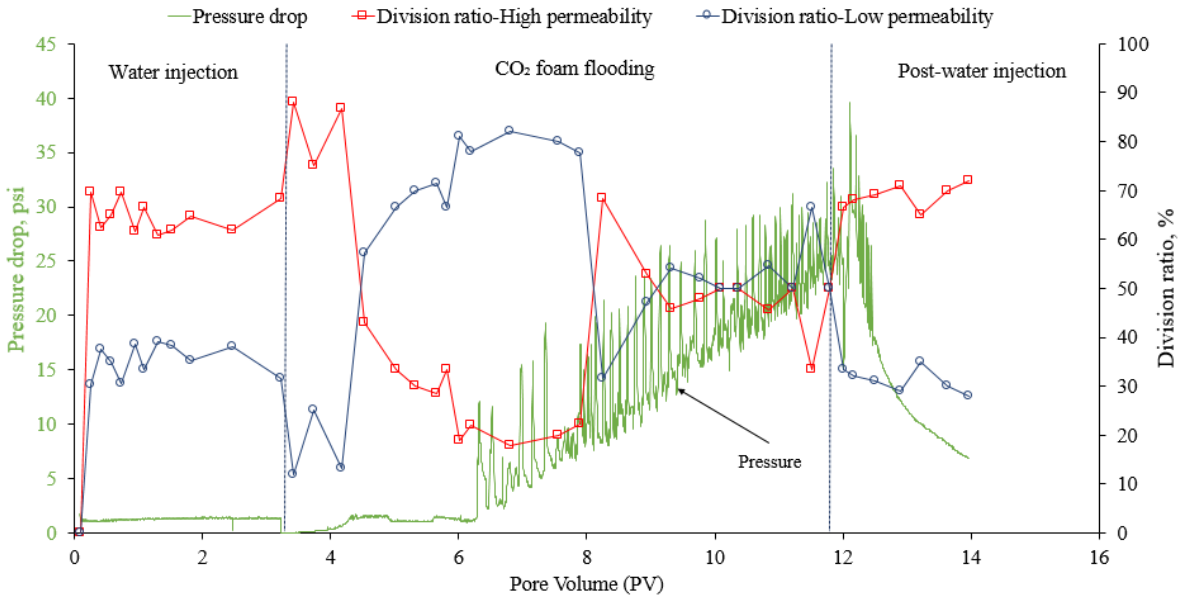

Figure 4-22. Dual core experiment with surfactant-stabilized CO_2 foam (0.5wt% AOS) at 25°C and 500 psi, permeability ratio V_k=2.

During the post-water injection, the division ratio for the high permeability core increased markedly from 50 to 70%, while production volume from the low permeability core dropped substantially. Furthermore, the pressure gradient decreased significantly from 40 psi to 7 psi as 2 PV of brine was injected into the cores. These results indicate that foam could survive, at least in a weakened form, and slightly reduce water flow during several pore volumes of injection. Overall, this experiment demonstrates the effective flow-controlling ability of surfactant-stabilized CO_2 foam at this level of heterogeneity. CO_2 foam was able to effectively block flow in the high permeability core and divert fluid to the low permeability core.

Figure 4-23 illustrates the variation in pressure and division ratio during a parallel core foam flooding experiment using a mixture of surfactant and nanoparticles. The permeability contrast in this experiment was around 8, which was notably higher than in the previous experiment, indicating medium heterogeneity. During primary water injection, the diversion ratio for the high-permeability core was nearly 100% because of the high level of heterogeneity. As a result, the fluid production from the low permeability was almost zero. The pressure drop during the water injection remained stable at around 2 psi.

Once surfactant-nanoparticles stabilized CO_2 foam was initiated, the division ratio for the low permeability core gradually increased, while the opposite changes were observed for the high permeability core. After 3 PV of CO_2 foam injection, the division ratio for the low permeability core reached 50% and continued to rise, reaching 80% by the end of the CO_2 foam flooding. Conversely, the division ratio in the high permeability core decreased due to a barrier formed in pores by the injected CO_2 foam.

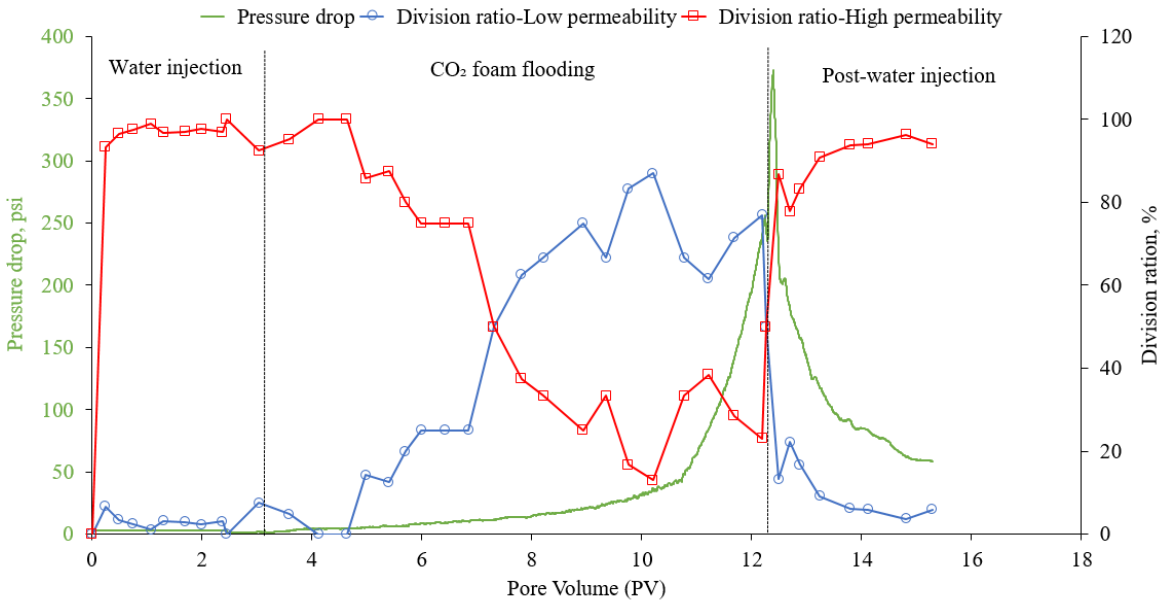

Figure 4-23. Dual core experiment with surfactant-nanoparticle-stabilized CO_2 foam (0.5wt% AOS+0.05wt% SiO_2) at 25°C and 500 psi, permeability ratio Vk=8.

The pressure drop showed a gradual increase during the first 8 PV of CO_2 foam flooding, indicating foam generation in the core. This was followed by a rapid increase, indicating foam generation in small pores required higher entry pressure. The pressure reached around 250 psi by the end of CO_2 foam flooding and continued to rise during the subsequent water injection, peaking at 350 psi. However, by the end of the post-water injection, the division ratio in the low permeability core had rapidly decreased to 10%, while it increased to 90% in the high permeability core. Meanwhile, the pressure gradient significantly decreased to 50 psi after 2 PV of water injection.

As shown in the Figures 4-22 and 4-23, the maximum pressure drop for the mixture reached 350 psi, while using surfactant alone resulted in a significantly lower pressure drop of 40 psi. Surfactant-stabilized foam experiments were conducted using core samples with permeabilities of 28 md and 65md, while core samples with permeabilities of 87 md and 11 md were utilized in the presence of nanoparticles. The permeability contrast between the lower-permeability core samples used in these experiments is approximately 3, while the observed ratio of pressure drop during the foam flooding is about 9. Given that all other parameters were the same, this difference indicates that the mixture produced stronger foam, resulting in a significantly higher pressure drop compared to surfactant only experiment. These findings reinforce the previous conclusions, emphasizing the benefits of nanoparticles in enhancing the properties of surfactant-stabilized CO_2 foam.

4.5 Oil Recovery Experiments

A series of oil recovery experiments were conducted to evaluate the recovery efficiency of foam flooding stabilized either with surfactant or with a mixture of surfactant and nanoparticles. In all experiments, waterflooding was performed first to achieve two-phase saturation of brine and residual oil in the core. The waterflooding began at an injection rate of 0.5 cc/min until no more was produced. The injection rate was then increased to 2 cc/min to overcome the capillary end effect and further reduced oil saturation. Afterward, CO_2 flooding was initiated at 1 cc/min, followed by CO_2 foam flooding as a tertiary EOR method. Co-injection of CO_2 and the foaming solution was performed at a constant total injection rate of 1 cc/min, with a gas fractional flow at 70% throughout all experiments.

Two sets of oil recovery experiments were conducted to investigate the ability of CO_2 foam to enhance oil recovery. One experiment used a 0.5 wt% AOS solution, while a mixture of 0.5 wt% AOS and 0.05 wt% SiO_2 was used for the second experiment. Both experiments were carried out under high and low temperature conditions to compare the impact of temperature on foam performance. The properties of the core samples and experimental conditions are given in Table 4-4.

Table 4-4. Core and experimental conditions for oil recovery experiments.

Core	Porosity, %	Permeability, mD	Experimental Conditions	Injection fluid
Ind12	18.8	45	1500 psi/80ºC	0.5% AOS solution
Ind13	18.9	39	1500 psi/80ºC	0.5% AOS + 0.05% SiO_2 solution
Ind14	19.5	63	1500 psi/40ºC	0.5% AOS solution
Ind15	19.5	45	1500 psi/40ºC	0.5% AOS + 0.05% SiO_2 solution
Ind16	20.1	175	500 psi/40ºC	0.5% AOS solution
Ind17	19.5	630	500 psi/40ºC	0.5% AOS solution

4.5.1 Oil Recovery Experiment at Elevated Temperature

Oil recovery and pressure drop for surfactant-stabilized CO_2 foam flooding were measured throughout the experiment, as shown in Figure 4-24. The oil recovery was calculated based on the produced oil volume and mass balance. The initial oil saturation in the Ind12 core was 0.62. Water breakthrough was observed at 0.37 PV, with an oil recovery factor of 27% OOIP at that point. The relatively early water breakthrough may have been caused by the discrepancy between the viscosities of the injected brine and oil, leading to an unfavorable viscosity ratio of 6. As a result, the water displacement front was unstable, and the injected brine bypassed some areas inside the homogeneous core, leaving behind trapped oil. Waterflooding at an injection rate of 0.5 cc/min recovered 49.3% of the OOIP, reducing

the oil saturation to 0.31. The pressure drop during this stage stabilized at around 8 psi. Increasing the brine injection rate to 2 cc/min resulted in an additional 10% of oil recovery, with a steady-state pressure at 22 psi. In total, 5 PV of brine were flooded into the core, recovering 58.4% of OOIP.

Following waterflooding, CO_2 flooding was conducted at a constant injection rate of 1 cc/min. CO_2 flooding recovered an additional 8% of OOIP after 2.5 PV of injection, reducing oil saturation to 0.21%. The pressure drop during CO_2 injection stabilized at around 2–3 psi.

In the subsequent step, the surfactant-stabilized CO_2 foam flooding gave an additional 8.9% of OOIP recovery after 3 PV of injection. The total oil recovery reached 75.3% of OOIP, with a final residual oil saturation of 0.15 During foam flooding, pressure drop gradually increased up to 12 psi before declining to 8.3 psi due to the reduction of oil saturation. Notably, no foam was observed in the production tube after the BPR during CO_2 foam flooding, indicating weak foam generation in the presence of oil inside the porous media.

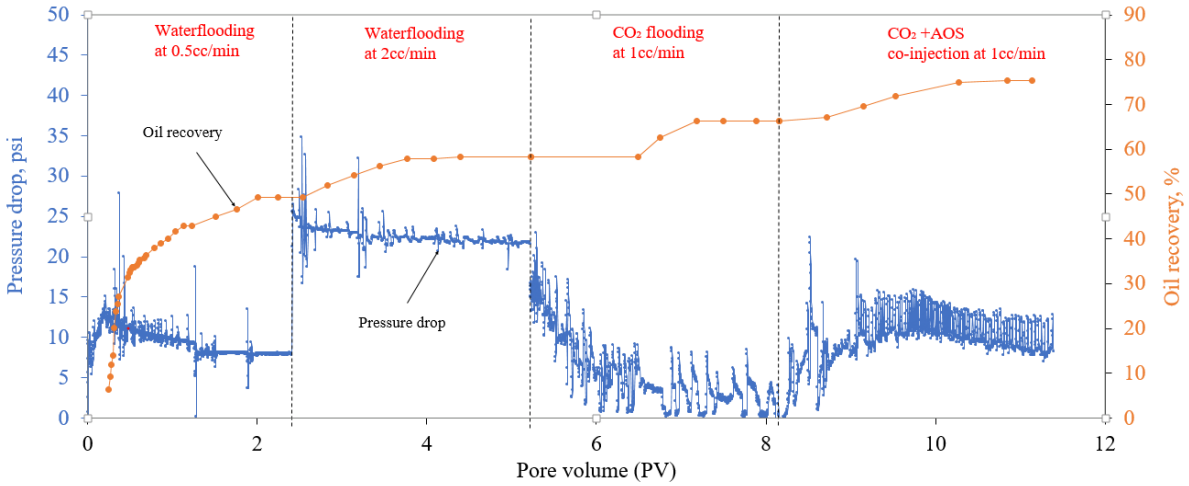

Figure 4-24. Oil recovery with surfactant-stabilized CO_2 foam (0.5wt% AOS) at 80ºC, 1500 psi.

The second experiment, as illustrated in Figure 4-25, involved the mixture of surfactant and NPs. The initial oil saturation in the Ind13 core was 0.59. The same injection procedures as in the previous experiment were followed in this run. Waterflooding recovered

approximately 61% of OOIP, with a steady-state pressure at 35 psi. As in the first experiment, at least 5 PV of brine was injected into the core until no oil production was observed to diminish the capillary end effects that might exist.

The oil recovery following CO_2 flooding was about 9.5% of the OOIP, reducing oil saturation to 0.17. Subsequent surfactant-nanoparticle-stabilized CO_2 foam flooding was able to produce an additional 12.1% of OOIP, even in the presence of oil. In total, the oil recovery following CO_2 foam flooding in the second experiment was around 82.8% of the OOIP. The pressure gradient during CO_2 foam flooding decreased and stabilized at around 20 psi.

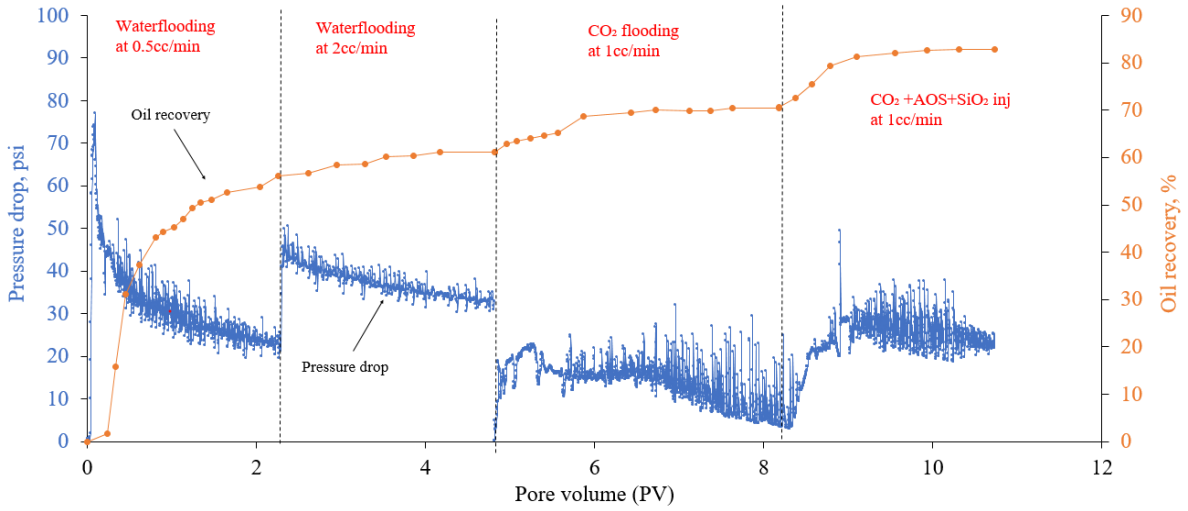

Figure 4-25. Oil recovery with surfactant-nanoparticle-stabilized CO_2 foam (0.5wt% AOS+0.05wt% SiO_2) at 80ºC and 1500 psi.

Oil recovery results and oil saturation prior to each injection schemes under high temperature conditions are presented in Figure 4-26. The oil recovery by CO_2 foam flooding in the presence of nanoparticles was approximately 3.2% higher compared to the experiment with surfactant alone. Additionally, the average pressure drop during CO_2 foam flooding with the nanoparticle mixture was 10 psi higher compared to the run with surfactant only. These results demonstrate the ability of nanoparticles to stabilize foam, further reducing CO_2 mobility and improving gas sweep efficiency, ultimately leading to greater oil recovery.

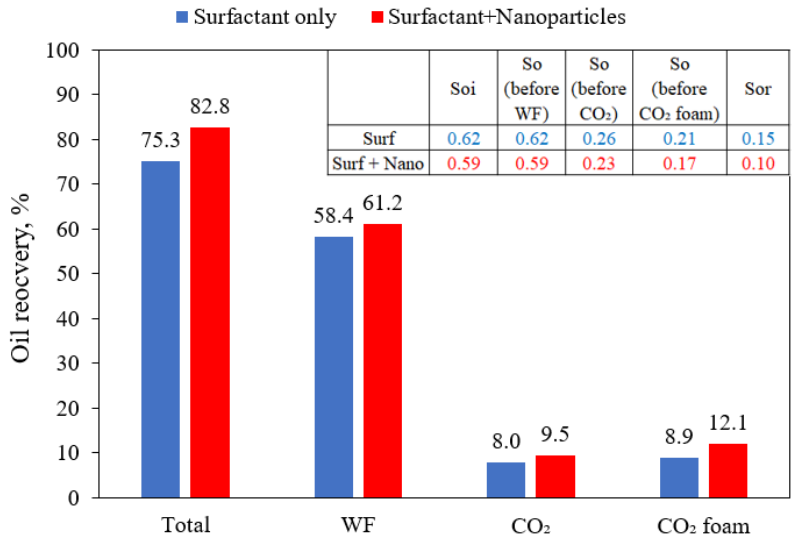

Figure 4-26. Oil recovery in the absence and presence of nanoparticles at 80ºC and 1500 psi.

4.5.2 Oil Recovery Experiment at Low-Temperature

Two oil recovery experiments were conducted at a low temperature of 40ºC, while the pressure was maintained at 1500 psi, consistent with the previous experiment. These experiments aimed to assess the ability of CO_2 foam to recover oil in the presence and absence of nanoparticles at low temperatures. Similar to the previous experiments, a 0.5 wt% AOS solution was used for the first experiment, while the second experiment was carried out using a mixture of 0.5% AOS and 0.05% SiO_2. Initial oil saturation in Ind14 core was 0.57.

In the surfactant-only experiment, waterflooding recovered about 48.9% of the OOIP as shown in Figure 4-27, reducing oil saturation to 0.28. As in the previous experiments, at least 5 PV of brine was injected to diminish the capillary end effect and ensure no further oil production during this process. CO_2 flooding recovered about 6.1% of OOIP with the steady-state pressure at 5 psi. Co-injection of CO_2 and surfactant solution produced about 14.2% of OOIP, reducing oil saturation to 0.16. During the surfactant-stabilized CO_2 foam flooding, the pressure gradient gradually increased and reached approximately 65 psi after 6 PV injections. The average pressure drop at low temperatures was significantly higher than at the high-temperature experiment at 80ºC. This suggests that high temperature has an adverse effect on foam stability in porous media, proving the results of bulk tests.

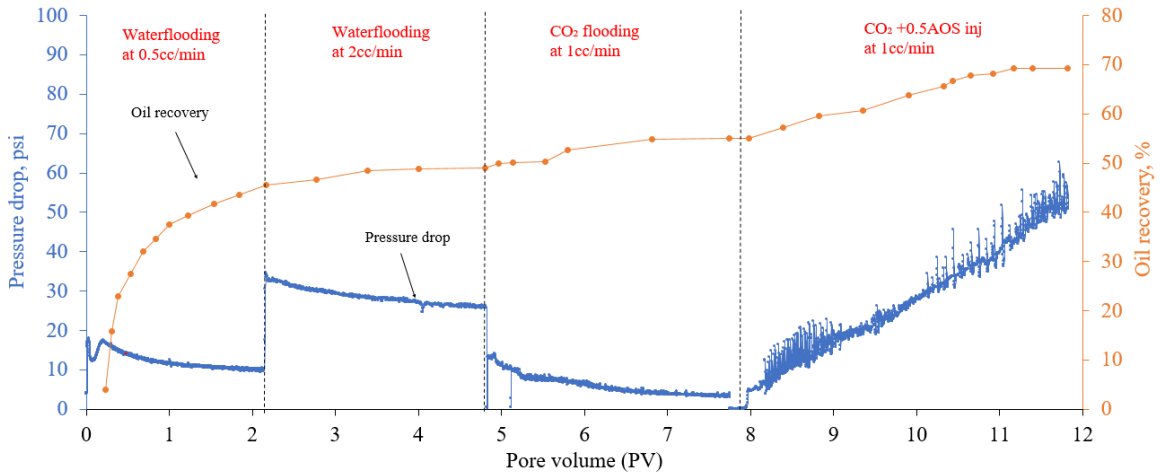

Figure 4-27. Oil recovery with surfactant-stabilized CO_2 foam (0.5wt% AOS) at 40ºC, 1500 psi.

In the subsequent experiment, as shown in Figure 4-28, a mixture of surfactant and nanoparticles was used. The same injection procedure as in the previous experiment was employed for this run. The initial oil saturation in the Ind15 core was 0.62. After 2 PV of brine injection at 0.5 cc/min, the oil recovery factor was 49% of the OOIP. However, only a minor amount of additional oil was produced when the injection rate was increased to 2 cc/min. The total oil recovery following extensive waterflooding was 49.5% of the OOIP, reducing oil saturation to 0.3.

Following this, CO_2 flooding recovered an additional 11.3% of the OOIP, with a steady-state pressure drop stabilizing around 6 psi. The oil recovery following the co-injection of CO_2 and the surfactant nanoparticles was around 19.7% of the OOIP, reducing the oil saturation to 0.12. The total oil recovery following CO_2 foam flooding was 80.5%. Additionally, the pressure gradient gradually rose throughout the foam flooding and reached about 190 psi after 6 PV of injection. As observed in the previous experiment, CO_2 foam flooding at low temperatures in the presence of nanoparticles resulted in a significantly higher pressure gradient compared to the high-temperature experiment. Furthermore, the average pressure drop for the mixture was higher than that for surfactant only, indicating the ability of nanoparticles to generate stronger and more stable foam.

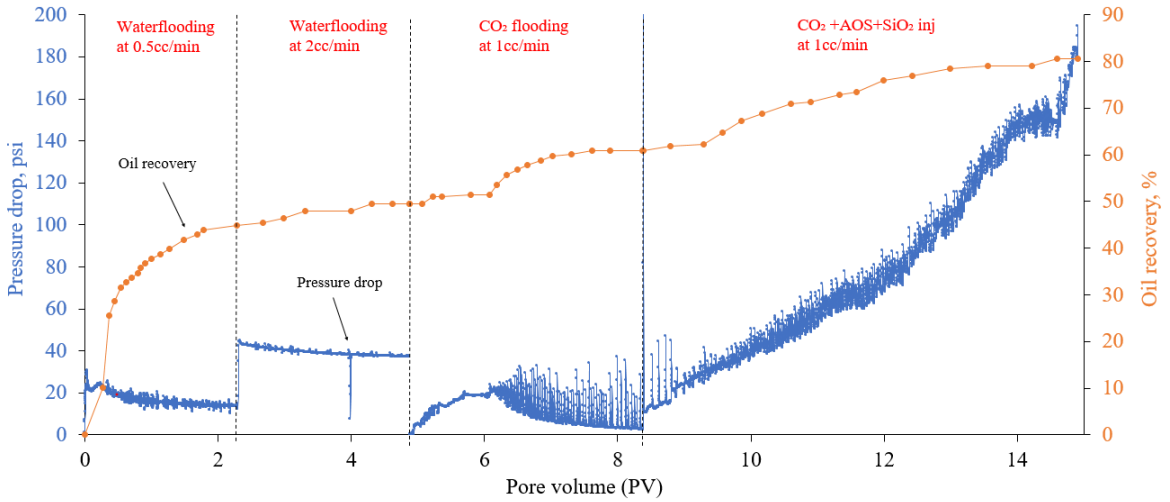

Figure 4-28. Oil recovery with surfactant-nanoparticle-stabilized CO_2 foam (0.5wt%AOS+0.05wt% SiO_2) at 40ºC and 1500 psi.

A comparison of the two oil recovery experiments and oil saturation changes at low temperature are presented in Figure 4-29. Similar to the high-temperature experiments, CO_2 foam stabilized by the mixture recovered 5.1% more oil compared to the surfactant-only case. These results demonstrate that the presence of nanoparticles leads to stronger and more stable foam generation, resulting in higher oil recovery and a greater pressure gradient.

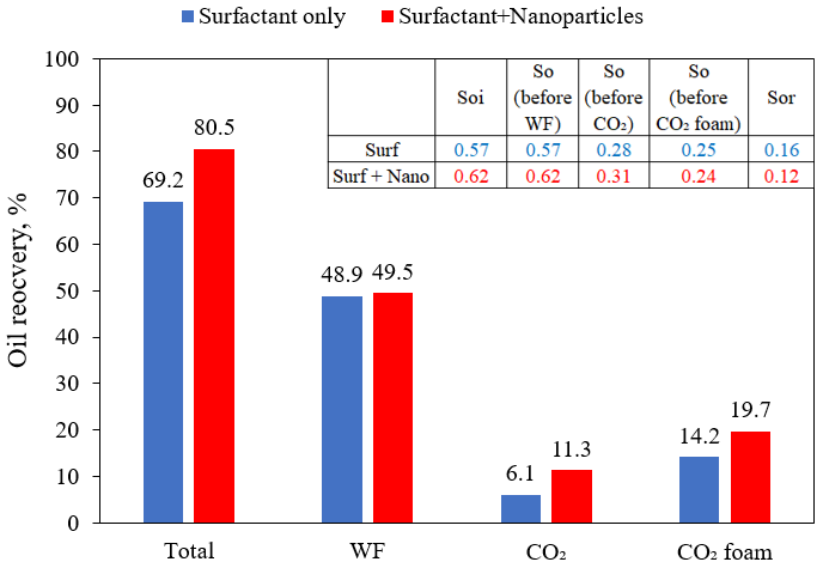

	Soi	So (before WF)	So (before CO_2)	So (before CO_2 foam)	Sor
Surf	0.57	0.57	0.28	0.25	0.16
Surf + Nano	0.62	0.62	0.31	0.24	0.12

Figure 4-29. Oil recovery in the absence and presence of nanoparticles at 40ºC and 1500 psi.

Total oil recovery was higher at high temperature compared to low temperature condition as the increase in temperature led to a reduction in oil viscosity. As shown in Figure 3-3, oil viscosity decreased from 20 cp to 5 cp when temperature rose from 40℃ to 80℃, reducing the viscosity ratio between injected water and oil. This resulted in improved sweep efficiency. Consequently, oil recovery followed by waterflooding was around 60% of OOIP at high temperature, compared to 50% OOIP at low temperature. Additionally, the reduction in oil viscosity at high temperature slightly increased oil recovery during CO_2 flooding due to more favorable mobility conditions.

However, CO_2 foam stabilized with either surfactant or surfactant-nanoparticles exhibited better oil recovery efficiency at low temperatures than at high temperatures. This can be attributed to the lower foamability and stability of CO_2 foam at high temperatures, as an increase in temperature accelerates the motion of molecules, causing faster coalescence and collapse of foam bubbles. At low temperatures, surfactant-stabilized CO_2 foam recovered 5.7% and 7.6% more oil in the absence and presence of nanoparticles, respectively, compared to high temperature conditions.

Overall, at both low and high temperatures, the presence of nanoparticles resulted in higher oil recovery compared to their absence, demonstrating the ability of nanoparticles to enhance and stabilize foam, even in the presence of oil. However, as seen in Figures 4-26 and 4-29, residual oil saturation before surfactant-stabilized CO_2 foam was slightly higher than before injection of surfactant-nanoparticle-stabilized CO_2 foam, with a difference ranging from 0.02 to 0.04. This difference is considered negligible, and its impact on foam stability can be ignored. Nonetheless, it is recommended to investigate the oil saturation on foam stability in the presence and absence of nanoparticles in future works.

4.5.3 The Co-injection of CO_2 and Brine

Two sets of core flooding experiments were conducted to evaluate the oil recovery performance of CO_2 and brine co-injection, with and without a foam agent, under both high and low temperature conditions. The injection scheme in this run was the same as in the previous experiment with oil, except that a co-injection of CO_2 and brine was conducted before CO_2 foam flooding stabilized with 0.5 wt% AOS. This sequential injection approach allowed for a direct comparison between conventional CO_2/brine co-injection and CO_2 foam

flooding, providing insights into the impact of foam generation on oil recovery under varying thermal conditions.

First oil recovery experiments was conducted using Ind16 core with an absolute permeability of 175 mD at 500 psi, while the temperature was kept at 80ºC. Under this experimental condition CO_2 was in the gas phase. The initial oil saturation in this experiment was 0.62. The cumulative oil recovery and differential pressure profile are shown in Figure 4-30. Initially, 2 PV of brine was injected at 0.5 cc/min, which reduced oil saturation to 0.24 and recovered around 60% of oil. Then the core was flooded with 3 PV of brine at 2 cc/min to avoid capillary end effect. During this stage, the volume of oil production was insignificant, and total oil recovery following waterflooding was around 63% of the OOIP. The pressure drop was around 6 and 16 psi during the first and second stages of waterflooding, respectively.

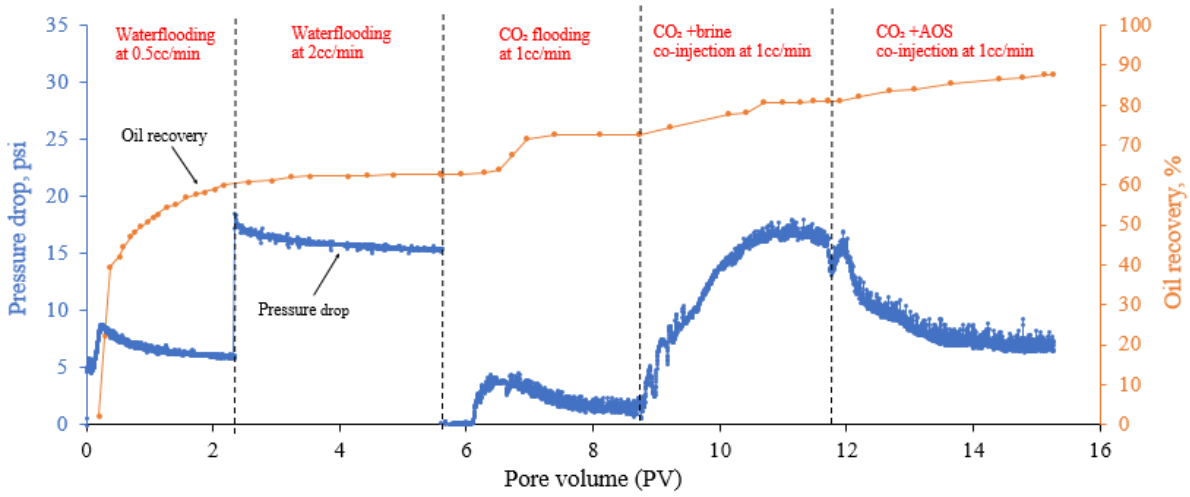

Figure 4-30. Oil recovery following waterflooding, CO_2 flooding, CO_2 +brine and foam injection, at 80ºC and 500 psi.

Following this, gas CO_2 flooding at 1cc/min was started. CO_2 flooding was able to produce approximately 10% of the OOIP and the average pressure drop was about 9 psi. Next, the co-injection of CO_2 and brine was conducted at 1 cc/min with a fixed gas fractional flow of 70%. An additional 8.5% of the OOIP was produced by co-injection of CO_2 and brine. The average pressure drop continuously increased until stabilized at around 16 psi at the end of the injection stage. This means that the co-injection of brine with CO_2 reduced gas mobility, improving the displacement efficiency and resulting in incremental oil

recovery. Co-injection of CO_2 and 0.5wt% AOS surfactant was then started at 1 cc/min rate with constant gas fractional flow of 70%. The injection was continued up to 5 PV of injection and recovered an additional 6.5% of the OOIP. Initially, the pressure drop was 14.3 psi and gradually decreased to 7 psi during foam injection. In-situ generated foam displaced water; thus, water saturation decreased and gas saturation increased, which resulted in a pressure reduction. Overall, ultimate oil recovery after all stages was 87.5% and the remaining oil saturation was 7.5%.

Second oil recovery experiments was conducted using a 630 mD Ind17 core sample at 40℃ and 500 psi. The injection process was conducted following the same injection scheme as in the previous test. The cumulative oil recovery and differential pressure profile are shown in Figure 4-31. The initial oil saturation was 58.4%. Waterflooding was able to recover 46.5% of the OOIP and reduced oil saturation to 31.4%. Overall, 7 PV of brine was injected to overcome the capillary end effect, and the pressure drop was 17 psi at 1c/min, and doubled at 2 cc/min.

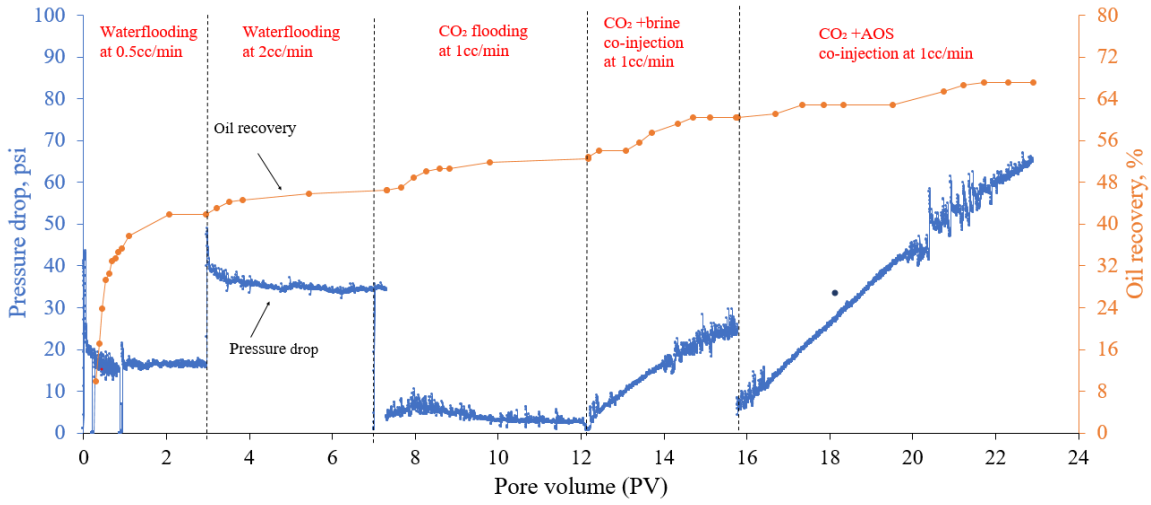

Figure 4-31. Oil recovery following waterflooding, CO_2 flooding, CO_2 +brine and foam injection, at 40ºC and 500 psi.

Following the waterflooding, CO_2 was injected at 1cc/min and produced an additional 6% of the OOIP. The pressure drop during this stage stabilized at around 2.5 psi. The subsequent co-injection of CO_2 and brine at 1 cc/min with 70% ratio significantly increased pressure difference by 25 psi after 3 PV of injection and another 8% of the OOIP was recovered. Then, the co-injection of CO_2 and 0.5% AOS solution was initiated, and the

pressure drop rose rapidly during this stage, reaching 65 psi at the end of the injection stage. 7 PV of gas and surfactant solution in total were co-injected, which gave around 7% of the OOIP. The ultimate oil recovery reached 67.14%, and the residual oil saturation was 19.5%.

The experimental studies with oil-saturated cores show that the co-injection of CO_2 and 0.5wt% AOS surfactant enhanced oil recovery by 6–9% despite extensive secondary IOR, which indicates the ability of foam to increase even microscopic displacement efficiency by mitigating preferential flow paths- and heterogeneity even at the core scale.

As illustrated in Figures 4-30 and 4-31, the pressure drop observed during the co-injection of CO_2 and brine at elevated temperature was slightly higher than that recorded during CO_2 foam flooding. This indicates that little to no stable foam was generated in the porous media because of detrimental effect of oil and elevated temperature. Despite this, the co-injection of CO_2 with the surfactant solution resulted in some additional oil recovery, likely attributed to the improved mobility control by the co-injection method. However, when the temperature was reduced to 40 °C, a notably higher pressure drop was observed during surfactant-stabilized CO_2 foam flooding relative to the co-injection without foam. Furthermore, the pressure profile for CO_2 foam showed a more rapid increase, suggesting more effective foam propagation and resistance to gas flow.

These findings demonstrate that at lower temperatures, surfactant-stabilized CO_2 foam provides better mobility control and oil recovery performance compared to CO_2/brine co-injection. The results also highlight the adverse impact of elevated temperature and crude oil on foam generation and stability, which compromises the effectiveness of foam-assisted gas injection under such conditions.

4.6 Summary

Anionic surfactant, alpha-olefin sulfonate, and silicon oxide nanoparticles were used in this study to improve the stability of CO_2 foam under various reservoir conditions. A series of bulk tests were conducted to assess the ability of surfactant and nanoparticles to stabilize CO_2 foam under various temperatures, salinities, and oil presence in bulk fluid. Dynamic foam flooding experiments using brine-saturated Indiana limestone cores were carried out to evaluate foam generation and propagation in porous media. The oil recovery efficiency of surfactant and surfactant-nanoparticle stabilized CO_2 foam was examined

through several coreflooding experiments at both elevated- and low-temperature conditions. A dual-core holder system was used to assess the flow diversion efficiency of CO_2 foam generated in porous media. Based on the results, the following conclusions can be drawn from this study:

- The variation of AOS surfactant concentration from 0.1% to 1 wt% in brine, which mimics the salinity of Caspian seawater, had a minimal effect on foam-half life and generated foam volume during bulk tests at ambient conditions. The surfactant-stabilized foam demonstrated the same stability as temperature increased from 20℃ to 50℃, however, it became significantly less stable with the further increases in temperature to 80℃. Increasing oil saturation from 0 to 5% at ambient conditions negatively affected foam stability. The addition of 0.05% nanoparticles to the 0.5wt% surfactant solution slightly improved foam stability at ambient conditions, however, further increasing nanoparticle concentration led to precipitation.
- A gas fraction of 0.7 generated the strongest foam during the foam quality scan, achieving a pressure drop of 100 psi with a 0.5 wt% surfactant concentration at 40°C and 1500 psi, compared to pressure drop of 5 psi without foaming agents, demonstrating the foam's ability to mitigate CO_2 mobility. The presence of SiO_2 improved surfactant-stabilized foam stability, increasing the apparent viscosity from 20 cp to 31 cp under reservoir conditions. Both surfactant- and surfactant–nanoparticle-stabilized CO_2 foams exhibited higher apparent viscosity as the temperature decreased from 80 °C to 40 °C, underscoring the negative impact of elevated temperatures on foam properties in porous media.
- Dual-core experiments showed that the both surfactant- and surfactant-nanoparticle stabilized CO_2 foam effectively diverted flow from high-permeability areas to low-permeability areas in cores with various permeability ratio.
- Positive entering and bridging coefficients, obtained during IFT measurements, suggest that oil will penetrate the lamellae and form a bridge between two liquid interfaces, while a positive spreading coefficient indicates that oil spreads on foam bubble surfaces, destabilizing the foam. These effects suggest that crude oil reduces foam stability, which is consistent with bulk test results.
- Oil recovery experiments were conducted at 80℃ and 40℃ temperatures. The injection sequence for oil recovery included waterflooding, followed by CO_2 flooding, and

finally CO_2 foam flooding as a tertiary method. At elevated temperature, the synergistic effect of nanoparticle-surfactant resulted in 12% incremental oil recovery, 3.2% higher than surfactant alone. At low temperature, CO_2 stabilized by surfactant and nanoparticles recovered 19.7% OOIP, while 14.6% oil was achieved with surfactant-stabilized CO_2 foam flooding. These results highlight the benefits of nanoparticles in stabilizing CO_2 foam for enhanced oil recovery.

- The combined effect of elevated temperature and crude oil resulted in weak and poorly stable CO_2 foam generation within the porous media. As a result, the mobility control efficiency of the surfactant-stabilized CO_2 foam under these conditions was comparable to that of CO_2 and brine co-injection without a foaming agent.

CHAPTER 5. Numerical Simulation of CO_2 Foam Mobility Control

In reservoir engineering, numerical modeling plays a crucial role by enabling project simulations without the need for costly and time-consuming trial and error in real-world scenarios [174]. Accurate reservoir modeling is essential for predicting the desired production performance of hydrocarbon reservoirs under varying conditions. Simulators are an essential component for preparation needed for a successful flooding operation [175].

In conjunction with experimental research, numerical modeling can be used to study CO_2 foam. In order to create models that can precisely forecast reservoir performance under different operational conditions, numerical modeling integrates mathematics, physics, computer programming, and reservoir engineering [176, 177]. This section outlines the simulation techniques employed to investigate gas injection and gas foam enhanced oil recovery (EOR) methods

5.1 Methodology

5.1.1 Reservoir Model Parameters

Prior to foam flooding, the oil recovery efficiencies of various gases, namely methane (CH_4), CO_2, and sour gas, were compared using a 2D reservoir model. Sour gas is defined as natural gas containing a significant amount of hydrogen sulfide. In this study, a 15.9% H_2S composition of sour gas produced from an oil reservoir in Kazakhstan was used. The sour gas was chosen for our study as sour gas injection has been successfully implemented in several large oil fields in Kazakhstan to support reservoir pressure and improve oil displacement [178]. Table 5-1 lists the properties of gases used in this study under reservoir conditions (1500 pressure and 80°C).

Table 5-1. Viscosity and density of different gases

Gas type	Viscosity, cp	Density, g/cm^3
CH_4	0.020	0.146
Sour	0.031	0.267
CO_2	0.051	0.639

A 2D homogeneous reservoir model with dimensions of 1040 feet by 20 feet by 100 feet was constructed to gain a better understanding of the vertical sweep efficiency of various gas injections. The reservoir model has 52 x 1 x 20 grid blocks with a permeability of 50 md and a porosity of 0.2. The production well's BHP was set at 1500 psi, while the reservoir's initial pressure was 1750 psi. The initial oil saturation was 0.2, and the initial reservoir temperature was 40℃, which was selected as the highest temperature for stable foam flooding based on the experimental study. Both the production and injection wells were perforated through every vertical layer with a steady reservoir flow rate.

To investigate the effect of permeability heterogeneity on gas injection, the study employed a 2D heterogeneous reservoir model with a geostatistically generated permeability. The heterogeneity permeability field was generated based on the methods described by [179]. The horizontal permeability was in the range from 0.003 to 1000 md, and the vertical permeability to horizontal permeability was taken as 0.1. Figure 5-1 displays the permeability distribution profile on a log scale. The reservoir and well parameters were the same as those in the homogeneous model. During gas flooding, the gas was injected into the bottom layer, while oil was produced from the upper layer to minimize the effect of gravity segregation and improve sweep efficiency during gas flooding. The simulated gas flooding was conducted for ten years. The same 2D heterogeneous and homogeneous models were used further to study CO_2 foam flooding.

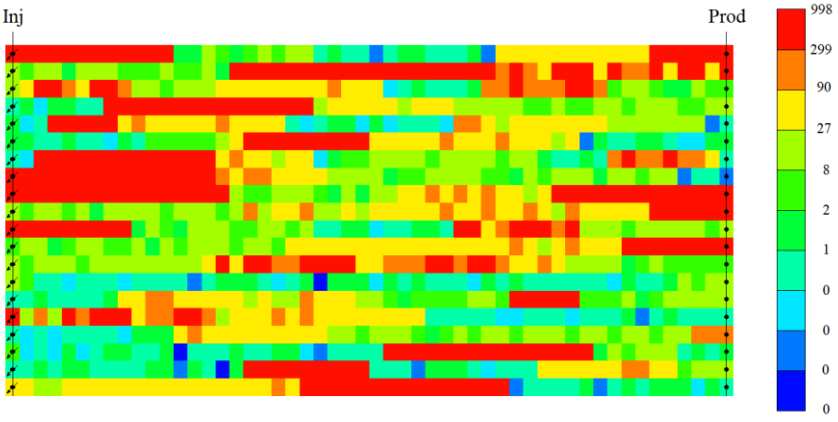

Figure 5-1. Heterogeneous permeability field in log scale.

3D heterogeneous reservoir model

A 3D heterogeneous reservoir model was used for comparison between various injection methods, namely CO_2 flooding, the co-injection of CO_2 and brine, and CO_2 foam flooding. Using the 3D model shown in Figure 5-2 gives opportunities to assess both vertical and areal sweep efficiency of EOR methods considered in this study. The reservoir model is 1200 feet long, 1250 feet wide, and 150 feet thick. The reservoir model measures 24 x 25 x 15 on the Cartesian grid. The parameters of the reservoir simulation model are as follows: the porosity is 0.2, the initial reservoir pressure is 1750 psi, and the temperature is 40ºC. The horizontal permeability is in the range from 0.003 to 300 md, and the vertical permeability to horizontal permeability is taken as 0.1. The heterogeneity permeability field was generated based on the methods described by [179]. Two injection wells were considered to simulate foam flooding: one for gas injection and one for water injection. In the water injection well, the surfactant is mixed with water. During the foam flooding, both production and injection wells were perforated across all layers.

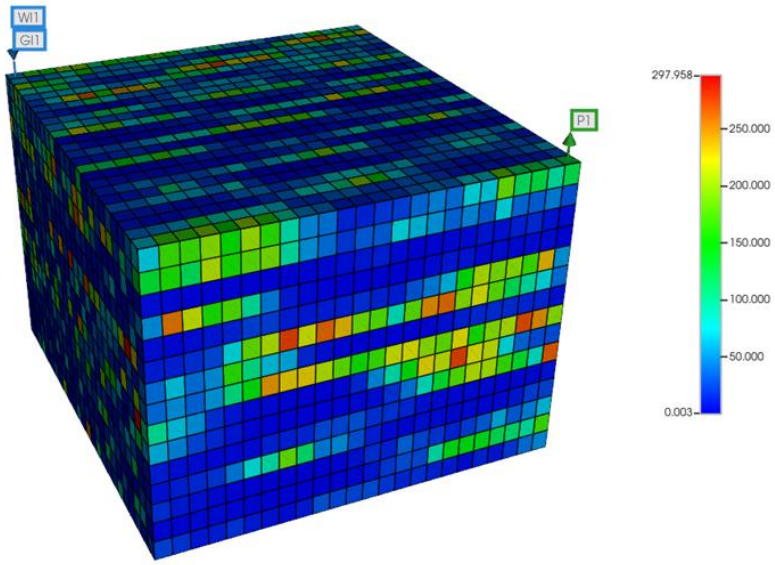

Figure 5-2. 3D heterogeneous reservoir model.

Figure 5-3 displays the oil, gas, and water relative permeability curves utilized in our analysis. Table 5-2 lists the main reservoir model parameters as well as the injection and production wells operating conditions.

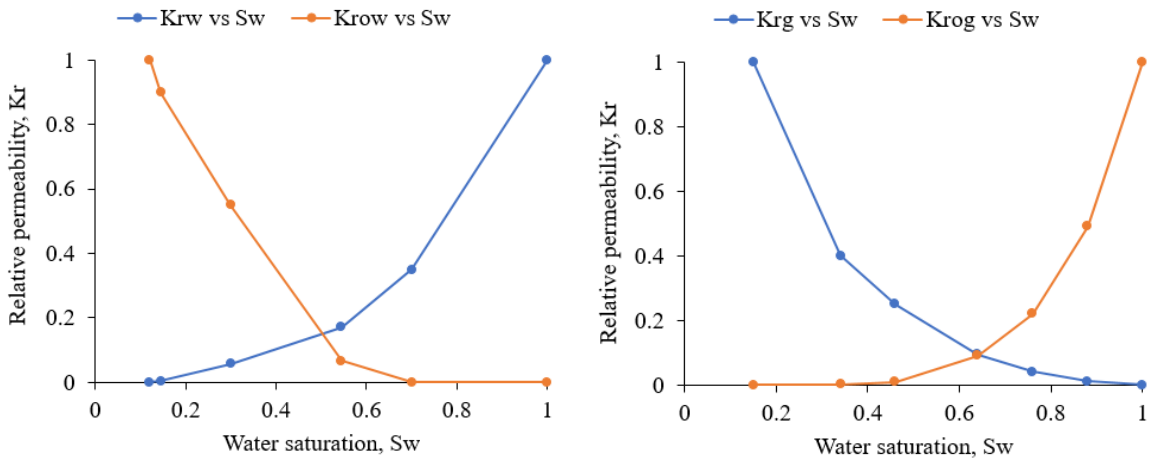

Figure 5-3. Relative permeability curves used in this study.

Table 5-2. Input parameters of the base 3D reservoir model.

Parameter	Value
Number of grid blocks	24×25×15
Block dimensions (W×L×H)	50ft×50ft×10 ft
Porosity	0.2
Reservoir temperature	212 °F
Initial reservoir pressure	1750 psi
Initial water saturation	0.12
Residual oil saturation	0.3
Minimum producer BHP	1500 psi
Maximum producer gas rate	3 MMscf/D

5.1.2 STARS Foam Modeling

To simulate CO_2 foam flooding, the STARS simulator developed by Computer Modeling Group LTD. was employed. The STARS foam model is widely recognized as the

most popular commercial simulator for foam flooding [180, 181]. In this model, the foam flow is assumed to be at the local equilibrium condition. In STARS simulator, apparent viscosity refers to the effective viscosity of the foam, which is influenced by factors like foam quality, water saturation, and shear rate. The simulator uses a local equilibrium (LE) foam model where foam behavior is introduced by modifying the gas relative permeability [182]. In the presence of foam, the gas relative permeability, k_{rg}^{f}, is determined by multiplying a dimensionless interpolation factor (FM) by the gas permeability without foam, k_{rg}^{nf}, as shown in Equation 5.1:

$$k_{rg}^{f} = k_{rg}^{nf} * FM \tag{5.1}$$

where k_{rg}^{f} is the gas permeability during foam injection, k_{rg}^{nf} is the gas permeability without foam.

FM is a weighting factor used to characterize foam strength. FM is equal to 1 in the absence of foam, and decreases as foam becomes stronger. FM can be determined by Equation 5.2:

$$FM = \frac{1}{1+fmmob*F_{water}*F_{surf}*F_{shear}*F_{oil}*\ldots..} \tag{5.2}$$

In Equation 5.2, fmmob is the base foam mobility reduction factor without the effects of various factors. Different factors affecting fmmob are surfactant concentration, water and oil saturation, gas flow rate, and capillary number. These factors are determined by Equations 5.3 to Equation 5.4:

$$F_{water} = 0.5 + \frac{\arctan[epdry(S_w - fmdry)}{\pi} \tag{5.3}$$

$$F_{surf} = \begin{cases} (\frac{C_{sw}}{fmsurf})^{epsurf} & for\ C_{sw} < fmsurf \\ 1 & for\ C_{sw} \geq fmsurf \end{cases} \tag{5.4}$$

$$F_{shear} = (\frac{fmcap}{N_{ca}})^{epcap} \tag{5.5}$$

$$F_{oil} = \begin{cases} 0 & for\ S_o > floil \\ \left(\frac{fmoil - S_o}{fmoil - floil}\right)^{epoil} & for\ floil < S_o < fmoil \\ 1 & for\ S_o < floil \end{cases} \quad (5.6)$$

In the F_{water} function, S_w is the water saturation in grids, fmdry is the critical water saturation, and epdry is the parameter that controls the relative permeability curve's slope close to the critical water saturation. In the F_{surf} function, C_{sw} is the surfactant concentration in grids, fmsurf is the critical surfactant fraction when foam strength begins to deteriorate due to a drop in surfactant content, and epsurf is the factor that governs the effects of the concentration of surfactant on gas mobility. In the F_{shear} function, N_{ca} is the capillary number, fmcap is the capillary number for the reference foam, and epcap is the parameter that governs the effect of the capillary number on FM function. In the F_{oil} function, S_o is the oil saturation in grids, fmoil is the maximum oil saturation when foam totally collapses, floil is the lowest oil saturation, below which oil does not have an effect on foam strength, and epoil is the parameter that controls the oil saturation contribution in the FM function. In the STARS, foam forms quickly anywhere there is simultaneous presence of gas, water, and surfactant.

The CMG-STARS was used to simulate the CO_2 foam flooding using the parameters derived from the experimental data of surfactant-stabilized CO_2 foam in the core. All of these parameters were derived from the two-phase flow (gas/surfactant) foam flooding experiments. Using various oil saturation-dependent function parameters, epoil and fmoil, a sensitivity analysis was conducted to examine their effect on oil saturation or CO_2 saturation.

5.2 Simulation Results

5.2.1 Effect of Gas Type on Oil Recovery

Figure 5-4 shows the impact of the different gases on GOR. The findings show that CH_4 injection led to the earliest gas breakthrough time because of low density and viscosity, as shown in Table 5-1. In contrast, the injection of CO_2, due to its higher density and viscosity, significantly delayed gas breakthrough. The GOR for sour gas injection was slightly higher compared to CO_2 but lower than during CH_4 injection. This can be attributed to the presence of H_2S in the injected gas, resulting in higher density and viscosity.

Figure 5-4. Gas oil ratio for three gas injection scenarios.

Figure 5-5 compares the oil recovery efficiency of injecting different gases into the 2D homogenous model. The earliest gas breakthrough of CH_4 resulted in the lowest oil recovery, while sour gas injection achieved a slightly higher oil recovery because of its better oil displacement efficiency and later gas breakthrough. CO_2, performs significantly better than both CH_4 and sour gas, recovering almost 76% OOIP.

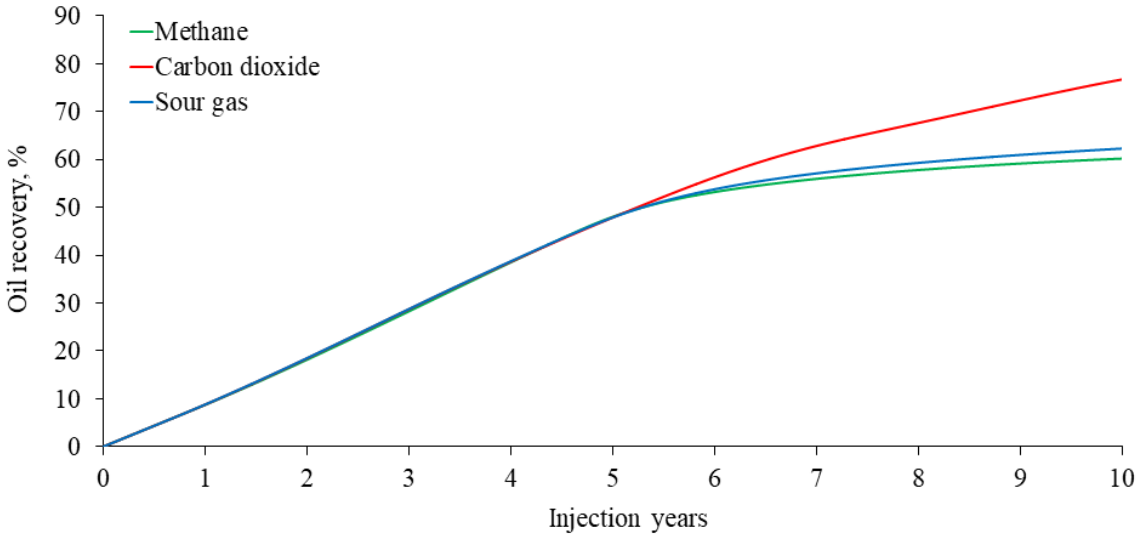

Figure 5-5. Oil recovery of injecting various gases into the 2D homogenous model.

Gravity segregations, resulting from the density differential between the injected gas and reservoir oil, significantly affect the effectiveness of oil displacement across the 2D model's cross-section. Vertical sweep efficiency is reduced because the injected gas tends to migrate to the top layer due to its lower density compared to oil. The change in vertical sweep efficiency can be quantitatively assessed using the viscous gravitational number (N_{gv}). The following equation can be used to express the viscous gravitational number [183]:

$$N_{gv} = \frac{k_v k_{rs} \Delta\rho g cos\alpha AL}{q_s \mu_s h} \tag{5.7}$$

where k_v is the vertical permeability, k_{rs} the relative permeability, $\Delta\rho$ is density difference between displacing and displaced phases, A is the cross section area, L is the reservoir length, q_s is the flow rate of the displacing phase, μ_s is the viscosity of displacing phase, g is gravity acceleration constant, and h is the reservoir thickness. If N_{gv}< 0.1, viscous forces dominate, if N_{gv}> 10, gravity dominates, and 0.1 < N_{gv} < 10 indicates intermediate balance.

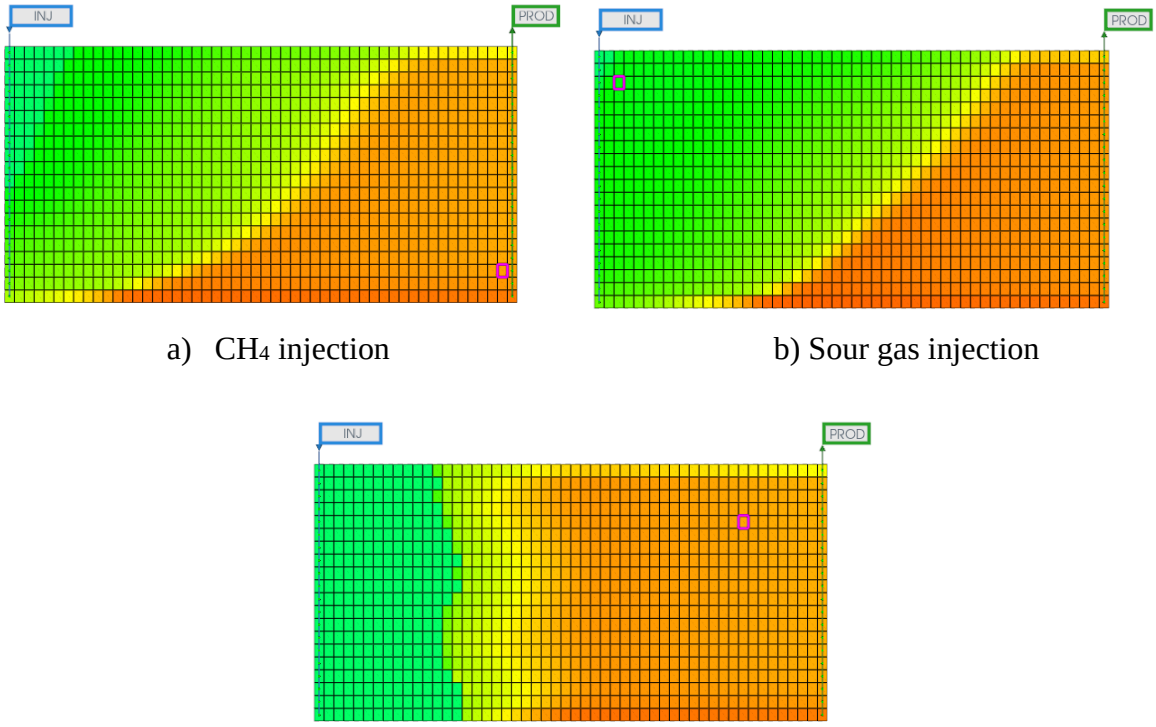

a) CH_4 injection

b) Sour gas injection

c) CO_2 injection

Figure 5-6. Oil saturation distribution.

Table 5-1 shows that the density of CO_2 is the highest viscosity and density under reservoir conditions. Thus, as Figure 5-6 confirms, gravity segregation should be more noticeable in sour gas and CH_4 injection. As can be seen, sour gas and CH_4 both overrode oil and caused early gas breakthrough, whereas CO_2 produced almost vertical displacement fronts that are advantageous for obtaining greater oil recovery

5.2.2 Effect of Heterogeneity

Figure 5-7 compares the effects of permeability heterogeneity on the GOR and oil recovery performance of CO_2 flooding. In a heterogeneous reservoir, CO_2 injection led to earlier gas breakthrough in high-permeability zones, causing a faster decline in the oil production rate compared to a homogeneous reservoir. As a result, CO_2 injection into the heterogeneous oil reservoir achieved 63% oil recovery, while the homogeneous model resulted in 76% oil recovery.

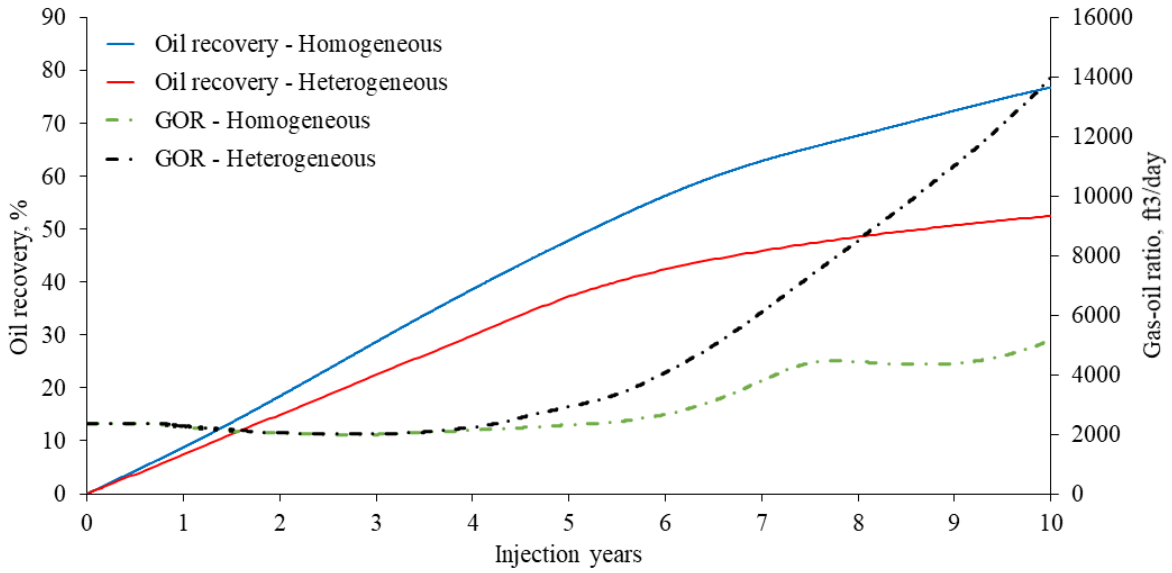

Figure 5-7. Effect of permeability heterogeneity on oil recovery during CO_2 flooding.

The oil saturation distribution after 1 year of CO_2 injection into both homogeneous and heterogeneous reservoirs is displayed in Figure 5-8. As seen in the figure, in the heterogeneous reservoir, the gas front moves more quickly through the high-permeability zones in the horizontal direction compared to the homogeneous model. As a result, the bottom layers of the heterogeneous reservoir are not adequately swept, leading to a

significant reduction in oil recovery. This comparison shows that the permeability heterogeneity negatively impacts CO_2 EOR under the selected reservoir characteristics, emphasizing the need for mobility control techniques, such as foam flooding.

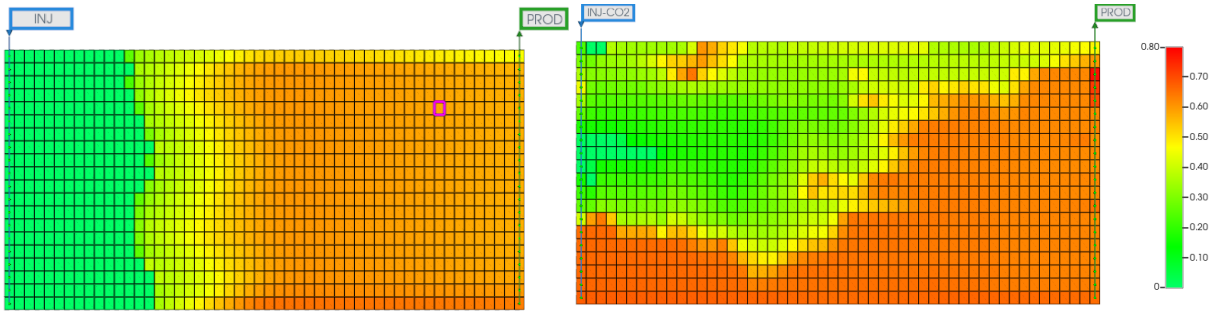

a) Homogeneous reservoir b) Heterogeneous reservoir

Figure 5-8. Gas-oil displacement fronts after one year of CO_2 flooding.

5.2.3 Foam Simulation Input Parameters

The validation of the foam model against experimental results was not performed in this study due to time constraints. Instead, it has been proposed as part of future work, which will incorporate validation based on experimental data, mineralogy, reservoir heterogeneity, well spacing, and field operating conditions. Nevertheless, the STARS simulation parameters presented in this section were derived from foam flooding experimental results.

In order to estimate the fmmob, epsurf, and fmsurf values—which are subsequently used for foam simulation—the foam quality scan data was fitted using the foam dry - out function. The continuous curve in Figure 5-9 represents the fitting curve derived from the STARS foam model. As shown in the figure, the CO_2 foam stabilized by 0.5 wt% AOS surfactant exhibited a high apparent viscosity of approximately 50 cp when the gas fractional flow was maintained at 70%. The rest of the foam parameters are given in Table 5-3. Fmoil and epoil value was selected based on the EOR experiments.

Table 5-3. STARS parameters.

STARS parameters	fmmob	fmsurf	fmcap	fmoil	epsurf	epcap	epoil
Fitted values	190	0.00047	1.2E-06	0.5	0.215	0.71	1

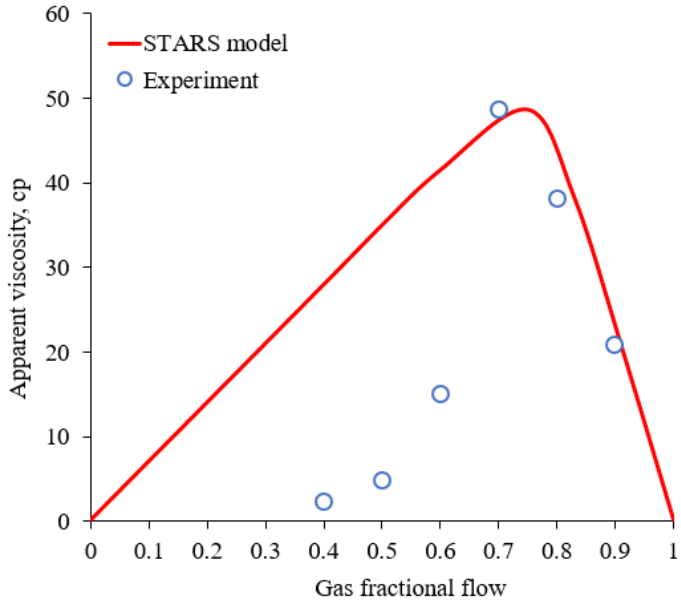

Figure 5-9. Experimental results for CO_2 foam quality scan and fitting with STARS model.

5.2.4 2D Reservoir Foam Simulation

Three distinct injection scenarios were compared using the 2D heterogeneous reservoir model, namely CO_2 flooding, the co-injection of CO_2 and brine, and CO_2 foam flooding. The total gas and liquid rates at reservoir conditions were kept consistent across all three scenarios. In both co-injection cases, in the absence and presence of surfactant, the fractional flow of CO_2 and liquid at reservoir conditions was maintained at 70%, which was determined as the optimal foam quality during the foam flooding experiments. The reservoir gas injection rate was 2400 ft^3/day, and the water injection rate was 1060 ft^3/day. The initial reservoir pressure was 1750 psi, and the bottomhole pressure of the production well was 1500 psi. The reservoir temperature was 40°C, the same as in the previous gas flooding simulations. The reservoir models were simulated for 15 years. The oil saturation distribution after 5 years of injection and GOR at the production well under surface conditions for all three injection scenarios are shown in Figure 5-10 and Figure 5-11, respectively.

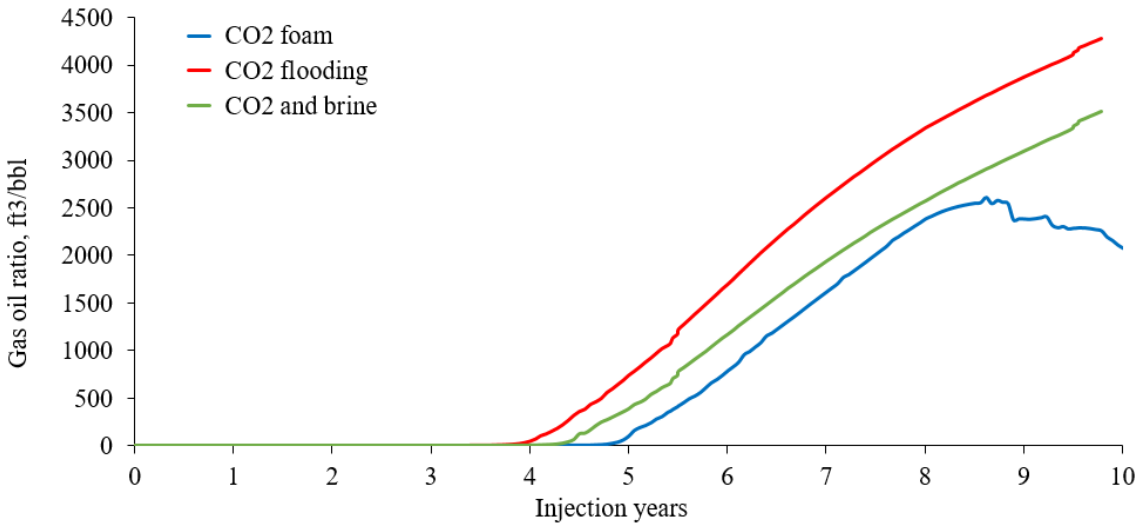

Figure 5-10. Gas-oil ratio for different injection scenarios using a 2D heterogeneous model.

As seen in the figures, in the heterogeneous reservoir, during CO_2 flooding, the injected gas expanded and became more mobile, causing the front of the injected CO_2 gas to move faster than in the other two scenarios. This resulted in higher gas saturation in the layer and deeper penetration of CO_2 into the high-permeability areas. As a result, the injected CO_2 moved more quickly than the viscous reservoir oil, bypassing reservoir areas with low permeability. Consequently, gas breakthrough occurred earlier at the production wells, leading to a sharp increase in GOR and reduced sweep efficiency.

In contrast, when CO_2 foam flooding was conducted, the displacement front moved slower compared to CO_2 flooding as foam reduced CO_2 mobility and selectively blocked high- permeability areas. Therefore, CO_2 foam flooding exhibited a uniform displacement and higher vertical sweep efficiency than the other injection scenarios. Additionally, CO_2 foam flooding delayed the gas breakthrough through the production well, resulting in a lower produced GOR.

The co-injection of CO_2 and brine, in the absence of surfactant, demonstrated better sweep efficiency than gas flooding. However, compared to CO_2 foam flooding, this method left more unswept areas in the upper part of the reservoir. As a result, during the the co-injection, gas breakthrough occurred slightly earlier than with CO_2 foam flooding. These results highlight the effectiveness of foam flooding in reducing CO_2 mobility, delaying gas breakthrough, and improving sweep efficiency.

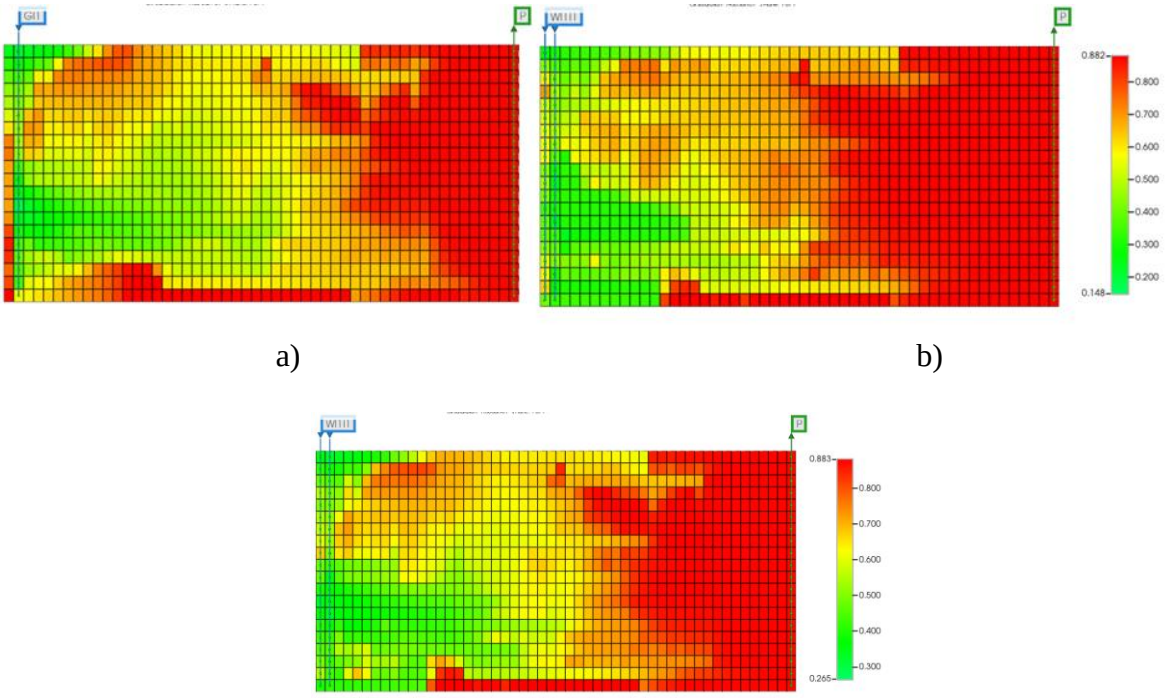

Figure 5-11. Oil saturation distribution after 5 years of a) CO_2 flooding b) CO_2 foam flooding c) the co-injection of CO_2 and brine.

Figure 5-12 compares the oil recovery efficiency of three injection scenarios. As shown, the oil recovery curve follows the same trend for all three scenarios before gas breakthrough due to the constant liquid production rate. However, after CO_2 breakthrough, the oil recovery for CO_2 flooding increased more slowly compared to the co-injection cases. The ultimate oil recovery following CO_2 flooding was 42%, while the co-injection of CO_2 and brine achieved 44% oil recovery. This is because the co-injection of CO_2 and brine reduces gas relative permeability, thereby decreasing CO_2 mobility. CO_2 foam flooding demonstrated the highest oil recovery, reaching 46%, which is 4% higher than CO_2 flooding and 2% higher than the co-injection of CO_2 and brine. The higher oil recovery in CO_2 foam flooding can be attributed to foam's ability to reduce CO_2 mobility and improve sweep

efficiency by blocking higher-permeability areas and diverting the injected fluid into lower-permeability areas.

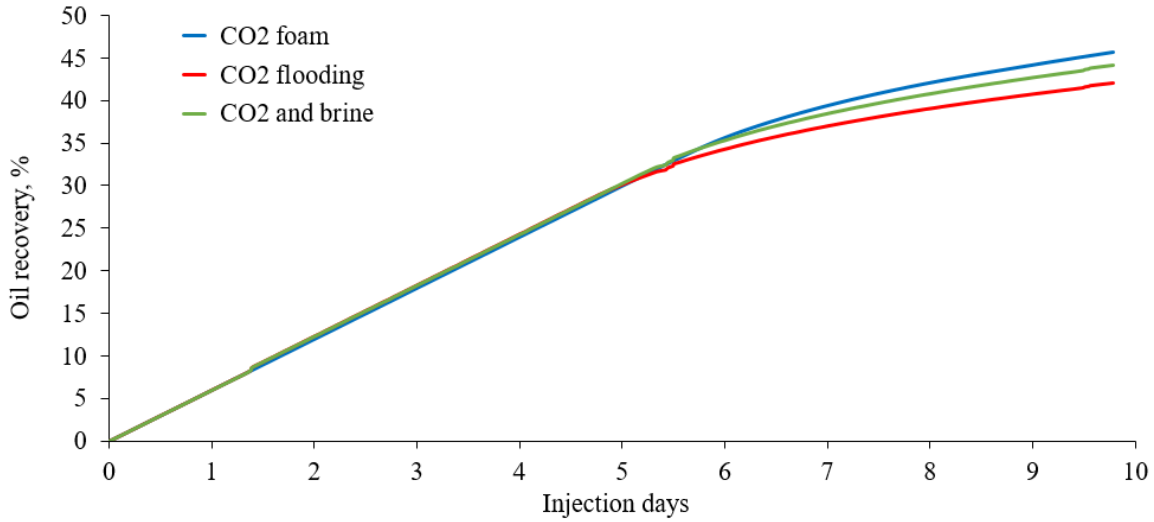

Figure 5-12. Comparison the oil recovery efficiency of three injection scenarios.

5.2.5 3D Reservoir Foam Simulation

In this study, a 3D heterogeneous model was employed to evaluate the oil recovery performance of three injection schemes: CO_2 flooding, the co-injection of CO_2 and brine, and CO_2 foam flooding. These scenarios were simulated over the 25-year period using the CMG STARS reservoir simulator. The well parameters were the same as in the 2D simulation. The co-injection of gas and brine, in the absence and presence of surfactant, was conducted, keeping a constant gas fractional flow of 70%. The produced GOR and oil production rate are shown in Figures 5-13 and 5-14.

In the 3D heterogeneous reservoir, CO_2 flooding led to earlier gas breakthrough at the production well due to the higher mobility of gas compared to the reservoir fluid. As illustrated in the figures, GOR during CO_2 flooding began to rise after 5 years of production and reached around 20000 ft^3/day by the end of the 25-year period. The early gas breakthrough caused a significant decline in oil production rate compared to other injection scenarios.

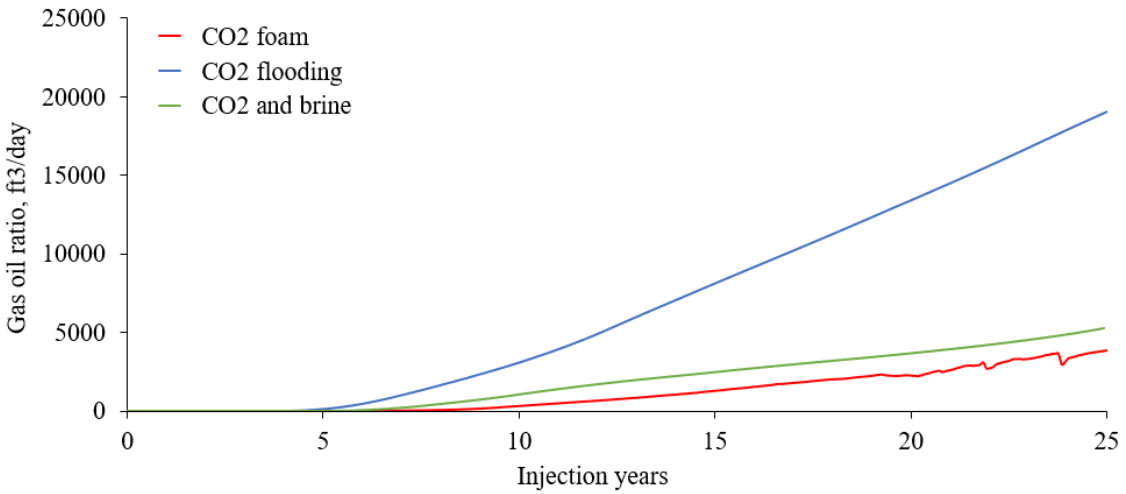

Figure 5-13. Gas oil ratio for three injection scenarios.

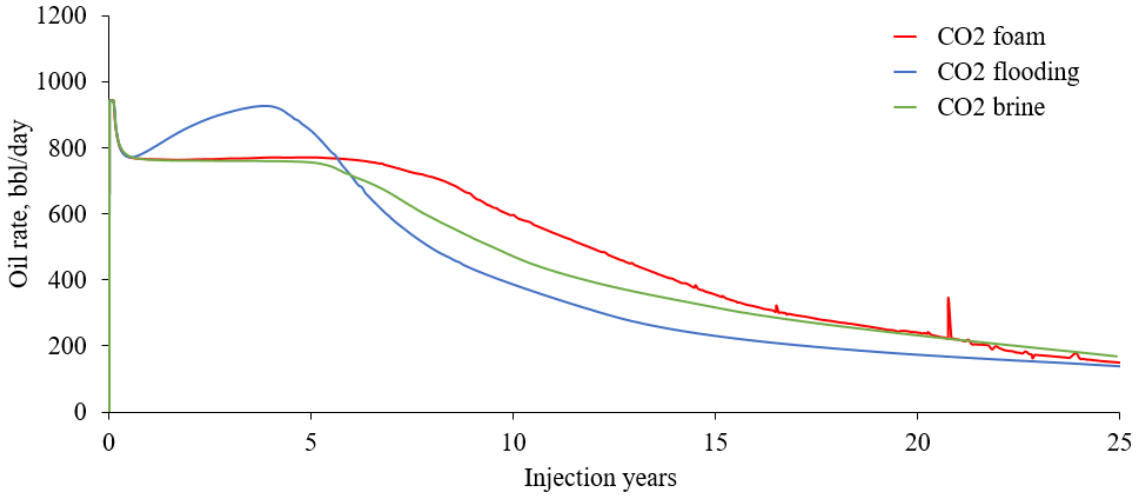

Figure 5-14. Oil rate for three injection scenarios.

As illustrated in the figures, the co-injection of CO_2 and brine slightly delayed gas breakthrough, and the GOR increased at a significantly slower rate compared to CO_2 flooding. After 25 years of the co-injection of CO_2 and brine, the GOR reached approximately 5000 ft^3/day, demonstrating the ability of the process to control and mitigate CO_2 mobility. The oil production rate during the co-injection of CO_2 and brine exhibited a longer plateau period and declined slower compared to CO_2 flooding.

In the third scenario, where CO_2 foam flooding was applied, the gas breakthrough occurred significantly later compared to the other two injection methods. After the breakthrough, the GOR rose slower compared to the co-injection of CO_2 and brine process

and reached 3851 ft^3/day by the end of the 25-year period. The oil production rate during CO_2 foam flooding exhibited a slower decline rate compared to the other injection scenarios. These results indicate that CO_2 foam flooding effectively reduced gas relative permeability in the heterogeneous reservoir, delaying the gas breakthrough and sustaining a higher oil production rate.

Figure 5-15 compares the oil recovery efficiency of three injection scenarios. In the heterogeneous reservoir, oil recovery following CO_2 flooding was approximately 43.7%, primarily due to early gas breakthrough. The co-injection of CO_2 and brine demonstrated a slightly higher oil recovery efficiency than CO_2 flooding, reaching 47.9%.

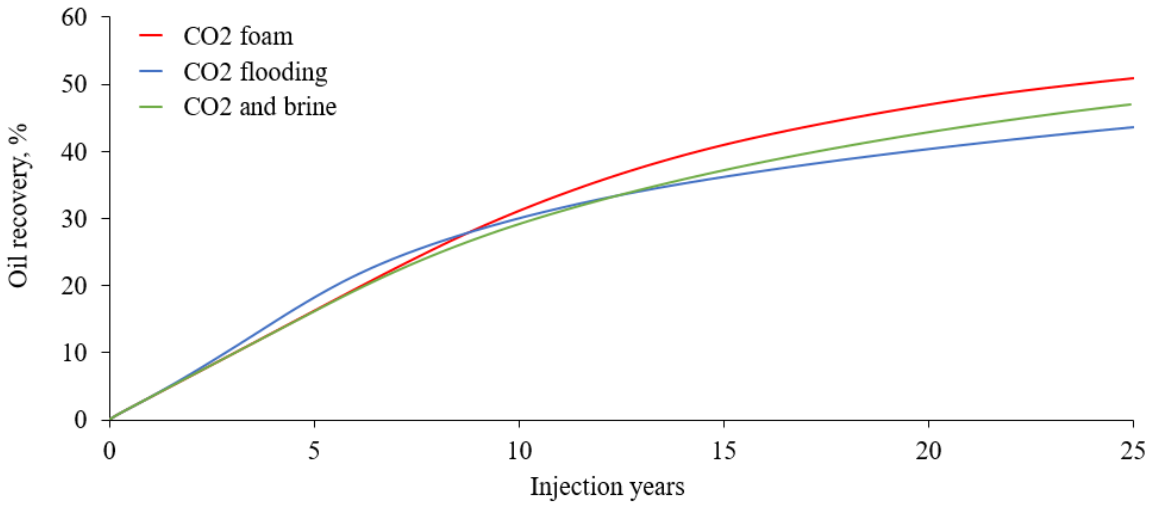

Figure 5-15. The oil recovery for three injection scenarios.

As expected, CO_2 foam flooding had a positive effect on oil recovery by mitigating CO_2 mobility. Oil recovery following CO_2 foam flooding reached nearly 50.9%, significantly higher than both the co-injection of CO_2 and brine, and CO_2 flooding. The superior oil recovery efficiency of CO^2 foam flooding can be attributed to the reduction in gas mobility due to foam generation, which delayed gas breakthrough and improved both areal and vertical oil sweep efficiency. Overall, these results demonstrate that CO_2 foam flooding was more effective in oil recovery than CO_2 flooding or the co-injection of CO_2 and brine, thanks to reduced gas mobility, resulting in better sweep efficiency.

5.2.6 Sensitivity Analysis of Oil Parameters on Foam Performance.

A series of foam simulations using the same STARS foam parameters, shown in Table 5-3, were conducted to assess the impact of fmoil and epoil values on foam performance.

In the first case, epoil was set to 1, while the fmoil value was varied. The fmoil represents the limiting oil saturation at which foam completely decays. The aim of this simulation was to evaluate the performance of CO_2 foam flooding for different crude oils, each specified by varying fmoil values. CO_2 foam is not sensitive to oil when fmoil value is high, whereas it decays rapidly when fmoil values are low.

Figure 5-16 illustrates the variation in GOR over 25 years of foam flooding as fmoil increased from 0.2 to 0.8. At fmoil = 0.2, the gas breakthrough occurred earlier compared to other cases, and GOR values increased rapidly, reaching approximately 5100 ft^3/day by the end of the foam injection. When fmoil = 0.5, the gas breakthrough time was significantly delayed, and GOR was reduced compared to the fmoil = 0.2 case. At fmoil = 0.8, foam flooding further reduced GOR and extended the gas breakthrough time to almost 15 years compared to the case with a fmoil value of 0.2.

Figure 5-16. Gas-oil ratio at various fmoil values.

Figure 5-17 shows the oil recovery following CO_2 foam flooding with different fmoil values. For the cases with fmoil = 0.2, the oil recovery achieved through CO_2 foam flooding was 43%. Setting fmoil to 0.5 increased the oil recovery to 50%, while further increasing fmoil to 0.8 recovered 57% of oil.

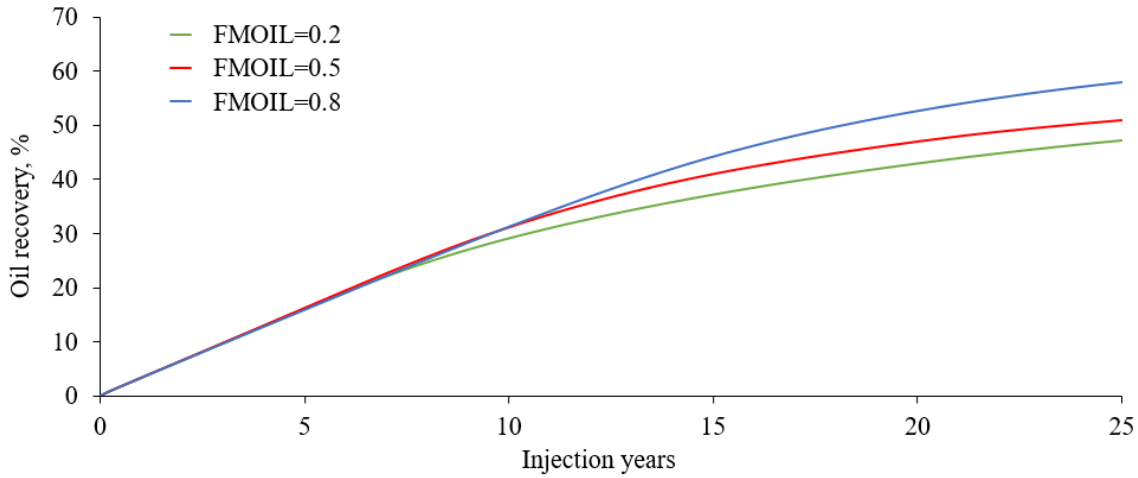

Figure 5-17. Oil recovery at various fmoil values.

The simulation results indicate that CO_2 foam stabilized by 0.5 wt% AOS performs better in terms of mobility control when the oil fraction (fmoil) is higher under reservoir conditions. However, if the oil negatively affects the foam, the fmoil value will decrease, resulting in poor mobility control performance.

In the second case, the same STARS foam parameters were again used, however, fmoil was set to 0.5 with the changing value of epoil from 1 to 9. The value of epoil shows the sharpness of foam decays. The value of epoil depends on the response of CO_2 foam on contact with crude oils. A higher value of epoil suggests that foam decays faster with increasing oil saturation.

Figure 5-18 shows the GOR of the production well during CO_2 foam flooding for various epoil values. As depicted in the figure, increasing the epoil value led to earlier gas breakthrough and higher GOR. For the case with a low epoil value of 1, stronger foam was generated due to reduced oil saturation, resulting in good foam stability. However, as epoil increases, the strength of the foam decreases more rapidly. The oil recovery efficiency of CO_2 foam flooding for different epoil values is shown in Figure 5-19. The highest oil

recovery was achieved at low epoil values, indicating better mobility control when epoil is lower.

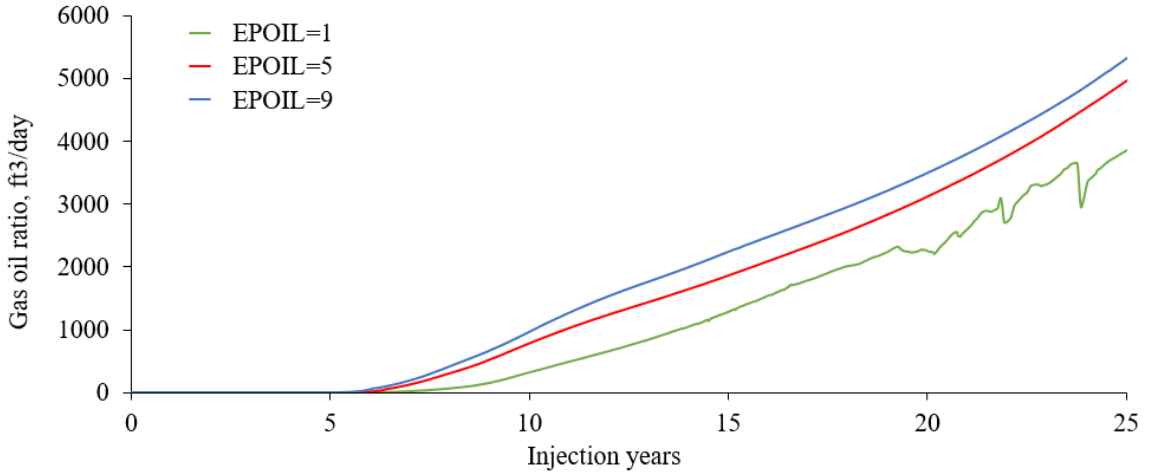

Figure 5-18. Gas-oil ratio at various epoil values.

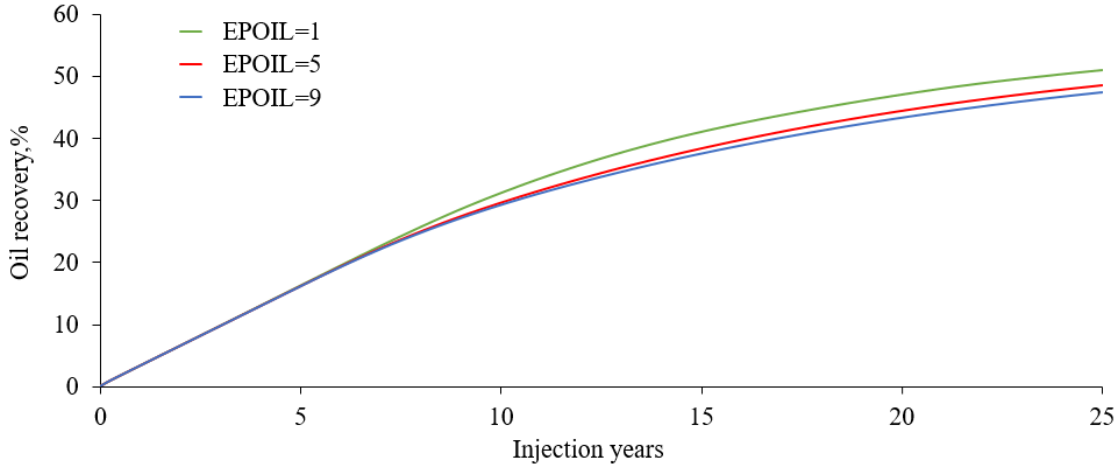

Figure 5-19. Oil recovery at various epoil values.

Overall, the mobility efficiency of CO_2 foam flooding is strongly influenced by crude oil properties. CO_2 foam flooding demonstrates better mobility control efficiency at higher fmoil values and lower epoil values. This highlights the importance of oil-foam interactions when studying the performance of CO_2 foam flooding in oil recovery.

5.3 Summary

This chapter has focused on reservoir-scale simulations to enhance understanding of the oil recovery performance of CO_2 foam flooding. The numerical results indicate that CO_2 foam effectively reduces CO_2 mobility, resulting in improved sweep efficiency, and consequently, a higher rate of oil recovery.

- A comparison of the different gas injections, namely methane, carbon dioxide, and sour gas, revealed that CO_2 flooding exhibited the highest oil recovery performance. The higher density and viscosity of CO_2 under reservoir conditions are the factors contributing to a more efficient oil displacement compared to other gases.
- The injection of CO_2 into a homogeneous 2D reservoir led to uniform oil displacement. However, in the heterogeneous reservoir, the injected CO_2 preferentially flowed through high-permeability areas, leading to early gas breakthrough and poor sweep efficiency. As a result, oil recovery following CO_2 flooding was significantly lower in the heterogeneous reservoir compared to the homogeneous one, highlighting the need for CO2 mobility control methods, such as foam flooding.
- A comparison of CO_2 flooding, the co-injection of CO_2 and brine, and CO_2 foam flooding was conducted using a 2D heterogeneous reservoir model. CO_2 foam flooding effectively reduced CO_2 mobility, delaying gas breakthrough and improving vertical sweep efficiency. As a result, CO2 foam flooding achieved the highest oil recovery, outperforming both CO_2 flooding and the co-injection of CO_2 and brine.
- The use of a 3D heterogeneous reservoir model further demonstrated the efficiency of CO_2 foam flooding in controlling CO_2 mobility and enhancing both areal and vertical sweep efficiency. In comparison to CO_2 flooding and the co-injection of CO_2 and brine, CO_2 foam demonstrated a higher oil recovery performance.
- The strength and stability of CO_2 foam highly depend on oil-foam interactions, represented by fmoil and epoil values. When CO_2 is less sensitive to oil, fmoil value is high, indicating greater foam stability. In contrast, a low fmoil value suggests the fast decay of foam upon contact with oil. CO_2 foam demonstrated better performance when the epoil value was low.

In conclusion, the simulations underscore the advantages of CO_2 foam flooding in enhancing oil recovery, particularly in heterogeneous reservoirs. The ability of CO_2 foam to control CO_2 mobility and improve sweep efficiency highlights its potential for future applications in enhanced oil recovery.

CHAPTER 6. Conclusions and future works

6.1 Conclusions

This thesis presents experimental findings on the performance of surfactant and surfactant-nanoparticle-stabilized CO_2 foams as an enhanced oil recovery method. Key parameters such as foam stability, foamability in the absence and presence of oil, foam-oil interactions, foam boosting performance of nanoparticles, and the enhanced oil recovery capacity of foam generated in porous media were investigated through bulk static tests and core flooding dynamic experiments under various pressure and temperature conditions. Specifically, alpha-olefin sulfonate (AOS) surfactant and the combination of AOS with silicon oxide (SiO_2) nanoparticles were tested as a foaming agent for CO_2 foam. Additionally, numerical reservoir models were developed based on experimental results to evaluate the foam's ability to reduce CO_2 mobility and assess the impact of oil-foam interactions. The following points highlight the key findings of this research:

Bulk foam screening tests:

In this thesis, bulk tests were carried out to evaluate the foamability and stability of foaming solutions at various surfactant concentrations, temperature conditions, the presence and absence of nanoparticles as well as crude oil.

- Increasing the AOS concentration from 0.1 wt% to 1 wt% had minimal effect on the observed foam volume and half-life at ambient conditions. These concentrations were well above the critical micelle concentration for AOS, beyond which the surfactant forms a double layer and surface activity plateaus, limiting further foam stability improvements. Moreover, there are no additional available sites at the gas-liquid interface for surfactant molecules to adsorb. Consequently, increasing the surfactant concentration in this experiment did not lead to an improvement in surface activity and foam stability as a result.
- In bulk foam tests, stability of foam declined as the temperature rose. For a 0.5 wt% AOS solution, the foam half-life dropped from approximately 270 secs to 100 secs as the temperature increased from 20℃ to 80℃. This decline in stability is due to increased molecular motion at higher temperatures, which accelerates the coalescence and collapse of foam bubbles. Additionally, foam behavior showed minimal sensitivity to salinity, as the salinity of tested brine solutions was relatively low, ranging from 0 to 13,000 ppm.

- The presence of nanoparticles slightly improved the stability of surfactant-stabilized CO_2 foam in bulk tests conducted at ambient conditions. This improvement is attributed to nanoparticles ability to adsorb at the gas-water interface, enhancing film strength and reducing coalescence. Moreover, nanoparticles helped to reduce liquid drainage due to gravity, which is one of the key reasons for foam destabilization during bulk tests.
- The presence of oil during the bulk tests accelerated the degradation of CO_2 foam, significantly reducing its stability. In this study, the effect of foam was more pronounced at higher oil concentrations. Increasing oil concentration from 0 to 5% halved the stability of foam stabilized with a 0.5 wt% AOS solution. The measurement of IFT in oil-CO_2-surfactant solution system demonstrated positive entering, bridging and spreading coefficients, indicating that oil enters the lamellae and spreads across it, leading to foam destabilization. These observations suggest that crude oil decreases foam stability, aligning with the findings from bulk tests.

Foam dynamic experiments in the absence of oil:

- The foam's apparent viscosity increased as the gas fractional flow increased, reaching a 70% transition point. The apparent viscosity of the foam decreased above the transition point. This supports the concept of a critical capillary pressure for foam instability.
- In the absence of oil, temperature negatively impacted the behavior of foam transport in porous media. Beyond a certain point, foam strength and stability drastically declined as reservoir temperature rose, limiting effectiveness at or above 80ºC.
- Pressure drop across cores increased with increasing AOS concentration during foam flooding tests. This effect became more apparent after a sufficient volume of the surfactant was injected. This is crucial for meeting the minimal chemical requirement.
- Foam stabilized with 0.05 wt% SiO_2 and 0.5 wt% AOS exhibited higher apparent viscosity, approximately 31 cp at elevated temperature, in porous media compared to the foam stabilized with surfactant only, which had the viscosity of 20 cp. The apparent viscosity of CO_2 foam stabilized with a mixture of surfactant and nanoparticles reached 80 cP, whereas the surfactant-stabilized foam exhibited a viscosity of 29 cP in porous media as the temperature decreased from 80 °C to 40 °C. This highlights the detrimental effect of elevated temperature on foam stability. Overall, experiments conducted at both elevated and low

temperatures demonstrate that the presence of nanoparticles reinforces the foam's thin films, preventing collapse and coalescence.

- The combination of nanoparticles and surfactants showed greater stability in porous media at 40°C after foam injection stopped, compared to surfactant alone. This improved foam stability helped maintain better control of CO_2 mobility for a longer period when nanoparticles were present, even after foam injection ceased.

Dual-core experiments:

- In double core experiments, approximately 60-70% of injected water was produced from the higher permeability core under a weak heterogeneity environment (Vk=2). However, after surfactant-stabilized CO_2 foam injection, flow was effectively diverted, increasing the division ratio in the lower permeability core from 30 to 80%. This indicates that the foam blocked some high-permeability core areas, diverting the fluid into the lower permeability core, thus improving the sweep efficiency. However, when foam injection ceased, the division ratio for the higher permeability core sharply increased, highlighting the low foam stability of foam in the porous media.

- In the case of severe heterogeneity (Vk = 8), almost all of the injected water was produced from the higher permeability core. After initiating the injection of surfactant-nanoparticles-stabilized CO_2 foam, the division ratio in the lower permeability core gradually increased to 70-80%, demonstrating the effectiveness of foam to divert flow in porous media. However, similar to the previous experiment, the division ratio in the high permeability core showed a rapid increase as foam injection ceased.

- Comparing the pressure drop observed in both experiments revealed that foam stabilized with nanoparticles demonstrated stronger generation and stability than foam stabilized with surfactant alone, highlighting the benefits of nanoparticles in enhancing foam stability.

Oil recovery experiments:

- Oil recovery experiments conducted at both elevated and low temperatures demonstrated better foam performance in the presence of nanoparticles compared to their absence. At elevated reservoir temperature (80°C), surfactant-nanoparticle-stabilized CO_2 foam flooding resulted in an additional 12.1% OOIP recovery compared to 8.9% OOIP recovered by surfactant-stabilized CO_2 foam after extensive water and CO_2 flooding. At low

temperature (40°C), the incremental oil recovery in the presence of nanoparticles reached 19.7% of OOIP, while approximately 14.7% OOIP was recovered without them. Both experiments demonstrated that the addition of nanoparticles enhanced oil recovery of surfactant-stabilized CO_2 foam by strengthening thin liquid film, reducing the liquid drainage, and producing stronger foam in porous media.

- At elevated temperature, the pressure drop during surfactant-stabilized CO_2 foam flooding was 20 psi with nanoparticles and 10 psi without. At low temperature, pressure drop in the absence of nanoparticles gradually increased and reached around 70 psi, while the addition of nanoparticles led to 180 psi, indicating the contribution of nanoparticles in generating stronger and more stable foam.

Numerical simulation

- In a 2D homogeneous reservoir model, CO_2 flooding achieved 76% OOIP oil recovery, significantly outperforming ethane (60%) or sour gas injection (61%). However, oil recovery efficiency of CO_2 flooding dropped to 52.5% in a heterogeneous reservoir model due to early gas breakthrough and gas channeling, which reduced sweep efficiency.
- In a 3D heterogeneous reservoir model, CO_2 foam flooding recovered 50.9% OOIP, significantly higher than CO_2 flooding (43.8%) and the co-injection of CO_2 and brine (47.9%). Overall, the results demonstrate that CO_2 foam is more effective at mitigating CO_2 mobility issues, leading to higher oil recovery.

6.2 Novelty of the study

CO_2 foam flooding has shown great potential for improving sweep efficiency and controlling mobility in carbonate reservoirs. However, optimizing foam stability and performance remains a challenge, particularly when considering local reservoir conditions and available injection fluids. This study addresses these challenges by exploring the use of surfactant–nanoparticle-stabilized CO_2 foams in the context of Kazakhstani carbonate oil fields, with a focus on practical injection media and advanced stabilization mechanisms. The main contributions of this work are summarized as follows:

- This study introduces a novel investigation into surfactant–nanoparticle-stabilized CO_2 foam, tested in both homogeneous and heterogeneous porous media under

elevated temperature and pressure conditions, simulating the reservoir conditions of deep Kazakhstani carbonate oil fields.

- Caspian Sea water was employed as the injection medium for CO_2 foam flooding, providing new insights into its impact on foam behavior and its potential suitability for future enhanced oil recovery projects in the region.
- The research enhances understanding of the synergistic stabilization effects between SiO_2 nanoparticles and AOS surfactant. Systematic evaluation demonstrated improved foam stability, enhanced oil recovery, and increased flow diversion capacity.

Lessons learned:

Based on the experimental work conducted in this study, several important observations and lessons were identified:

- CO_2 exhibits high solubility in brine, which leads to rapid foam bubble collapse; thus, it was difficult to obtain long-time stable foam [184]. In this study, the half-life time of CO_2 foam ranged from 200 to 300 seconds, making it complicated to analyze foam bubble behavior due to rapid decay. The use of a simple experimental setup and potentially unsuitable porous frit for bulk tests possibly may accelerate foam degradation. As a result, some bulk test outcomes did not align with trends reported in the previous literature [6, 117].
- Zeta potential measurements and visual observations indicated low stability of SiO_2 nanoparticles, especially at high concentrations, in the brine used in this study. Consequently, a low (0.05 wt%) concentration of nanoparticles was selected for foam experiments in porous media, conducted at elevated pressure and temperature conditions. However, the coreflood system required approximately four hours to reach thermal equilibrium, during which time the stability of the nanoparticle solution may have deteriorated, leading to precipitation. Evidence of precipitation included a sharp increase in pressure drop across the core during CO_2 foam flooding and visible white deposits on the inlet plug of the core holder. For this reason, it is important to investigate the long-time stability of nanoparticles under elevated temperature conditions.
- In foam dynamic experiments, higher-pressure drop observed in the presence of nanoparticles compared to its absence may not necessarily indicate improved foam strength. It is possible that these increases were due to nanoparticle precipitation, which may block

flow paths in porous media. Therefore, selecting thermally compatible nanoparticles is critical for foam flooding applications in porous media.

- Both the AOS surfactant and SiO_2 nanoparticles used in this study exhibit negative surface charge, while carbonate rock surfaces are positively charged. Electrostatic attraction between these oppositely charged components can result in the adsorption of foaming agents onto rock surfaces, leading to significant loss of active agents within the porous medium. In several of the foam dynamic tests, particularly at elevated temperature, very weak foam was observed. One of the possible reasons, except for elevated temperature, was insufficient presence of foaming agent in porous media due to adsorption. As a result, discussing foam behavior in porous media was complicated due to the unknown degree of foaming agent loss. For this reason, it is crucial to use compatible foaming agents.

- In oil recovery experiments, CO_2 flooding prior to foam injection may have influenced foam performance. CO_2 dissolution in oil and mixing during CO_2 flooding may have affected the subsequent foam flooding process. As a result, it was challenging to determine whether observed incremental oil recovery during CO_2 foam flooding was due to reduced CO_2 mobility by foam or simply due to CO_2-oil interaction, which could enhance oil displacement.

6.3 Future works

This dissertation demonstrates the potential of combining surfactants with nanoparticles to improve the stability of CO_2 foam for enhancing oil recovery. However, some uncertainties were present in the experimental results due to limitations of experimental equipment:

- The experimental setup used for bulk tests included a gas flow meter that was calibrated for N_2 rather than CO_2. Furthermore, the porous frit used to generate foam had pores with various radii, causing non-uniform foam formation on its surface, potentially affecting foamability. To address these challenges, it is recommended to repeat bulk static tests using a commercially available foam analyzer equipped with a calibrated gas flow meter, an automatic data acquisition system, and a heating oven for more accurate foam volume and stability measurements.

- In this thesis, the efficiency of CO_2 foam flooding in diverting flow within a heterogeneous environment was investigated by conducting dual-core experiments at ambient conditions and in the absence of oil. However, to ensure the reliability of CO_2 foam flooding, further research is needed to consider high-temperature and high-pressure reservoir conditions and oil-foam interactions in heterogeneous environments.
- The reaction of CO_2 with water forms carbonic acid, which may dissolve carbonate minerals in a core, potentially creating flow fingers and altering the rock's properties. This may affect foam generation and propagation; thus, it is important to understand the scale of carbonate mineral dissolution during CO_2 foam flooding. To address this problem, further research using X-ray computed tomography (CT) is recommended to visualize the alteration of rock properties.
- Rock wettability is another critical factor influencing foam stability, as it affects fluid flow and foam behavior under different wettability conditions. In this thesis, core flooding experiments were conducted using only water-wet cores and a single oil, while most carbonate reservoirs are typically oil-wet or mixed-wet wettability [185]. There are two contradictory theories among researchers regarding the effect of wettability on foam stability. One group of researchers argues that water-wet conditions are favorable for successful foam performance [112], while others suggest that stable foam can be generated in oil-wet porous media due to wettability alteration from hydrophobic to hydrophilic conditions [187]. However, either surfactants or nanoparticles have been used to study the effect of wettability on foam stability. Therefore, further studies are required to evaluate the impact of rock wettability on nanoparticle-surfactant stabilized foam stability.
- Certain assumptions were made in reservoir simulations, such as homogeneous porosity, constant well parameters, uniform grid size, and a small reservoir sector model. However, these assumptions can lead to errors and uncertainties in the results; therefore, future studies should incorporate real field data such as rock property, field conditions, field history, well spacing and controls to construct a more accurate reservoir model and validate it properly against experimental results.

References

(1) U.S. Energy Information Administration (EIA). International Energy Outlook 2013, Washington, D.C., United States, July, 2013. Report is available at www.eia.gov.

(2) Orr, F. M., Heller, J. P., & Taber, J. J. (1982). Carbon dioxide flooding for enhanced oil recovery: Promise and problems. Journal of the American Oil Chemists Society, 59, 810A-817A.

(3) Manrique, E. J., Muci, V. E., & Gurfinkel, M. E. (2007). EOR field experiences in carbonate reservoirs in the United States. SPE Reservoir Evaluation & Engineering, 10(06), 667-686.

(4) Xu, Z. X., Li, S. Y., Li, B. F., Chen, D. Q., Liu, Z. Y., & Li, Z. M. (2020). A review of development methods and EOR technologies for carbonate reservoirs. Petroleum Science, 17, 990-1013.

(5) Schramm, L. L. (1994). Foam sensitivity to crude oil in porous media.

(6) Talebian, S. H., Masoudi, R., Tan, I. M., & Zitha, P. L. J. (2014). Foam assisted CO_2-EOR: A review of concept, challenges, and future prospects. Journal of Petroleum Science and Engineering, 120, 202-215.

(7) Worthen, A., Taghavy, A., Aroonsri, A., Kim, I., Johnston, K., Huh, C., ... & DiCarlo, D. (2015, September). Multi-scale Evaluation of Nanoparticle-stabilized CO_2-in-water Foams: From the Benchtop to the Field. In SPE Annual Technical Conference and Exhibition? (p. D011S009R006). SPE..

(8) McLendon, W. J., Koronaios, P., Enick, R. M., Biesmans, G., Salazar, L., Miller, A., ... & Crandall, D. (2014). Assessment of CO_2-soluble non-ionic surfactants for mobility reduction using mobility measurements and CT imaging. Journal of Petroleum Science and Engineering, 119, 196-209.

(9) Yekeen, N., Manan, M. A., Idris, A. K., Padmanabhan, E., Junin, R., Samin, A. M., ... & Oguamah, I. (2018). A comprehensive review of experimental studies of nanoparticles-stabilized foam for enhanced oil recovery. Journal of Petroleum Science and Engineering, 164, 43-74.

(10) Liu, Y., Grigg, R. B., & Svec, R. K. (2005, April). CO_2 foam behavior: influence of temperature, pressure, and concentration of surfactant. In SPE Oklahoma City Oil and Gas Symposium/Production and Operations Symposium (pp. SPE-94307). SPE.

(11) Blaker, T., Aarra, M. G., Skauge, A., Rasmussen, L., Celius, H. K., Martinsen, H. A., & Vassenden, F. (2002). Foam for gas mobility control in the Snorre field: the FAWAG project. SPE Reservoir Evaluation & Engineering, 5(04), 317-323.

(12) AlYousef, Z., Almobarky, M., & Schechter, D. (2017). Enhancing the stability of foam by the use of nanoparticles. Energy & Fuels, 31(10), 10620-10627.

(13) Enick, R. M., Olsen, D., Ammer, J., & Schuller, W. (2012, April). Mobility and conformance control for CO_2 EOR via thickeners, foams, and gels-a literature review of 40 years of research and pilot tests. In SPE Improved Oil Recovery Conference? (pp. SPE-154122). SPE.

(14) Rezaei, A., Riazi, M., Escrochi, M., & Elhaei, R. (2020). Integrating surfactant, alkali and nano-fluid flooding for enhanced oil recovery: A mechanistic experimental study of novel chemical combinations. Journal of Molecular Liquids, 308, 113106.

(15) Grigg, R. B., & Mikhalin, A. A. (2007, February). Effects of flow conditions and surfactant availability on adsorption. In SPE International Conference on Oilfield Chemistry? (pp. SPE-106205). SPE.

(16) Heller, J. P., Lien, C. L., & Kuntamukkula, M. S. (1985). Foamlike dispersions for mobility control in CO_2 floods. Society of Petroleum Engineers Journal, 25(04), 603-613.

(17) Bera, A., Kumar, T., Ojha, K., & Mandal, A. (2013). Adsorption of surfactants on sand surface in enhanced oil recovery: Isotherms, kinetics and thermodynamic studies. Applied Surface Science, 284, 87-99.

(18) Osei-Bonsu, K., Shokri, N., & Grassia, P. (2015). Foam stability in the presence and absence of hydrocarbons: From bubble-to bulk-scale. Colloids and Surfaces A: Physicochemical and Engineering Aspects, 481, 514-526.

(19) Worthen, A. J., Bryant, S. L., Huh, C., & Johnston, K. P. (2013). Carbon dioxide-in-water foams stabilized with nanoparticles and surfactant acting in synergy. AIChE Journal, 59(9), 3490-3501.

(20) Singh, R., & Mohanty, K. K. (2014, April). Synergistic stabilization of foams by a mixture of nanoparticles and surfactants. In SPE Improved Oil Recovery Conference? (pp. SPE-169126). SPE.

(21) Adkins, S. S., Gohil, D., Dickson, J. L., Webber, S. E., & Johnston, K. P. (2007). Water-in-carbon dioxide emulsions stabilized with hydrophobic silica particles. Physical Chemistry Chemical Physics, 9(48), 6333-6343.

(22) Ahmadi, M. A., & Shadizadeh, S. R. (2013). Induced effect of adding nano silica on adsorption of a natural surfactant onto sandstone rock: experimental and theoretical study. Journal of Petroleum Science and Engineering, 112, 239-247.

(23) Rossen, W. R., & Shen, C. (2007, June). Gravity segregation in gas-injection IOR. In SPE Europec featured at EAGE Conference and Exhibition? (pp. SPE-107262). SPE.

(24) Vikingstad, A. K., Aarra, M. G., & Skauge, A. (2006). Effect of surfactant structure on foam–oil interactions: comparing fluorinated surfactant and alpha olefin sulfonate in static foam tests. Colloids and Surfaces A: Physicochemical and Engineering Aspects, 279(1-3), 105-112.

(25) Simjoo, M., Dong, Y., Andrianov, A., Talanana, M., & Zitha, P. L. (2013). Novel insight into foam mobility control. SPE Journal, 18(03), 416-427.

(26) Yekeen, N., Idris, A. K., Manan, M. A., Samin, A. M., Risal, A. R., & Kun, T. X. (2017). Bulk and bubble-scale experimental studies of influence of nanoparticles on foam stability. Chinese Journal of Chemical Engineering, 25(3), 347-357.

(27) Babamahmoudi, S., & Riahi, S. (2018). Application of nano particle for enhancement of foam stability in the presence of crude oil: Experimental investigation. Journal of Molecular Liquids, 264, 499-509.

(28) Yekeen, N., Idris, A. K., Manan, M. A., & Samin, A. M. (2017). Experimental study of the influence of silica nanoparticles on the bulk stability of SDS-foam in the presence of oil. Journal of Dispersion Science and Technology, 38(3), 416-424.

(29) Al Yousef, Z. A., Almobarky, M. A., & Schechter, D. S. (2020). Surfactant and a mixture of surfactant and nanoparticles to stabilize CO_2/brine foam, control gas mobility, and enhance oil recovery. Journal of Petroleum Exploration and Production Technology, 10, 439-445.

(30) Alooghareh, M. H., Kabipour, A., Sisakht, S. M. M., & Razavifar, M. (2022). Effects of different gases on the performance of foams stabilized by Cocamidopropyl betaine surfactant and silica nanoparticles: A comparative experimental study. Petroleum, 8(4), 546-551.

(31) Wei, P., Pu, W., Sun, L., Pu, Y., Wang, S., & Fang, Z. (2018). Oil recovery enhancement in low permeable and severe heterogeneous oil reservoirs via gas and foam flooding. Journal of Petroleum Science and Engineering, 163, 340-348.

(32) Ding, M. C., Li, Q., Yuan, Y. J., Wang, Y. F., Zhao, N., & Han, Y. G. (2022). Permeability and heterogeneity adaptability of surfactant-alternating-gas foam for recovering oil from low-permeability reservoirs. Petroleum Science, 19(3), 1185-1197.

(33) Green, D. W., & Willhite, G. P. (1998). Enhanced Oil Recovery. Richardson, TX: Henry L. Doherty Memorial Fund of AIME, Society of Petroleum Engineers

(34) Sheng, J. J. (2010). Modern chemical enhanced oil recovery: theory and practice. Gulf Professional Publishing.

(35) Wardlaw, N. C. (1996). Factors affecting oil recovery from carbonate reservoirs and prediction of recovery. Developments in Petroleum Science, 44, 867-903.

(36) Romero-Zern, L. (Ed.). (2012). Introduction to Enhanced Oil Recovery (EOR) Processes and Bioremediation of Oil-Contaminated Sites. InTech. doi: 10.5772/2053

(37) Lake, L.W. Enhanced Oil Recovery, Prentice Hall, New Jersey, 1989.

(38) Hirasaki, G. J., Miller, C. A., & Puerto, M. (2011). Recent advances in surfactant EOR. SPE journal, 16(04), 889-907.

(39) Needham, R. B., & Doe, P. H. (1987). Polymer flooding review. Journal of petroleum technology, 39(12), 1503-1507..

(40) Zerpa, L. E., Queipo, N. V., Pintos, S., & Salager, J. L. (2005). An optimization methodology of alkaline–surfactant–polymer flooding processes using field scale numerical simulation and multiple surrogates. Journal of Petroleum Science and Engineering, 47(3-4), 197-208.

(41) Hirasaki, G., & Zhang, D. L. (2004). Surface chemistry of oil recovery from fractured, oil-wet, carbonate formations. Spe Journal, 9(02), 151-162.

(42) Levitt, D. B., & Pope, G. A. (2008, April). Selection and screening of polymers for enhanced-oil recovery. In SPE Improved Oil Recovery Conference? (pp. SPE-113845). SPE.

(43) Zhang, D. L., Liu, S., Yan, W., Puerto, M., Hirasaki, G. J., & Miller, C. A. (2006, April). Favorable attributes of alkali-surfactant-polymer flooding. In SPE Improved Oil Recovery Conference? (pp. SPE-99744). SPE.

(44) Liu, S. (2008). Alkaline Surfactant Polymer enhanced oil recovery process. Rice University.

(45) Lee, S., & Kam, S. I. (2013). Enhanced oil recovery by using CO_2 foams: fundamentals and field applications. In Enhanced Oil Recovery Field Case Studies (pp. 23-61). Gulf Professional Publishing

(46) Whorton, L. P., Brownscombe, E. R., & Dyes, A. B. (1952). U.S. Patent No. 2,623,596. Washington, DC: U.S. Patent and Trademark Office.

(47) Holm, L. W., & Josendal, V. A. (1974). Mechanisms of oil displacement by carbon dioxide. Journal of petroleum Technology, 26(12), 1427-1438.

(48) Langston, M. V., Hoadley, S. F., & Young, D. N. (1988, April). Definitive CO_2 flooding response in the SACROC unit. In SPE Improved Oil Recovery Conference? (pp. SPE-17321). SPe.

(49) Manrique, E., Thomas, C., Ravikiran, R., Izadi, M., Lantz, M., Romero, J., & Alvarado, V. (2010, April). EOR: current status and opportunities. In SPE Improved Oil Recovery Conference? (pp. SPE-130113). SPE.

(50) Jarrell, P. M., Fox, C. E., Stein, M. H., & Webb, S. L. (2002). Practical aspects of CO2 flooding. (No Title), 22.

(51) Verma, M. K. (2015). Fundamentals of carbon dioxide-enhanced oil recovery (CO_2-EOR): a supporting document of the assessment methodology for hydrocarbon recovery using CO_2-EOR associated with carbon sequestration (No. 2015-1071). US Geological Survey.

(52) Lemmon, E. W. (2010). Thermophysical properties of fluid systems. NIST chemistry WebBook.

(53) Martin, D. F., & Taber, J. J. (1992). Carbon Dioxide Flooding. Society of Petroleum Engineers. Society of Petroleum Engineering.

(54) Skarestad, M., & Skauge, A. (2012). PTEK213 Reservoarteknikk II. Bergen, Norway: University of Bergen.

(55) Holm, L. W. (1986). Miscibility and miscible displacement. Journal of Petroleum Technology, 38(08), 817-818.

(56) Lambert, M. R., Marino, S. D., Anthony, T. L., Calvin, M. W., Gutierrez, S., & Smith, D. P. (1996, March). Implementing CO_2 floods: no more delays!. In SPE Permian Basin Oil and Gas Recovery Conference (pp. SPE-35187). SPE.

(57) Fernø, M. A., Eide, Ø., Steinsbø, M., Langlo, S. A. W., Christophersen, A., Skibenes, A., ... & Graue, A. (2015). Mobility control during CO_2 EOR in fractured carbonates using foam: Laboratory evaluation and numerical simulations. Journal of Petroleum Science and Engineering, 135, 442-451.

(58) Heller, J. P. (1994). CO_2 Foams in Enhanced Oil Recovery. In Foams: Fundamentals and Applications in the Petroleum Industry (Vol. 242, pp. 201-234): American Chemical Society

(59) Bond, D.C., and Holbrook, O.C. Gas Drive Oil Recovery Process, U.S. Patent 2,866,507, 1958

(60) Mast, R. F. (1972, October). Microscopic behavior of foam in porous media. In SPE Annual Technical Conference and Exhibition? (pp. SPE-3997). SPE.

(61) Patton, J. T., Holbrook, S. T., & Hsu, W. (1983). Rheology of mobility-control foams. Society of Petroleum Engineers Journal, 23(03), 456-460.

(62) Castanier, L. M. (1989). Steam with additives: field projects of the eighties. Journal of Petroleum Science and Engineering, 2(2-3), 193-206.

(63) Hirasaki, G. J. (1989). A review of steam-foam process mechanisms. paper SPE, 19518..

(64) Schramm, L. L., & Schramm, L. L. (Eds.). (2000). Surfactants: fundamentals and applications in the petroleum industry. Cambridge university press..

(65) Dickson, J. L., Binks, B. P., & Johnston, K. P. (2004). Stabilization of carbon dioxide-in-water emulsions with silica nanoparticles. Langmuir, 20(19), 7976-7983.

(66) Xue, Z., Panthi, K., Fei, Y., Johnston, K. P., & Mohanty, K. K. (2015). CO_2-soluble ionic surfactants and CO_2 foams for high-temperature and high-salinity sandstone reservoirs. Energy & Fuels, 29(9), 5750-5760.

(67) Falls, A. H., Hirasaki, G. J., Patzek, T. E. A., Gauglitz, D. A., Miller, D. D., & Ratulowski, T. (1988). Development of a mechanistic foam simulator: the population balance and generation by snap-off. SPE reservoir engineering, 3(03), 884-892.

(68) Farajzadeh, R., Andrianov, A., Krastev, R., Hirasaki, G. J., & Rossen, W. R. (2012, April). Foam-oil interaction in porous media: Implications for foam assisted enhanced oil recovery. In SPE EOR Conference at Oil and Gas West Asia (pp. SPE-154197). SPE.

(69) Radke, C. J., & Ransohoff, T. C. (1986). Mechanisms of foam generation in glass bead packs (No. CONF-861080-). Univ. of California.

(70) Liu, Q., Qu, H., Liu, S., Zhang, Y., Zhang, S., Liu, J., ... & Luo, D. (2020). Modified Fe_3O_4 nanoparticle used for stabilizing foam flooding for enhanced oil recovery. Colloids and Surfaces A: Physicochemical and Engineering Aspects, 605, 125383.

(71) Zhou, Y., Wu, X., Zhong, X., Sun, W., Pu, H., & Zhao, J. X. (2019). Surfactant-augmented functional silica nanoparticle based nanofluid for enhanced oil recovery at high temperature and salinity. ACS applied materials & interfaces, 11(49), 45763-45775.

(72) Rehman, M. M., & Meribout, M. (2012). Conventional versus electrical enhanced oil recovery: a review. Journal of Petroleum Exploration and Production Technology, 2, 169-179.

(73) Bhatt, S., Saraf, S., & Bera, A. (2023). Perspectives of foam generation techniques and future directions of nanoparticle-stabilized CO_2 foam for enhanced oil recovery. Energy & Fuels, 37(3), 1472-1494.

(74) Schramm, L.L., and Wassmuth, F. Foams: Basic Principles, in Foams: Fundamentals and Application in the Petroleum Industry (ed. Schramm, L.L.), American Chemical Society, Washington DC, 1994, pp. 3-45 (Chapter 1)

(75) Chambers, K. T., & Radke, C. J. (1991). Interfacial phenomena in petroleum recovery. New York: Marcel Dekker, 191-255.

(76) Exerowa, D., Gochev, G., Platikanov, D., Liggieri, L., & Miller, R. (Eds.). (2018). Foam films and foams: Fundamentals and applications. CRC Press.

(77) Almajid, M. M., & Kovscek, A. R. (2016). Pore-level mechanics of foam generation and coalescence in the presence of oil. Advances in colloid and interface science, 233, 65-82.

(78) Kovscek, A. R., & Radke, C. J. (1993). Fundamentals of foam transport in porous media (No. DOE/BC-93000174). Lawrence Berkeley National Lab.(LBNL), Berkeley, CA (United States).

(79) Dicksen, T., Hirasaki, G. J., & Miller, C. A. (2002, April). Conditions for foam generation in homogeneous porous media. In SPE Improved Oil Recovery Conference? (pp. SPE-75176). SPE.

(80) Haggerty, R., Zhang, D., Eun, J., & Li, Y. (2023). Characterization of bubble transport in porous media using a microfluidic channel. Water, 15(6), 1033.

(81) Sheng, J. J. (2013). Foams and their applications in enhancing oil recovery. In Enhanced oil recovery field case studies (pp. 251-280). Gulf professional publishing.

(82) Weaire, D. L., & Hutzler, S. (1999). The physics of foams. Oxford University Press.

(83) Saint-Jalmes, A. (2006). Physical chemistry in foam drainage and coarsening. Soft Matter, 2(10), 836-849.

(84) Metin, C. O., Lake, L. W., Miranda, C. R., & Nguyen, Q. P. (2011). Stability of aqueous silica nanoparticle dispersions. Journal of Nanoparticle Research, 13, 839-850.

(85) Khatib, Z. I., Hirasaki, G. J., & Falls, A. H. (1988). Effects of capillary pressure on coalescence and phase mobilities in foams flowing through porous media. SPE reservoir engineering, 3(03), 919-926.

(86) Ross, S., & McBain, J. W. (1944). Inhibition of foaming in solvents containing known foamers. Industrial & Engineering Chemistry, 36(6), 570-573.

(86) Skjæveland, S. M., & Kleppe, J. (1992). SPOR Monograph, Recent advances in improved oil recovery methods for north sea sandstone reservoirs. Norwegian Petroleum Directorate, Norway.

(87) Friedmann, F., & Jensen, J. A. (1986, April). Some parameters influencing the formation and propagation of foams in porous media. In SPE Western Regional Meeting (pp. SPE-15087). SPE.

(88) Hudgins, D. A., & Chung, T. H. (1990, April). Long-distance propagation of foams. In SPE Improved Oil Recovery Conference? (pp. SPE-20196). SPE.

(90) Aarra, M. G., Skauge, A., & Martinsen, H. A. (2002). A Breakthrough for EOR in the North Sea. In SPE Annual Technical Conference and Exhibition.

(91) Andrianov, A., Farajzadeh, R., Nick, M. M., Talanana, M., & Zitha, P. L. (2011, July). Immiscible foam for enhancing oil recovery: bulk and porous media experiments. In SPE Asia Pacific Enhanced Oil Recovery Conference (pp. SPE-143578). SPE.

(92) Borchardt, J. K. (1987, February). Foaming agents for EOR: correlation of surfactant performance properties with chemical structure. In SPE International Conference on Oilfield Chemistry? (pp. SPE-16279). SPE.

(93) Robinson, J. V., & Woods, W. W. (1948). A method of selecting foam inhibitors. Journal of the Society of Chemical Industry, 67(9), 361-365.

(94) Harkins, W. D. (1941). A general thermodynamic theory of the spreading of liquids to form duplex films and of liquids or solids to form monolayers. The Journal of Chemical Physics, 9(7), 552-568.

(95) Aarra, M. G., & Skauge, A. (1994, September). A foam pilot in a North Sea oil reservoir: preparation for a production well treatment. In SPE Annual Technical Conference and Exhibition? (pp. SPE-28599). SPE.

(96) Vikingstad, A. K. (2006). Static and dynamic studies of foam and foam-oil interactions.

(97) Garrett, P. R. (1980). Preliminary considerations concerning the stability of a liquid heterogeneity in a plane-parallel liquid film. Journal of colloid and interface science, 76(2), 587-590.

(98) Denkov, N. D. (2004). Mechanisms of foam destruction by oil-based antifoams. Langmuir, 20(22), 9463-9505.

(99) Schramm, L. L., & Novosad, J. J. (1990). Micro-visualization of foam interactions with a crude oil. Colloids and Surfaces, 46(1), 21-43.

(100) Bergeron, V., Fagan, M. E., & Radke, C. J. (1993). Generalized entering coefficients: a criterion for foam stability against oil in porous media. langmuir, 9(7), 1704-1713.

(101) Dalland, M., Hanssen, J. E., & Kristiansen, T. S. (1992, September). Oil interaction with foams at static and flowing conditions in porous media. In Paper at the 13th EOR workshop and symposium, Banff.

(102) Mannhardt, K., Novosad, J. J., & Schramm, L. L. (2000). Comparative evaluation of foam stability to oil. SPE Reservoir Evaluation & Engineering, 3(01), 23-34.

(103) Derikvand, Z., & Riazi, M. (2016). Experimental investigation of a novel foam formulation to improve foam quality. Journal of Molecular Liquids, 224, 1311-1318.

(104) Svorstol, I., Vassenden, F., & Mannhardt, K. (1996, April). Laboratory studies for design of a foam pilot in the Snorre field. In SPE Improved Oil Recovery Conference? (pp. SPE-35400). SPE.

(105) Hirasaki, G. J., & Lawson, J. B. (1985). Mechanisms of foam flow in porous media: apparent viscosity in smooth capillaries. Society of Petroleum Engineers Journal, 25(02), 176-190.

(106) Chambers, D. J. (1994). Foams for Well Stimulation. In Foams: Fundamentals and Applications in the Petroleum Industry (Vol. 242, pp. 355-404): American Chemical Society.

(107) Bennetzen, M. V., & Mogensen, K. (2014, December). Novel applications of nanoparticles for future enhanced oil recovery. In International petroleum technology conference (pp. IPTC-17857). IPTC.

(108) Grigg, R. B., & Bai, B. (2005, February). Sorption of surfactant used in CO_2 flooding onto five minerals and three porous media. In SPE International Conference on Oilfield Chemistry? (pp. SPE-93100). SPE.

(109) Yekeen, N., Manan, M. A., Idris, A. K., & Samin, A. M. (2017). Influence of surfactant and electrolyte concentrations on surfactant Adsorption and foaming characteristics. Journal of Petroleum Science and Engineering, 149, 612-622.

(110) Holmberg, K. (Ed.). (2003). Novel surfactants: preparation applications and biodegradability, revised and expanded (Vol. 114). Crc Press.

(111) Johnston, K. P., & da Rocha, S. R. (2009). Colloids in supercritical fluids over the last 20 years and future directions. The Journal of Supercritical Fluids, 47(3), 523-530.

(112) Rossen, W. R. (2017). Foams in enhanced oil recovery. In Foams (pp. 413-464). Routledge.

(113) Yu, J., An, C., Mo, D., Liu, N., & Lee, R. (2012, April). Foam mobility control for nanoparticle-stabilized CO_2 foam. In SPE Improved Oil Recovery Conference? (pp. SPE-153336). SPE.

(114) Emami, H., Ayatizadeh Tanha, A., Khaksar Manshad, A., & Mohammadi, A. H. (2022). Experimental investigation of foam flooding using anionic and nonionic surfactants: A screening scenario to assess the effects of salinity and ph on foam stability and foam height. ACS omega, 7(17), 14832-14847.

(115) Sun, Q., Li, Z., Li, S., Jiang, L., Wang, J., & Wang, P. (2014). Utilization of surfactant-stabilized foam for enhanced oil recovery by adding nanoparticles. Energy & Fuels, 28(4), 2384-2394.

(116) Ahmed, S., Elraies, K. A., Forooozesh, J., Bt Mohd Shafian, S. R., Hashmet, M. R., Hsia, I. C. C., & Almansour, A. (2017). Experimental investigation of immiscible supercritical carbon dioxide foam rheology for improved oil recovery. Journal of Earth Science, 28, 835-841.

(117) Ahmed, S., Elraies, K. A., Hashmet, M. R., Hanamartani, A. S., & Bt Mohd Shafian, S. R. (2018, April). Laboratory study of CO_2 foam for enhanced oil recovery: advanced screening, optimization, and evaluation. In SPE Kingdom of Saudi Arabia Annual Technical Symposium and Exhibition (pp. SPE-192351). SPE.

(118) San, J., Wang, S., Yu, J., Liu, N., & Lee, R. (2017). Nanoparticle-stabilized carbon dioxide foam used in enhanced oil recovery: effect of different ions and temperatures. Spe Journal, 22(05), 1416-1423.

(119) Zhu, T., Ogbe, D. O., & Khataniar, S. (2004). Improving the foam performance for mobility control and improved sweep efficiency in gas flooding. Industrial & engineering chemistry research, 43(15), 4413-4421.

(120) Martin, F. D., Stevens, J. E., & Harpole, K. J. (1995). CO_2-Foam Field Test at the East Vacuum Grayburg/San Andres Unit. SPE Reservoir Engineering, 10(04), 266-272.

(121) Kim, J. S., Dong, Y., & Rossen, W. R. (2004, April). Steady-state flow behavior of CO_2 foam. In SPE Improved Oil Recovery Conference? (pp. SPE-89351). SPE.

(122) Worthen, A. J., Bagaria, H. G., Chen, Y., Bryant, S. L., Huh, C., & Johnston, K. P. (2012, April). Nanoparticle stabilized carbon dioxide in water foams for enhanced oil recovery. In SPE Improved Oil Recovery Conference (pp. SPE-154285). SPE.

(123) Binks, B. P. (2002). Particles as surfactants—similarities and differences. Current opinion in colloid & interface science, 7(1-2), 21-41.

(124) Okubo, T. (1995). Surface tension of structured colloidal suspensions of polystyrene and silica spheres at the air-water interface. Journal of colloid and interface science, 171(1), 55-62.

(125) Binks, B. P., & Horozov, T. S. (2005). Aqueous foams stabilized solely by silica nanoparticles. Angewandte Chemie International Edition, 44(24), 3722-3725.

(126) Espinosa, D., Caldelas, F., Johnston, K., Bryant, S. L., & Huh, C. (2010, April). Nanoparticle-stabilized supercritical CO_2 foams for potential mobility control applications. In SPE Improved Oil Recovery Conference? (pp. SPE-129925). SPE.

(127) Zhang, T., Espinosa, D., Yoon, K. Y., Rahmani, A. R., Yu, H., Caldelas, F. M., ... & Huh, C. (2011, May). Engineered nanoparticles as harsh-condition emulsion and foam stabilizers and as novel sensors. In Offshore Technology Conference (pp. OTC-21212). OTC.

(128) Mo, D., Yu, J., Liu, N., & Lee, R. (2012, October). Study of the effect of different factors on nanoparticle-stablized CO_2 foam for mobility control. In SPE Annual Technical Conference and Exhibition (pp. SPE-159282). Spe.

(129) Zhang, T., Roberts, M. R., Bryant, S. L., & Huh, C. (2009, April). Foams and emulsions stabilized with nanoparticles for potential conformance control applications. In SPE International Conference on Oilfield Chemistry? (pp. SPE-121744). SPE.

(130) Yu, J., Liu, N., Li, L., & Lee, R. L. (2012, February). Generation of nanoparticle-stabilized supercritical CO_2 foams. In Carbon Management Technology Conference (pp. CMTC-150849). CMTC.

(131) Liu, Y., Grigg, R. B., & Bai, B. (2005, February). Salinity, pH, and surfactant concentration effects on CO_2-foam. In SPE International Conference on Oilfield Chemistry? (pp. SPE-93095). SPE.

(132) Fu, C., Yu, J., & Liu, N. (2018). Nanoparticle-stabilized CO_2 foam for waterflooded residual oil recovery. Fuel, 234, 809-813.

(133) Rognmo, A. U., Heldal, S., & Fernø, M. A. (2018). Silica nanoparticles to stabilize CO_2-foam for improved CO_2 utilization: Enhanced CO_2 storage and oil recovery from mature oil reservoirs. Fuel, 216, 621-626.

(134) Fameau, A. L., & Salonen, A. (2014). Effect of particles and aggregated structures on the foam stability and aging. Comptes Rendus. Physique, 15(8-9), 748-760.

(135) Stocco, A., Rio, E., Binks, B. P., & Langevin, D. (2011). Aqueous foams stabilized solely by particles. Soft Matter, 7(4), 1260-1267.

(136) Zhang, Y., Liu, Q., Ye, H., Yang, L., Luo, D., & Peng, B. (2021). Nanoparticles as foam stabilizer: Mechanism, control parameters and application in foam flooding for enhanced oil recovery. Journal of Petroleum Science and Engineering, 202, 108561.

(137) Ehtesabi, H., Ahadian, M. M., & Taghikhani, V. (2015). Enhanced heavy oil recovery using TiO_2 nanoparticles: investigation of deposition during transport in core plug. Energy & Fuels, 29(1), 1-8.

(138) Sun, X., Zhang, Y., Chen, G., & Gai, Z. (2017). Application of nanoparticles in enhanced oil recovery: a critical review of recent progress. Energies, 10(3), 345.

(139) Bakshi, S., He, Z. L., & Harris, W. G. (2015). Natural nanoparticles: implications for environment and human health. Critical Reviews in Environmental Science and Technology, 45(8), 861-904.

(140) Singh, R., & Mohanty, K. K. (2015). Synergy between nanoparticles and surfactants in stabilizing foams for oil recovery. Energy & Fuels, 29(2), 467-479.

(141) Guo, F., & Aryana, S. (2016). An experimental investigation of nanoparticle-stabilized CO_2 foam used in enhanced oil recovery. Fuel, 186, 430-442.

(142) Risal, A. R., Manan, M. A., Yekeen, N., Azli, N. B., Samin, A. M., & Tan, X. K. (2019). Experimental investigation of enhancement of carbon dioxide foam stability, pore plugging, and oil recovery in the presence of silica nanoparticles. Petroleum Science, 16, 344-356.

(143) Ibrahim, A. F., Emrani, A., & Nasraldin, H. (2017, July). Stabilized CO_2 foam for EOR applications. In Carbon Management Technology Conference (pp. CMTC-486215). CMTC.

(144) Aarra, M.G., Skauge, A., and Martinsen, H.A. A Breakthrough for EOR in the North Sea, Presented at SPE Annual Technical Conference and Exhibition, San Antonio, Texas, 29. Sep.-2. Oct., 2002. Paper SPE 77695.

(145) Skauge, A., Aarra, M.G., Surguchev, L.M, Martinsen, H.A., and Rasmussen, L. Foam Assisted WAG: Experience from the Snorre Field, Presented at the SPE/DOE Improved Oil Recovery Symposium, Tulsa, Oklahoma, 13-17. April, 2002. Paper SPE 75157.

(146) Vikingstad, A.K., and Aarra, M.G. Comparing the Static and Dynamic Foam Properties of a Fluorinated and an Alpha Olefin Sulfonate Surfactant, JPSE., Vol 65, 2009, pp.105-111.

(147) Mannhardt, K., and Svorstøl, I., Surfactant Concentration for Foam Formation and Propagation in Snorre Reservoir Core, JPSE, Vol. 30, Issue 2, July, 2001, pp.105-119

(148) Aarra, M. G.; Ormehaug, P. A.; Skauge, A.; Masalmeh, S. K. Experimental Study of CO_2- and Methane-Foam Using Carbonate Core Material at Reservoir Conditions. SPE Middle East Oil Gas Show Conf. MEOS, Proc. 2011, 2, SPE-141614-MS.

(149) Skauge, A., Solbakken, J., Ormehaug, P. A., & Aarra, M. G. (2020). Foam generation, propagation and stability in porous medium. Transport in Porous Media, 131(1), 5-21.

(150) Mannhardt, K., Schramm, L. L., & Novosad, J. J. (1992). Adsorption of anionic and amphoteric foam-forming surfactants on different rock types. Colloids and surfaces, 68(1-2), 37-53.

(151) Ghosh, P., & Mohanty, K. K. (2018). Novel application of cationic surfactants for foams with wettability alteration in oil-wet low-permeability carbonate rocks. SPE Journal, 23(06), 2218-2231.

(152) Shakeel, M., Samanova, A., Pourafshary, P., & Hashmet, M. R. (2021). Experimental analysis of oil displacement by hybrid engineered water/chemical EOR approach in carbonates. Journal of Petroleum Science and Engineering, 207, 109297.

(153) Muneer, R. (2023). Surface force analysis and application of DLVO modeling in predicting and controlling fines migration in sandstone reservoirs. School of Mining and Geosciences

(154) Bod, P. R., Borthakur, P. P., Baruah, E., & Kerolina, R. D. S. A Review of Properties, Synthesis Procedure, Characterization and Application for Silicon Oxide Nanoparticles.

(155) Freire-Gormaly, M., Ellis, J. S., MacLean, H. L., & Bazylak, A. (2016). Pore structure characterization of Indiana limestone and pink dolomite from pore network reconstructions. *Oil & Gas Science and Technology–Revue d'IFP Energies nouvelles*, *71*(3), 33.

(156) Kalam, S., Abu-Khamsin, S. A., Gbadamosi, A. O., Patil, S., Kamal, M. S., Hussain, S. M. S & Mohanty, K. K. (2023). Static and dynamic adsorption of a gemini surfactant on a carbonate rock in the presence of low salinity water. *Scientific Reports*, *13*(1), 11936.

(157) Alanazi, A., Baban, A., Ali, M., Keshavarz, A., Iglauer, S., & Hoteit, H. (2023). Residual trapping of CO_2, N_2, and a CO_2-N_2 mixture in Indiana limestone using robust NMR coreflooding: Implications for CO_2 geological storage. *Fuel*, *353*, 129221.

(158) Somasundaran, P., & Agar, G. E. (1967). The zero point of charge of calcite. *Journal of Colloid and Interface Science*, *24*(4), 433-440.

(159) Safran, S. E. (2019). Nanoparticle-stabilized CO_2 foams to improve conventional CO_2 EOR process at Batı Raman field (Doctoral dissertation, Middle East Technical University (Turkey)).

(160) Guo, B. (2003). Proof of the Young–Laplace equation using the theory of calculus of variations applied to petroleum fluids. Petroleum science and technology, 21(7-8), 1159-1165.

(161) EI Elliott 2004. https://web.archive.org/web/20190712202752/http://people.ds.cam.ac.uk/jae1001/cus/teaching/materials/M6_lecture_6.pdf

(162) Energy Institute. Good Plant Design and Operation for Onshore Carbon Capture Installations and Onshore Pipelines, first edition, London, September, 2010.

(163) Salaudeen, I., Rehan Hashmet, M., & Pourafshary, P. (2021, October). Synergistic effects of engineered water-nanoparticle on oil/brine/rock interactions in carbonates. In SPE Europec featured at EAGE Conference and Exhibition (p. D022S002R003). SPE.

(164) Shirazi, M., Kord, S., & Tamsilian, Y. (2019). Novel smart water-based titania nanofluid for enhanced oil recovery. Journal of Molecular Liquids, 296, 112064.

(165) Majeed, T., Sølling, T. I., & Kamal, M. S. (2020). Foamstability: The interplay between salt-, surfactant-and critical micelle concentration. Journal of Petroleum Science and Engineering, 187, 106871.

(166) Solbakken, J. S., & Aarra, M. G. (2021). CO_2 mobility control improvement using N_2-foam at high pressure and high temperature conditions. International Journal of Greenhouse Gas Control, 109, 103392.

(167) Schramm, L. L. (1994). Foam sensitivity to crude oil in porous media.

(168) Kumar, S., & Mandal, A. (2017). Investigation on stabilization of CO_2 foam by ionic and nonionic surfactants in presence of different additives for application in enhanced oil recovery. Applied Surface Science, 420, 9-20.

(169) Hurtado, Y., Beltran, C., Zabala, R. D., Lopera, S. H., Franco, C. A., Nassar, N. N., & Cortes, F. B. (2018). Effects of surface acidity and polarity of SiO2 nanoparticles on the

foam stabilization applied to natural gas flooding in tight gas-condensate reservoirs. Energy & fuels, 32(5), 5824-5833.

(170) Aarra, M.G., Skauge, A., Solbakken, J., Ormehaug, P.A., April 2014. Properties of N2- and CO_2-foams as a function of pressure. JPSE 116, 72–89.

(171) AlSumaiti, A. M., Hashmet, M. R., AlAmeri, W. S., & Anto-Darkwah, E. (2018). Laboratory study of CO_2 foam flooding in high temperature, high salinity carbonate reservoirs using Co-injection Technique. Energy & Fuels, 32(2), 1416-1422.

(172) Alvarez, J. M., Rivas, H. J., & Rossen, W. R. (2001). Unified model for steady-state foam behavior at high and low foam qualities. SPE journal, 6(03), 325-333.

(173) Li, B. F., Zhang, M. Y., Li, Z. M., Kovscek, A., Xin, Y., & Li, B. L. (2023). Flow characteristics and regime transition of aqueous foams in porous media over a wide range of quality, velocity, and surfactant concentration. Petroleum Science, 20(2), 1044-1052.

(174) Schlumberger. (2016). ECLIPSE Industry-Reference Reservoir Simulator Technical Description: Schlumberger.

(175) Ramirez, W. F., Fathi, Z., & Cagnol, J. L. (1984). Optimal injection policies for enhanced oil recovery: part 1—theory and computational strategies. Society of Petroleum Engineers Journal, 24(03), 328-332.

(176) Ertekin, T., Abou-Kassem, J. H., & King, G. R. (2001). Basic applied reservoir simulation. (No Title).

(177) Batycky, R., Thiele, M., Coats, K., Grindheim, A., Ponting, D., Settari, T. Whitson, C. (2007). Chapter 17 - Reservoir Simulation. In Petroleum Engineering Handbook, Vol. 5 - Reservoir Engineering and Petrophysics.

(178) Urazgaliyeva, G., King, G. R., Darmentaev, S., Tursinbayeva, D., Dunger, D., Howery, R. & Aitzhanov, A. (2014, November). Tengiz sour gas injection project: An update. In SPE Annual Caspian Technical Conference (pp. SPE-172284). SPE.

(179) Christie, M. A., & Blunt, M. J. (2001). Tenth SPE comparative solution project: A comparison of upscaling techniques. SPE Reservoir Evaluation & Engineering, 4(04), 308-317.

(180) Farajzadeh, R., Lotfollahi, M., Eftekhari, A. A., Rossen, W. R., & Hirasaki, G. J. H. (2015). Effect of permeability on implicit-texture foam model parameters and the limiting capillary pressure. Energy & fuels, 29(5), 3011-3018.

(181) Zeng, Y., Ma, K., Farajzadeh, R., Puerto, M., Biswal, S. L., & Hirasaki, G. J. (2016). Effect of surfactant partitioning between gaseous phase and aqueous phase on CO_2 foam transport for enhanced oil recovery. Transport in Porous Media, 114(3), 777-793.

(182) Vicard, A., Atteia, O., Bertin, H., & Lachaud, J. (2022). Estimation of local equilibrium foam model parameters as functions of the foam quality and the total superficial velocity. *ACS omega*, *7*(20), 16866-16876.

(183) Chugh, S., Baker, R., Cooper, L., & Spence, S. (2000). Simulation of horizontal wells to mitigate miscible solvent gravity override in the Virginia Hills Margin. Journal of Canadian Petroleum Technology, 39(02).

(184) Amani, P., Salehi, A., Wang, J., & Firouzi, M. (2025). Enhancing CO_2 foam stability with hexane vapours: Mitigating coarsening and drainage rates. *Colloids and Surfaces A: Physicochemical and Engineering Aspects*, *707*, 135867.

(185) Chilingar, G. V., & Yen, T. F. (1983). Some notes on wettability and relative permeabilities of carbonate reservoir rocks, II. *Energy Sources*, *7*(1), 67-75.

(186) Mannhardt, K. (1999). Core Flood Evaluation of Solvent Compositional and Wettability Effects on Hydrocarbon Solvent Foam Performance. Journal of Canadian Petroleum Technology, 38(13).

Appendix

A. Crude oil composition

Научно-исследовательский лабораторный центр АО «НИПИнефтегаз»

Республика Казахстан. 130000, г. Актау, 8 мкр. административное здание АО «НИПИнефтегаз», телефон: (7292) 600208 доб. 128; e-mail: sl@nipi.kz

Республика Казахстан, 060014, г. Атырау, мкр. Балыкшы, ул. Айнакн Байжигитовой, строение 57, телефон: (7122) 933039 доб. 612; e-mail: atyrau@nipi.kz

KZ.T.13.1064 TESTING

Аттестат аккредитации № KZ.T.13.1064 от 12 октября 2020 года

Утверждаю
Генеральный директор
АО «НИПИнефтегаз»
д-р техн.наук
О.С. Герштанский

ОТЧЕТ ОБ ИСПЫТАНИИ № 16/22 от 26.07.2022 г.

Лабораторные исследования по определению компонентного состава дегазированной нефти

Направление: исследования пластовой нефти

Наименование и адрес заказчика: Школа горного дела и наук о Земле АО «Назарбаев Университет», 130000, Республика Казахстан, г. Нур-Султан, проспект Кабанбай батыра, 53, тел.: +7 (7172) 694 628

Наименование образца, выданное заказчиком: нет

Место проведения испытаний: АО НИПИнефтегаз, НИЛЦ

Внутренний идентификационный код образца: Н-259/22

Место отбора образца: нет

Дата и время отбора образца: нет.

Объем пробы: 1 л

Вид тары: пластиковая емкость

Дата поступления образца в лабораторию: 25.07.2022 г.

Описание образца: дегазированная нефть

Параметры окружающей среды: температура 25,0 °С, барометрическое давление 101,4 кПа, относительная влажность 52 %

Дата проведения испытаний: 25.07.2022 г.

Согласно Письму № 25-23/46 от 20.06.2022 г. в НИЛЦ АО «НИПИнефтегаз» 25.07.2022 г. поступила проба дегазированной нефти на определение компонентного состава от Школы горного дела и наук о Земле АО «Назарбаев Университет».

Компонентный состав дегазированной нефти определен согласно ASTM D 2887-2013 г. «Стандартный метод распределения температурных пределов кипения нефтяных фракций с помощью газовой хроматографии» на хроматографе «Кристалл 5000.2».

Результаты исследований дегазированной нефти представлены в таблице ниже.

Таблица 1 – Результаты исследования компонентного состава дегазированной нефти

Наименование	Н-259/22	
	% масс.	% мол.
Изо-пентан	1,485	2,990
Н–пентан	5,498	11,071
Гексан	7,803	13,156
Циклогексан	0,030	0,052
Бензол	1,067	1,985
Гептан	6,867	10,394
М-Ц-гексан	0,380	0,562
Толуол	0,193	0,304
Октан	9,615	13,056
Этилбензол	0,141	0,193
мета/пара-ксилол	1,147	1,570
ортоксилол	0,265	0,362
Нонан	1,789	2,148
1,2,4 три метил бензол	0,459	0,555
Деканы	1,749	1,897
Ундеканы	5,391	5,329
Додеканы	4,841	4,369
Тридеканы	5,442	4,518
Тетрадеканы	4,972	3,802
Пентадеканы	4,343	3,063
Гексадеканы	4,189	2,741
Гептадеканы	3,706	2,272
Октадеканы	3,813	2,207
Нонадеканы	3,576	1,976
Эйкозаны	3,048	1,611
Генейкозаны	2,994	1,495
Докозаны	2,235	1,065
Трикозаны	2,434	1,112
Тетракозаны	1,721	0,756
Пентакозаны	1,916	0,807
Гексакозаны	1,562	0,632
Гептакозаны	1,426	0,554
Октакозаны	1,218	0,456
Нонакозаны	1,142	0,413

Наименование	Н-259/22	
	% масс.	% мол.
Триконтаны	0,870	0,304
Гентриконтаны	0,451	0,153
Дотриконтаны	0,112	0,037
Тритриконтаны	0,040	0,013
Тетратриконтаны	0,022	0,007
Пентатриконтаны	0,021	0,006
Гексатриконтаны	0,008	0,002
Гептатриконтаны	0,007	0,002
Октатриконтаны	0,004	0,001
Нонатриконтаны	0,004	0,001
Тетраконтаны+	0,003	0,001
Ароматические (сумма)	3,272	4,968

Директор НИЛЦ С.В. Лозовая

Руководитель НИПН Л.Л. Алькина

B. Surfactant datasheet

Stepan

+1-847-446-7500
1-800-457-7573
Tech Services:
+1-800-745-7837

Certificate of Analysis

Print Date: 04-NOV-2022 13:51:52 CET
Page: 1 / 1
Customer Code:

Material No. & Description: 1082215 BIO-TERGE AS-40 KSB
Specification number: PA006_STP Issue: 2 (31-JUL-2015)

Batch/Lot: 0008745542

Location: STALYBRIDGE, CH GB

Date of Manufacture: 10-AOU-2022
Certification Date: 15-AOU-2022
Recommended Retest Date: 10-AOU-2023

Description		Limits	In Out	Result	Units
110-0	APPEARANCE (@ 25C)	Clear Liquid, PFM	IN	Conforme	
058-0	PH (10% in Water)	5,0 - 6,5	IN	6,4	
117-D	ACTIVE (%) (EW 320)	37,0 - 39,0	IN	37,7	%
125-0	FREE OIL (%)	1,8 Max.	IN	1,4	%
098-G	SODIUM SULFATE (%)	2,0 Max.	IN	1,0	%
119-0	SODIUM CHLORIDE (%)	1,00 Max.	IN	0,01	%
024-0	VISC (CPS) (@ 25C)	500 Max.	IN	70	cPs
006-E	COLOR KLETT (5% Active in Water)	100 Max.	IN	35	
320-A	ISOTHIAZOLINONES (CIT/MIT) (ppm)	5,0 - 15,0	IN	12,0	ppm

This certificate is electronically generated and is valid without a signature.

THIS ANALYSIS IS NOT TO BE CONSTRUED AS A WARRANTY, EXPRESSED OR IMPLIED. The preceding data is provided at the request of and for the convenience of the customer and does not relieve the customer of its responsibility to verify data contained on this report and to perform any other analysis necessary to determine suitability of the product described above for the use intended by the customer.

DEDICATED TO CONTINUOUS IMPROVEMENT THROUGH SQC & SPC

C. Nanoparticles (SiO_2) oxide size measurement

PARTICLE METRIX

ZETAVIEW®

www.particle-metrix.com

Electrophoresis & Brownian Motion
Video Analysis
Laser Scattering Microscopy

Nazarbayev University - School of Science
53 Kabanay Ave. - Block C4, Room 628
010000 Astana
Kazakhstan
Video Operator: ZetaUser

Operator (Report): ZetaUser

Sample Parameters
Sample Name:
Sample Info 1:
Sample Info 2:
Sample Info 3:
Electrolyte:
Temperature: 23.93 °C sensed
pH 7.0 entered
Conductivity: 13575.00 µS/cm sensed

Instrument Parameters
Laser Wavelength: 488 nm
Filter Wavelength: Scatter
Sensitivity: 60
Shutter: 200

SOP: <No SOP>
Size Distribution 1 Cycle 11 Positions
Description:

Result (sizes in nm)

	Number	Concentration	Volume
Median (X50)	164.8	164.8	301.9
StdDev	89.8	89.8	246.5

Concentration: 1.0E+11 Particles / mL
Dilution Factor: 1000
Original Concentration: 1.0E+14 Particles / mL

Quality
Average Counted Particles per Frame: 232
Number of Traced Particles: 2823

Analysis Parameters
Max Area 1000, Min Area 5, Min Brightness 25, nm/Class: 30

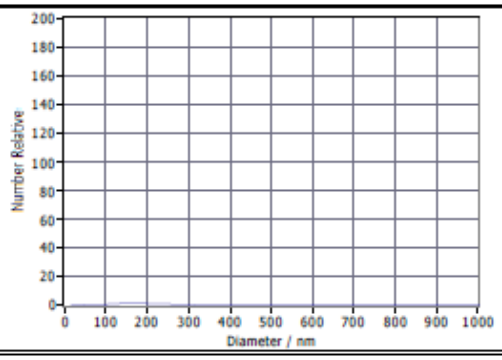

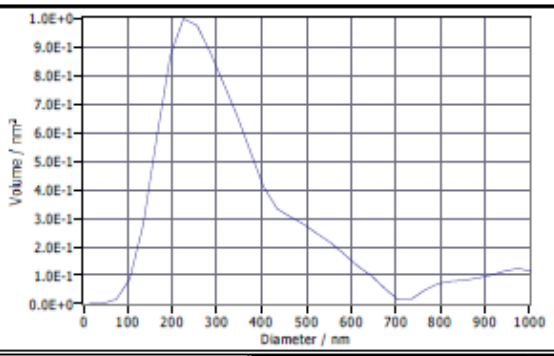

Peak Analysis (Concentration)

Diameter / nm	Number Absolute	FWHM / nm	Percentage
168.6	4.9E+2	151.5	100.0

X Values (all sizes are given in nm)

	Number	Concentration	Volume
X10	88.6	88.6	165.2
X50	164.8	164.8	301.9
X90	284.1	284.1	824.1
Span	1.2	1.2	2.2
Mean	195.4	195.4	398.6
StdDev	89.8	89.8	246.5

Comment

(Signature)

Analyzed Video: Z:\Madiyar\20231124_0007_01-1000-size_size_488.avi

Experiment: 2023-11-24 16:21 ZetaView S/N 23-866, Software ZetaView (version 8.05.16 SP3)

Report: 2023-11-24 16:23 Software ZetaView (version 8.05.16 SP3)

D. Characteristics of Aflas O-Rings

030 O-RING AFLAS
80 DUROMETER BLACK
CS: .070″ (1.78MM)
ID: 1.614″ (41.00MM)

A80030

LOGIN TO SEE PRICES

Stock & Availability (ea)

- In Stock: **491**
- Inbound Stock: 0
- Offsite Stock: 0 ($50 Line Min)
- New Production: Unlimited ($250 Line Min)
  Expedited Shipping*: 08/08/2025
  Standard Shipping: 10/27/2025

*Add your desired qty and click ADD TO CART to see expedite fees and options.

Additional information

Weight	*0.00115 lbs*
Shipping Dimensions	*1.754 × 1.754 × 0.07 in*
Material	*Aflas*
Color	*Black*
Durometer	*80*
Size	*030*
Minimum Temperature	*14*
Maximum Temperature	*428*

Description

SPEC SHEET: Tetrafluoroethylene-Propylene (AFLAS®) 80 Durometer.pdf

Tetrafluoroethylene-Propylene (AFLAS®)

Material Description

This elastomer is a copolymer of tetrafluoroethylene (TFE) and propylene. AFLAS®is unique due to its resistance to petroleum products, steam, phosphate esters and brake fluids. In some respects, it exhibits media compatibility properties similar to ethylene propylene
and fluorocarbon. It has fair resistance to brake fluids and phosphate esters while exhibiting good resistance to petroleum oils.

Cure system: Peroxide-cured

Standard AFLAS® compounds are peroxide-cured.

Temperature Range:

Standard Low Temp: -10°C (-14°F)

Standard High Temp: 220°C (428°F)